1-1-2013

Application of Computational Fluid Dynamics Methods to Improve Thermal Hydraulic Code Analysis

Dennis Shannon Sentell, Jr.
University of South Carolina

APPLICATION OF COMPUTATIONAL FLUID DYNAMICS METHODS TO IMPROVE THERMAL HYDRAULIC CODE ANALYSIS

by

Dennis Shannon Sentell, Jr.

Bachelor of Science
United States Military Academy, 1993

Master of Science
Massachusetts Institute of Technology, 2002

Submitted in Partial Fulfillment of the Requirements

For the Degree of Doctor of Philosophy in

Nuclear Engineering

College of Engineering and Computing

University of South Carolina

2013

Accepted by:

Travis W. Knight, Major Professor

Jamil A. Khan, Committee Member

Djamel Kaoumi, Committee Member

L. Larry Hamm, Committee Member

Lacy Ford, Vice Provost and Dean of Graduate Studies

DEDICATION

This work is dedicated to my loving and supportive wife, Amala, and our incredible sons—Gray, Sloan and Talbot. Their love and constant encouragement are the greatest inspiration and motivation towards all I strive to become and accomplish. No more school. I promise!

ACKNOWLEDGEMENTS

The United States Army and the United States Military Academy at West Point provided funding for this work based on educational requirements to be an Assistant Professor in the Department of Physics and Nuclear Engineering.

NO PANE, NO GAIN!

ABSTRACT

A computational fluid dynamics code is used to model the primary natural circulation loop of a proposed small modular reactor for comparison to experimental data and best-estimate thermal-hydraulic code results. Recent advances in computational fluid dynamics code modeling capabilities make them attractive alternatives to the current conservative approach of coupled best-estimate thermal hydraulic codes and uncertainty evaluations. The results from a computational fluid dynamics analysis are benchmarked against the experimental test results of a 1:3 length, 1:254 volume, full pressure and full temperature scale small modular reactor during steady-state power operations and during a depressurization transient. A comparative evaluation of the experimental data, the thermal hydraulic code results and the computational fluid dynamics code results provides an opportunity to validate the best-estimate thermal hydraulic code's treatment of a natural circulation loop and provide insights into expanded use of the computational fluid dynamics code in future designs and operations. Additionally, a sensitivity analysis is conducted to determine those physical phenomena most impactful on operations of the proposed reactor's natural circulation loop. The combination of the comparative evaluation and sensitivity analysis provides the resources for increased confidence in model developments for natural circulation loops and provides for reliability improvements of the thermal hydraulic code.

PREFACE

The design and development of evolutionary and innovative next generation nuclear reactors incorporate the use of passive systems to fulfill required functions and to provide confidence in the plant's ability to operate in steady-state conditions and to handle transients and accidents. These systems are characterized by no or very limited reliance on external input (power, signals or human action) and whose operation takes advantage of natural forces, such as natural circulation.

Therefore, these systems are required to accomplish their mission with a sufficient reliability margin that makes them attractive as an essential means of achieving two key goals. The first is design simplification and significant cost reduction for future plants. Second is an assurance of safety with a lesser dependence of the safety function of active components like pumps and diesel generators.

Since the magnitude of the natural forces that drive the operation of passive systems is relatively small, counter-forces such as friction, can be of comparable magnitude and cannot be ignored, as is generally the case with pumped systems. This concern leads to the consideration that despite the fact that passive systems, by definition, should be more reliable than active ones, there is always a probability that a physical phenomenon could lead to a failure mode once the system enters into operation.

The characteristics of this type of uncertainty and low driving forces for these passive systems justify a comparative evaluation of the best-estimate thermal-hydraulic code predictions to the rapidly expanding role of computational fluid dynamics models in new nuclear power plant design. The need to use computational fluid dynamics arises because the best-estimate thermal-hydraulic codes rely heavily on a network of one-dimensional volumes and correlation databases that could lead to artificial confidence in the passive systems.

It is obvious, however, that the flow patterns in most, if not all, components in the core of a nuclear power plant, are strongly three-dimensional. Natural circulation and complex channel flow and mixing are also essentially three-dimensional in nature. Representing such complex flows through the use of existing best-estimate thermal-hydraulic codes may not just be oversimplified, but, as stated earlier, could be misleading in their use in reliability assessments. The confidence in these code's accurate predictions could result in erroneous judgments about the reliability of these new designs as a whole. This research is one proposal to improve the confidence in evaluation of natural circulation in these passive systems.

TABLE OF CONTENTS

LIST OF TABLES

LIST OF FIGURES

LIST OF ABBREVIATIONS

1-D……..One-Dimensional

3-D……...Three-Dimensional

ADS……...Automatic Depressurization System

AHWR……..Advanced Heavy Water Reactor

AP600/1000……..……Advanced Plant 600/1000

BWR……..……..Boiling Water Reactor

CFD…….……Computational Fluid Dynamics

CHF……....Critical Heat Flux

CL…….…….....Cold Leg

CPV……...Cooling Pool Vessel

CRP…….……Coordinated Research Project

ECCS…….……Emergency Core Cooling System

EHRS…….……..Emergency Heat Removal System

EQN……...Equation

ESBWR……....Economic Simplified Boiling Water Reactor

FW…….…….....Feedwater

HL…….……...Hot Leg

HPC…….……High-Pressure Containment

HTSTR……Heat Structure

IAEA…….……International Atomic Energy Agency

ID……...Inside Diameter

IRIS……..…International Reactor Innovative and Secure

IRWST…….……In-containment Refueling Water Storage Tank

LOCA……Loss of Coolant Accident

LWR…….……..Light Water Reactor

MASLWR…….……Multi-Application Small Light Water Reactor

MPa……..Mega-pascals

MWe…….……Mega-watt Electric

MWt…….……...Mega-watt Thermal

NRC……..……..……Nuclear Regulatory Commission

NSSS…….……Nuclear Steam Supply System

OD……..Outside Diameter

OSU……..……Oregon State University

OSU-MASLWR……..…Oregon State University MASLWR Integral Test Facility

PDE……..Partial Differential Equation

PRHR…….……..Passive Residual Heat Removal

PZR……...Pressurizer

PWR……..……Pressurized Water Reactor

RPV……...Reactor Pressure Vessel

RHRS…….……..Residual Heat Removal System

RWST……..……...Refueling Water Storage Tank

SBLOCA……Small Break Loss of Coolant Accident

SG……...Steam Generator

SMART……...System Integrated Modular Advanced Reactor

SMR……..Small Modular Reactor

SNAP…….Symbolic Nuclear Analysis Package

SS……...Stainless-Steel

T-H……..……..Thermal-Hydraulic

TRACE……TRAC/RELAP Advanced Computational Engine

CHAPTER 1

INTRODUCTION

1.1 PASSIVE SYSTEM MOTIVATION IN ADVANCED NUCLEAR REACTOR DESIGNS

Designers of evolutionary and innovative nuclear reactors place an increased reliance on passive systems to reduce geographic footprints, minimize the number of components in use, and eliminate the need for human interaction during normal and transient operations. Passive systems, as defined by the International Atomic Energy Agency (IAEA), do not rely on external power sources or operator actions, or at least do so only to a very limited degree. Rather, these systems operate by exploiting various natural phenomena (e.g., conduction, condensation, gravity and/or natural circulation) to accomplish their function. The term “passive” identifies a system which is composed entirely of passive components and structures or a system which uses active components in a very restricted way to initiate an ensuing passive operation. (IAEA-TECDOC-626 1991)

Due to their reliance on inherent physical laws, passive systems are often thought to be more reliable than traditional active systems. (EPRI 2007) This is due to a number of factors. Considering that the reliability of active systems is more often limited by the availability of AC power or successful operator action, it can be surmised that passive systems, with a reliance on neither, would be more

reliable. Secondly, passive systems are often thought to be less expensive than their active counterparts, as a passive system would preclude many of the costly redundant components present in an active system. Furthermore, passive systems can eliminate complex backup systems, such as diesel generators or off-site power grid connections, which result in an increase in both reliability and economic attractiveness. Thus, it is the passive systems' potential to achieve enhanced reliability at a lower cost that motivates the use of them in evolutionary and innovative reactor designs.

In addition to these features, these reactors will be licensed within a framework that will be risk-informed and performance-based. Probabilistic risk assessments of passive systems will serve as a cornerstone requirement for the licensing of advanced nuclear generating plants. As such, the applications of passive systems to reactor operation and safety are numerous, and these applications must be accurately accounted for in any probabilistic risk assessment of the design. The reliability assessment of passive systems requires, as a first step, the identification of all the relevant failure modes. Thus, the final result is generally a statement about the proneness to failure, which is conditional on the assumptions that all significant failure modes have been duly identified and accounted.

The IAEA currently recognizes four categories of passive systems, as listed in Table 1.1. (IAEA-TECDOC-626 1991) Several examples of systems that fall into each category are also listed. There are unique challenges for evaluation of the system reliability in each of these categories. For Category A systems,

structural-reliability analysis methods can estimate reliability through the application of the principles of probabilistic structural mechanics theory. For Category C and D equipment, operating experience data can provide the basis for the reliability calculation. However, there is so far no agreed approach regarding reliability assessments of Category B passive systems. Numerous advanced reactor designs, including the Westinghouse AP1000 and General Electric's economic simplified boiling water reactor (ESBWR), currently rely heavily on category B passive systems, and they will be explored further in Chapter 2.

Table 1.1. IAEA Classification for Passive Systems

Category	*Description*	*Example*
A	Physical barriers and static structures	Cladding, piping, Containment
B	Moving fluid with no moving parts	Natural circulation cooling Systems
C	Moving fluid with moving parts	Gravity-driven make-up tanks and accumulators with check valves
D	Active Initiation/Passive Execution	Gravity-driven control rods requiring active initiation

1.2 Statement of The Problem

As part of the safety assessment and licensing procedure for new nuclear power plant designs, a wide range of analyses are carried out using best-estimate thermal-hydraulic (T-H) codes. These codes have been developed to evaluate system response during an extensive array of scenarios, including normal and transient operations. In these codes, the partial differential equations (mass, momentum and energy balance equations) that describe flow and heat transfer are usually solved by finite-difference methods based on one-

dimensional (1-D) approximations. Accordingly, the T-H modeling employs an appropriate set of correlations and physical models. The model for a specific nuclear power plant is then built by connecting 1-D modular components (pipes, tees, pumps, valves, heat structures, etc.) and relying on these correlations to accurately predict system behavior. The reliance on passive systems for both steady-state and transient conditions and their inclusion in these 1-D models increases the chance of erroneously predicting the system behavior.

T-H code uncertainties can come from uncertainties in the imperfect modeling of the physical geometry of the system, uncertainties in the value and/or precision of input parameters, and uncertainties in the modeling of the physical processes as a result of solution methods that use imperfect correlations or numerical-solution techniques. Potential T-H effects include 1-D versus multi-dimensional effects, physical asymmetries, two-phase flow instabilities, T-H oscillations, and the effects of non-condensable gases. As such, the uncertainties related to both the code's output, through model development and user input, combined with the inherent uncertainty of several types of natural phenomenon, leads to deviations in the predicted behavior of these systems.

The advent of small modular reactors (SMRs) and advanced reactor designs relying on natural circulation for primary coolant flow and passive safety systems introduces certain accident scenarios previously unforeseen, in which strong asymmetries may exist in the natural properties of the coolant and residual heat removal systems (RHRS). As a simple example, these asymmetries can be due to differences in temperature in large mixing volumes.

The temperature distributions at the core inlet depend largely on the coolant mixing taking place in the downcomer and in the lower plenum of the pressure vessel. Such mixing phenomena are strongly three-dimensional (3-D) and are influenced by turbulence. Therefore, 1-D approximations and data correlations utilized in the T-H code calculations are unsuitable for this class of problem. Natural circulation further complicates this flow as the driving forces involved are orders of magnitude less than those systems with a driving head from numerous coolant and heat removal pumps.

Among the modeling assumptions adopted in T-H system codes, whose adequacy is highly questionable when dealing with stability analyses even in single-phase natural circulation loops, the following can be mentioned: (Wulff 2011)

- the neglect of developing boundary layer conditions (e.g., thermal entry effects) in heated and cooled sections;
- the use of first-order numerical schemes, which are prone to dissipative and dispersive effects that could lead to qualitative changes in the predicted behavior with respect to a well converged solution;
- the use of 1-D balance equations based on cross-section averaged variables.

However, in the context of single and two-phase natural circulation, computational fluid dynamics (CFD) codes have reached a satisfactory level of maturity for providing a complementary capability to T-H system codes for accurately characterizing 3-D flows. Comparisons between the 1-D best estimate code and the 3-D CFD codes against existing experimental data can provide useful insights into the limitations posed by utilization of the 1-D T-H

codes in assessments of next generation nuclear power plants' and SMRs' reliance on natural circulation.

Furthermore, sensitivity analysis utilization can facilitate model developments for natural circulation and provide for more reliable validation of the T-H code. The inclusion of a more refined T-H code output or, in more advanced computational efforts, a coupled T-H and computational fluid dynamic code output, increases the overall probabilistic risk assessment in terms of minimizing the uncertainties associated with passive system performance.

1.3 Background of the Study

There is a clear motivation for expanding the use of passive systems in advanced reactor designs. Several new designs, some of which have already received Nuclear Regulatory Commission (NRC) approval, depend on passive safety systems as the primary method of reactor decay heat removal during normal and transient conditions. Accurate assessments of the reliability of these passive safety systems and the accompanying uncertainty in these calculations are critical to the overall risk assessment of these designs.

Notwithstanding the fact that passive systems are considered by most as more reliable than active ones, because of the smaller unavailability due to hardware failure and human error, there is always a non-zero likelihood of the occurrence of physical phenomena leading to pertinent failure modes, once the system enters into operation. In fact, the deviations of the natural forces or physical principles, upon which they rely, from the expected conditions can impair the performance of the system itself.

Unfortunately, there is still a lot of uncertainty when addressing these phenomena, with most of them being unknown. The lack of operational and experimental data and, consequently, difficulties arise in performing meaningful reliability analysis and deriving credible reliability figures only magnifies this uncertainty. This type of uncertainty is designated as phenomenological, which becomes particularly relevant when innovative or untested technologies are applied, eventually contributing significantly to the overall uncertainty related to the reliability assessment. (Burgazzi 2004)

This is even more relevant when natural circulation is concerned, due to the small engaged driving forces and the T-H phenomena affecting the system performance. With reference to natural circulation passive systems, the coolant flows predicted to be delivered by these systems can be subject to significant uncertainties, which in turn can lead to a significant uncertainty in the predicted T-H performance of the plant under normal and transient conditions. The overall uncertainty relating to T-H analysis can be binned into two broad categories:

1) uncertainties related to correlations, data and codes needed for the deterministic description and evaluation of the system (i.e., assessment by T-H code), and
2) uncertainties related to natural circulation performance itself.

With reference to the former class, uncertainties may have different origins ranging from the approximation of the models characterizing any physical phenomena, to the approximation of the numerical solutions, to the lack of precision of the values adopted for boundary and initial conditions, and to the parameters that are the input to the phenomenological models, in addition to the analyzer effect for the numerical simulation of the plant (as for instance the

nodalization of the plant). The amount of uncertainty that affects a calculation strongly depends upon the involved area in the technology and upon the sophistication of the adopted models and modeling techniques. This research seeks to eliminate some of that uncertainty by increasing the confidence in the output of the best-estimate T-H codes.

1.4 Research Hypothesis

A CFD code is used to model the primary natural circulation loop of a proposed SMR for comparison to experimental data and best-estimate T-H code results. Recent advances in CFD code modeling capabilities make them attractive surrogates to the current conservative approach of coupled best-estimate thermal hydraulic codes and uncertainty evaluations. The results of the CFD analysis are benchmarked against the experimental test results of a 1:3 length, 1:254 volume, full pressure and full temperature scale SMR during steady-state power operations and during a depressurization transient. A comparative evaluation of the experimental data, the thermal hydraulic code results and the CFD code results provides an opportunity to validate the best-estimate thermal hydraulic code's treatment of a natural circulation loop and provide insights into expanded use of the CFD code in future designs and operations. Additionally, a sensitivity analysis is conducted to determine those physical phenomena most impactful on operations of the proposed reactor's natural circulation loop. The combination of the comparative evaluation and sensitivity analysis provides the resources for increased confidence in model

developments for natural circulation loops and provides for reliability improvements of the thermal hydraulic code.

1.5 Significance of Research

According to the information provided by the “Power Reactor Information System” of the IAEA, today 436 nuclear power reactors are in operation in the world providing a total installed electricity capacity of 371 giga-watts, five nuclear reactors are in long term shutdown and 62 units are under construction. (IAEA-PRIS 2012) This installed capacity is a direct reaction to the worldwide energy demand increase and projected 40% rise over the next three decades. The use of advanced evolutionary and innovative nuclear power plants must play a substantial role in the environmental and economic balance of producing energy in a safe and stable fashion.

Design simplifications and increased design margins have led to the inclusion of some advanced reactors, whose normal and transient operating systems, depend entirely on the use of natural circulation. As stated earlier, these reactors rely on natural circulation to remove core power during normal operating conditions and for removal of decay heat in a transient condition, providing for an increased level of safety reliability.

The renewed interest in natural circulation is a consequence of the above, in combination with, the potential for cost savings from increased use of natural circulation systems in plant designs. Relevant experiments directed to the characterization of natural circulation have been carried out in the past because of the importance of the related mechanisms for the safety of existing reactors.

Similarly, T-H codes have been validated through the comparison of predicted results and experimental data. The quality of recorded experimental data and the precision level of the available system codes, or the expected uncertainty in these predictions, are generally evaluated as satisfactory for the needs of the current reactors.

However, the demand posed by the more extensive use of the natural circulation in the design of evolutionary and innovative water cooled reactors require a re-evaluation of the code capabilities in comparison to the experimental data while considering the new phenomena and conditions involved. Additionally, there are no acceptable methodologies for incorporating the passive systems' reliability into the overall risk of these new designs. This research is a part of the re-evaluation effort.

CHAPTER 2

REVIEW OF LITERATURE

2.1 INTRODUCTION TO NATURAL CIRCULATION

The complex set of physical phenomena that occur in a gravity environment when a geometrically distinct heat sink and heat source are connected by a fluid flow path can be identified as natural circulation. No external sources of mechanical energy for the fluid motion are involved when natural circulation is established. The above definition includes the situations of a heater immersed into a fluid, of an in-surge of hot fluid into a pool of cold liquid, and of a heat source and sink (e.g. heater and cooler) consisting of separated mechanical components connected by piping and situated at different gravity elevations. Natural circulation also drives the occurrence of stratification in horizontal pipes. (IAEA-TECDOC-1474 2005)

Natural circulation will occur, in the absence of pumped flow, whenever buoyant forces caused by differences in loop fluid densities are sufficient to overcome the flow resistance of loop components including steam generators (SGs), primary coolant pumps, and pipe friction. The fluid density differences occur as a result of heating fluid in the core region, causing the liquid become less dense, and cooling fluid in the SGs, causing the fluid to become denser.

The buoyant forces resulting from those density differences cause fluid to circulate through the primary loops, providing a means of removing the core decay heat.

Natural circulation flow is driven by temperature induced density gradients, enhanced by a thermal center elevation difference between a hot core and a cold SG region in the primary loop. This density gradient produces a buoyancy effect that drives the natural circulation flow. Thus, single-phase natural circulation is the flow of an essentially sub-cooled primary liquid driven by liquid density differences within the primary loop.

Two-phase natural circulation is normally defined as the continuous flow of fluid and vapor. In this mode of natural circulation, vapor generated in the core enters the hot leg and flows along with the saturated liquid to the SG, where at least some of the vapor is condensed. Hence, density gradients are affected in two-phase mode not only by temperature differences, but also by the voids in the primary loop. In both single-phase and two-phase natural circulation, the mass flow rate is the most important heat removal parameter. A more detailed technical analysis of natural circulation is found in Chapter 3.

It appears the commercial utilization of natural circulation systems as heat transport devices began in the late 1800s. First large-scale use of these systems appears to have been in the automobile industry to cool the engine block. With the advent of internal combustion engines of high compression ratio, their use in the automobile industry ceased practically in the 1940s. However, natural circulation systems have found other applications in the chemical and power

generation industries. Thermo-syphon reboilers are extensively used in the chemical process industries. Many fossil-fueled power plants of low and medium capacity use natural circulation boilers. While deploying natural circulation boilers, no allowance is given with regard to the thermal performance. At the same time, however, natural circulation boilers have less maintenance and operating cost compared to assisted circulation (forced circulation) boilers. Due to this, it is not uncommon for plants with ratings greater than 900 mega-watt electric (MWe) to deploy two to three natural circulation boilers as opposed to forced circulation models. (IAEA-TECDOC-1474 2005)

In the current generation of nuclear plants, the natural circulation core power removal capability is exploited for accident situations to demonstrate the inherent safety features of the plant. Natural circulation is also occurring during various phases of the refueling. In reference to existing light water reactors (LWRs), the consideration of natural circulation is most clearly recognizable in the design of the layout of the primary coolant loop. The core is located at a lower elevation with respect to the SGs and the feedwater (FW) inlet location, in the cases of pressurized and boiling water reactors (PWR and BWR), respectively. In all of the adopted geometrical configurations, natural circulation allows the removal of the decay heat produced by the core, should the forced circulation driven by centrifugal pumps become unavailable. Furthermore, natural circulation is the working mode for the secondary side of most SGs in existing pressurized heavy and LWRs. It is essential as well for the core cooling in the unlikely event of loss of primary coolant.

In future generation of nuclear plants, natural circulation is planned to be used for ensuring the nominal operating conditions and for achieving safe cooling following accidents in a wider spectrum than foreseen for current generation reactors.

2.2 Natural Circulation in Transient Conditions

Many advanced reactors make use of passive safety systems based entirely on natural circulation for the removal of the decay power in transient conditions. For example, if the normal heat sink is not available, the decay heat can be removed by using a passive connection between the primary system and heat exchangers in PWRs. (Mascari et al. 2010)

For example, the Advanced Plant (AP) 600 and 1000 designs, include a passive residual heat removal (PRHR) system consisting of a C-Tube type heat exchanger immersed in the in-containment refueling water storage tank (IRWST) and connected to one of the hot legs (HL). (IAEA-TECDOC-1391 2004) A PRHR from the core via SG to the atmosphere, considered in the Water Moderated, Water Cooled Energy Reactor (WWER) 1000 design, consists of heat exchangers cooled by atmospheric air, while the PRHR via SGs, considered in the WWER-640 design, consists of heat exchangers immersed in emergency heat removal tanks installed outside the containment. (Kurakov et al. 2002)

In the Advanced Chinese (AC) 600, the PRHR heat exchangers are cooled by atmospheric air (Gou et al. 2009) and in the System Integrated Modular Advanced Reactor (SMART) the PRHR heat exchangers are submerged in an in-containment refueling water tank. (Lee and Kim 2008) The

International Reactor Innovative and Secure (IRIS) design includes a passive emergency heat removal system (EHRS) consisting of a heat exchanger immersed in the refueling water storage tank (RWST). The EHRS is connected to a separate SG feed and steam line, and the RWST is installed outside the containment structure. (Carelli et al. 2004)

In the advanced BWR designs the core water evaporates, removing the core decay heat, and condenses in a heat exchanger placed in a pool. Then the condensate comes back to the core. (Hicken and Jaegers 2002) For example, the Siede Wasser Reaktor (SWR) 1000 MWe design has emergency condensers immersed in a core flooding pool and connected to the core, while the ESBWR design uses isolation condensers immersed in external pools. (IAEA-TECDOC-1474 2005)

2.3 Natural Circulation in Steady-State Conditions

The designs of some advanced reactors rely on natural circulation for the removing of the core power during normal steady-state operation. Examples of these reactors are the CAREM, a natural circulation based PWR being developed in Argentina, the ESBWR, and the Multi-Application Small Light Water Reactor (MASLWR).

The CAREM nuclear power plant design is based on a light water integrated reactor. The entire primary system, core, SGs, primary coolant and steam dome, is contained inside a single pressure vessel. For low power modes, below 150 MWe, the flow rate in the reactor primary systems is achieved by natural circulation. Coolant enters the core from the lower plenum. After it's

heated the coolant exits the core and flows up through the riser to the upper dome. In the upper part, coolant leaves the riser through lateral windows to the external region. Then it flows down through modular SGs, decreasing its enthalpy. Finally, the coolant exits the SGs and flows down through the downcomer to the lower plenum, closing the circuit. The driving forces obtained by the differences in the density along the circuit are balanced by the friction and form losses, producing the adequate flow rate in the core. Reactor coolant natural circulation is produced by the location of the SGs above the core. (IAEA-TECDOC-1624 (2009)

The ESBWR relies on natural circulation and proven passive systems to improve safety, economics, and performance. In the ESBWR design concept, safety improvements are accomplished by eliminating the recirculation pump, thus relying on natural circulation cooling. The coolant is circulated by natural circulation as a result of the density difference between the high void, two-phase fluid in the chimney and the exterior single-phase liquid in the downcomer. The tall chimney not only enhances the natural circulation flow, but also ensures the ample time for core exposure before the emergency core cooling system (ECCS) is activated. Likewise, the emergency core cooling and containment cooling systems do not have an active pump injecting flows and the cooling flows are driven by pressure differences. Large volumes of suppression pool liquid functions not only as a primary heat sink during the initial blow down, but also as coolant inventory to prevent the core from becoming exposed.

By relying on natural circulation at operating pressures and increased chimney height, the ESBWR has enhanced natural circulation flow inside the vessel. The driving head of core flow is proportional to the core and chimney height and void fraction inside the downcomer shroud. The ESBWR design features results in an average core flow per bundle over three times greater than that of a conventional BWR under natural circulation at similar bundle power. The use of natural circulation eliminates pumps, motors, controls, piping and many other components that could possibly fail. (Ishii 2004)

Of particular interest is the MASLWR. This design is a small modular integral PWR relying on natural circulation during both steady-state and transient operation. Because MASLWR uses natural circulation for primary loop flow, reactor coolant pumps are not needed. In this regard, its primary flow loop is quite simple as illustrated in Figure 2.1. (Modro et al. 2003)

The long vertical tube in the center of the reactor vessel is called the riser and functions like a chimney to enhance the driving head of the natural circulation flow. Starting from the bottom of the riser, fluid enters the core, which is located in a shroud connected to the riser entrance. While the fluid travels through the core, it is heated and rises by buoyancy through the riser. Hot fluid in the surrounding annulus, outside the riser is cooled by convective heat transfer to a helical coil SG. The fluid inside the tubes is at a lower pressure, hence boiling occurs inside the tubes to generate superheated steam. The steam produced within the tube side of this coil travels on to the turbine generator set where it is used to produce electrical power. The cooled primary fluid in the

annulus is negatively buoyant and descends to the bottom of the vessel and the inlet of the core thereby completing its loop.

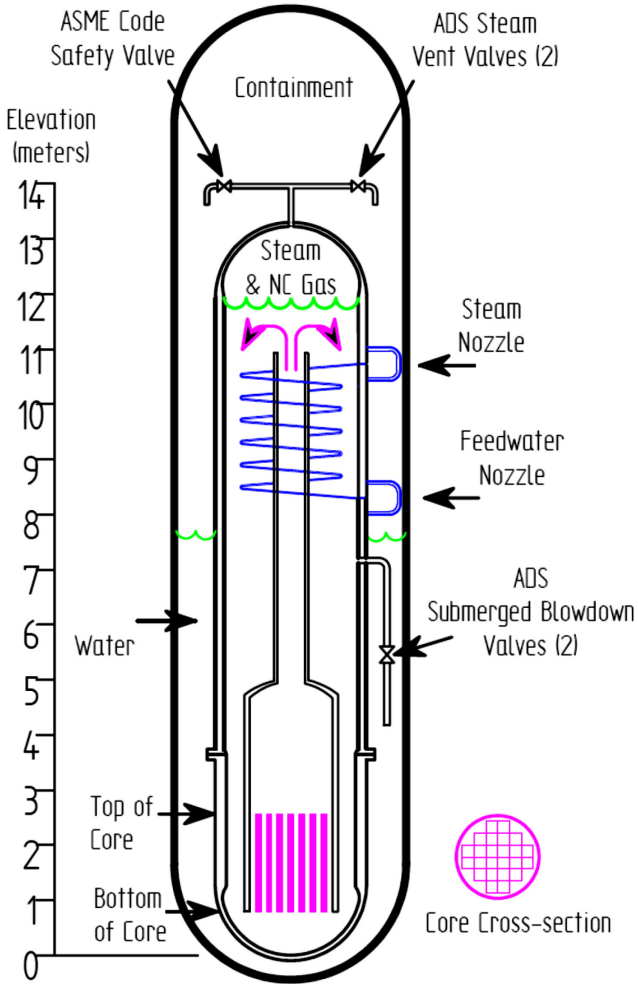

Figure 2.1. Schematic of MASLWR Primary Flow Loop (Modro et al. 2003)

2.4 Single and Two-Phase Fluid Natural Circulation Experimentation

In the development process of these new reactors, the analysis of single and two-phase fluid natural circulation in complex systems under steady state and transient conditions is crucial for the understanding of the physical and operational phenomena typical of these advanced designs. The use of experimental facilities is fundamental in order to characterize the T-Hs of these

phenomena and to develop an experimental database useful for the validation of the T-H computational tools necessary for the operation, design and safety analyses of these designs.

Because of the expense of conducting full-scale integral system tests, much of the thermal hydraulic testing for advanced reactor designs is conducted in “reduced-scale” integral system test facilities. The design of such facilities requires performing a thorough thermal hydraulic scaling analysis. The general objective of a scaling analysis is to obtain the physical dimensions and operating conditions of a reduced scale test facility capable of simulating the important flow and heat transfer behavior of the system under investigation.

To develop a properly scaled test facility, the following objectives must be met for each operational mode of interest. The thermal hydraulic processes that should be modeled must be identified, and the experimental criteria that should be preserved between the test facility and the full-scale prototype must be identified. Priorities for preserving the criteria are established because all of the criteria cannot be simultaneously preserved in a reduced scale facility. The specifications for the test facility design are established based on satisfying the most important similarity criteria, and biases due to scaling distortions can then be quantified. Lastly, the critical attributes of the test facility that must be preserved to meet quality assurance requirements must be identified. (IAEA-TECDOC-1474 2005)

Several scaled test facilities are currently in use worldwide. Most of the organizations responsible for the facilities described above are currently

participating in the IAEA Coordinated Research Project (CRP) on natural circulation phenomena, modeling and reliability of passive systems that utilize natural circulation. These facilities are representative of the broad spectrum of ongoing work in the area of natural circulation and passive system testing. A listing of current integral scaled test facilities with the major testing objectives is summarized in Table 2.1. (IAEA-TECDOC-1474 2005)

Table 2.1. Summary of Integral Scaled Test Facilities

Test Facility	*Major Testing Objectives*
CNEA Argentina	Study the dynamics of CAREM by means of power imbalance, with and without active control, and to validate T-H codes
ITL, BARC India	Simulate a variety of natural circulation phenomena in an advanced heavy water reactor (AHWR) design
LSTF Japan	Simulate the Tsuruga-2, a four loop 1100 MWe PWR during steady-state natural circulation
PANDA Switzerland	Full-height test facility for full capabilities simulation of the ESBWR
APEX-1000 USA	Low-pressure integral system test facility used for certification testing for the Westinghouse AP1000
OSU-MASLWR USA	Examine natural circulation phenomena of importance to integral reactors such as IRIS, CAREM, SMART and MASLWR
PUMA USA	Low-pressure test facility to simulate BWR instabilities at low pressure and low flow

It should also be noted that a significant amount of natural circulation and passive safety system data has been obtained in simple loop experiments and separate effects tests capable of providing detailed information under well-known

and carefully controlled system conditions. The simple loop experiments of the Bhabha Atomic Research Centre (BARC) are an excellent example.

2.5 THERMAL-HYDRAULIC COMPUTATIONAL METHODS

In order to analyze the T-H behavior of LWRs, the NRC developed and maintained four main codes: RAMONA, RELAP5, TRAC-B and TRAC-P. (Boyack and Ward 2000) In the last five years the NRC developed an advanced best estimate T-H system code named TRAC/RELAP Advanced Computational Engine (TRACE) to perform best estimate analysis for LWR designs. (TRACE V5.0 2008) Different analyses using the TRACE code have been applied to various types of reactor designs.

A TRACE model of the Almaraz nuclear power plant was used to study a loss of RHRS at mid-loop operation. (Queral, Gonzalez and Exposito 2008) A TRACE model of the Maanshan PWR was used to evaluate its effectiveness by simulating a turbine trip and load reduction transients and comparing the results with Maanshan data. (Wang et al. 2009) A TRACE model of ROSA/LSTF test facility was recently used to simulate a RPV upper head small break loss of coolant accident (SBLOCA) test. (Freixa and Manera 2010) Furthermore, the analysis of an inadvertent actuation of a submerged automatic depressurization system (ADS) valve, performed in the Oregon State University (OSU) MASLWR test facility, was conducted using TRACE, RELAP5/Mod3.3, and RELAP5-3D code. (Pottorf, Mascari and Woods 2009)

As expected, the results of the best-estimate code TRACE closely resembled the experimental data from the test facilities and operating reactors. It

should be noted, however, that these models, vice the last mentioned test facility, made wide use of active systems in their execution and the results only served to validate an already accepted combination of legacy codes in the newly developed TRACE.

Most recently, an assessment and validation process of the TRACE code was conducted for comparison to the natural circulation database developed in the OSU-MASLWR test facility. This facility was constructed at OSU under a U.S. Department of Energy grant in order to examine the natural circulation phenomena of importance to the MASLWR reactor design. Test series have been conducted at this facility in order to assess the behavior of the MASLWR concept in both normal and transient operation and to assess the passive safety systems under transient conditions.

In particular a series of tests investigated the primary system flow rates and secondary side steam superheat, used to control the facility, for a variety of core power levels and FW flow rates. More specifically, this analysis focused on an evaluation of the code's capability in predicting natural circulation phenomena and heat exchange from primary to secondary side by helical SGs in superheated condition and to evaluate the fidelity of various methods to model the OSU-MASLWR in TRACE along with a sensitivity analysis.

The analyses of the calculated data showed that the phenomena of interest of the OSU-MASLWR are predicted by the code to a fairly consistent degree, with some deviations occurring in the core inlet and outlet temperature

profiles and various coolant flow rate deviations at lower power settings. Figures 2.2 and 2.3 highlight these deviations. (Mascari et al. 2010)

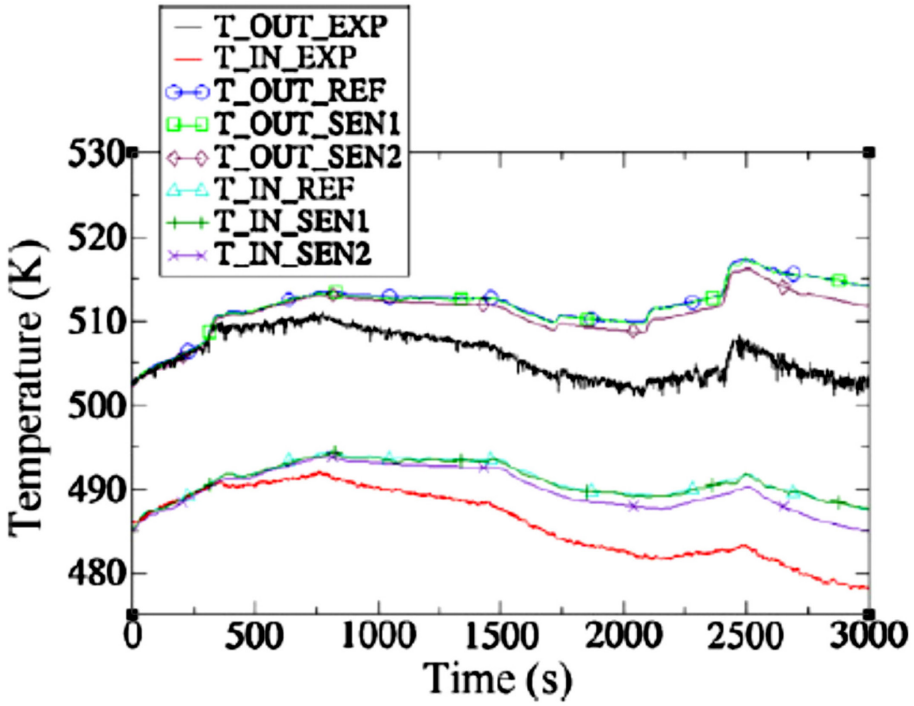

Figure 2.2. Coolant Temperature at the Core Inlet and Outlet

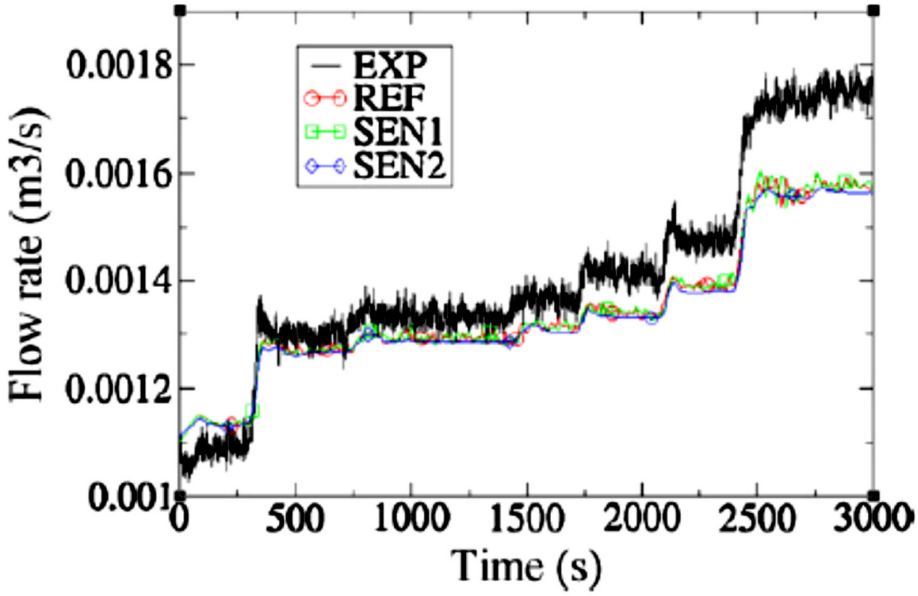

Figure 2.3. Primary Volumetric Flow Rate

2.6 COMPUTATIONAL FLUID DYNAMICS METHODS

With the advent of fast, digital computers in the late 1960s, it became possible to attempt the numerical solution of the Navier-Stokes equations. Initially the codes were highly “author” dependent, and most codes were merely special-purpose codes for specific university, laboratory or industry tasks. In the mid-1980s, the Concentration, Heat, and Momentum (CHAM) organization adopted a single code policy which led to the development of a new code system, PHOENICS. This first, genuinely multi-purpose CFD code was the template for all that followed.

PHOENICS was the first modular designed code. It featured a central solver, a pre-processor for mesh generation, a post-processor for graphical display, and modules designed to “link in” as needed. Most current CFD vendors follow this same hierarchy in codes such as FLUENT, CFX, STAR-CD and COMSOL.

As stated previously, the need to use CFD arises because many traditional reactor systems and containment T-H codes are based on a network of 1-D volumes and correlation databases that could lead to artificial confidence in the passive systems. It is obvious, however, that the flow patterns in most, if not all, components in the core of a nuclear power plant, are strongly 3-D. Natural circulation and complex channel flow and mixing are also essentially 3-D in nature. Representing such complex flows through the use of existing best-estimate T-H codes may not fully and accurately portray the actual physical phenomena involved. The T-H database correlations offer confidence in these

analyses, but data on the exchange of mass, momentum and energy between phases for 3-D flow are extremely limited.

The use of CFD to study the complex 3-D flow associated with natural circulation could offer a higher degree of quality by extending the computational results, and in turn, an increased confidence in the reliability of passive systems. This comes at a cost however, as the physical models utilized in the existing T-H codes are well established provided they are utilized with their acceptable ranges. The physical models required for CFD will require significant effort in both design and computational time to replicate real-time simulations for steady-state and transient operations.

In the mid-2000s, the IAEA formed three writing groups to perform a series of tasks to evaluate areas where CFD could lead to increases in passive system reliability. The results of this initiative highlighted several areas where the use of CFD codes could lead to increased benefits in terms of better understanding, quantification and improved reliability estimations. These include boron dilution, mixing and thermal fatigue, hot leg temperatures, pipe breaks, lower plenum flows, hydrogen accumulation, flow-induced vibrations and natural circulation. Consequently, several CFD studies were conducted to highlight the use of passive systems in both single and two-phase natural circulation loops.

An extensive analysis of unstable single-phase natural circulation was conducted by comparing a 1-D code to a CFD code for a very simple natural circulation loop. The analysis concluded the 1-D models provide a relatively accurate prediction of steady-state natural circulation, but begin to diverge when

evaluating wall friction, especially in the region of transition between laminar and turbulent flow. Additionally, the analysis indicated the CFD model provided improved modeling capabilities, specifically in the use of friction and heat transfer closure laws, mostly applicable in steady forced flow while dealing with oscillating natural circulation flow. The analysis also concluded a compromise must be reached between the improved capabilities of the CFD model and the consequent increase in computational cost of the related simulations. (Pilkhwal, Ambrosini and Forgione 2007)

Next, a coolant transient benchmark analysis was completed on the Belgian Vodo-Vodyanoi Energetichesky Reactor “water water power reactor” (VVER) 1000. The analysis shows that the CFD code results are in reasonable agreement for each measured parameter, with some exceptions for the core inlet velocity. The CFD simulations predicted the flow rotation qualitatively well, but their formation is characterized by more diffusion than in the measurements. The analysis concluded that the observed differences depend on the modeling assumptions, and on the degree of compliance with the best practice guidelines. Lastly, the analysis demonstrated that CFD codes still have limitations, but the developmental work for single-phase mixing is promising. (Kolev and Spasov 2010)

A more rigorous analysis of the coupling of a CFD code to the initial and boundary conditions of a best-estimate T-H code was performed. Verification of the coupled CFD and T-H code was first conducted on the basis of a simple test case consisting of a straight pipe filled with liquid subject to a sudden

acceleration. As a second validation step, measurements using advanced instrumentation were performed in a simple, specially constructed test facility consisting of two loops connected by a double T-junction. Comparisons of the experimental measurements were made with calculation results obtained using the coupled codes, as well as the individual codes in stand-alone mode. Although coupling of the codes provided for only small increases in the results, the stand-alone comparative assessment of the results showed that the CFD code more accurately represented the experimental data. (Bertolotto et al, 2009)

Most recently, the NRC conducted a CFD analysis of natural circulation flow in a PWR loop under severe accident conditions. The CFD model included the primary side of a SG, the hot leg, a portion of the pressurizer (PZR) surge line and a simplified reactor pressure vessel (RPV) upper plenum along with a section of the vessel itself. The FLUENT 6.3 CFD code was used for the analysis. A set of data at $1/7^{th}$ scale natural circulation flows were collected, and this data was used to benchmark the CFD predictions. The results of the analysis qualitatively show all of the flow features observed experimentally in the hot leg and SG regions. A sensitivity study was also conducted to provide feedback on variations to several key modeling parameters. The study recommended several areas where T-H code modeling technique could be improved, including average normalized temperatures in the SG tubes and surge line mass flow rates. (NUREG/CR-1922 2010)

CHAPTER 3

THEORETICAL DISCUSSION AND ANALYSIS

3.1 NATURAL CIRCULATION

As briefly discussed in Chapter 2, natural circulation is a complex set of T-H phenomena that occur in a gravity environment when geometrically or materially distinct heat sinks and heat sources are connected by a fluid. No external sources of mechanical energy for the fluid motion are involved when natural circulation is established (IAEA-TECDOC-1624 2009).

More specifically, a heat sink, a heat source and the pipes connecting them form the essential hardware of a natural circulation system. The pipes are connected to the sink and source in such a way that it forms a continuous circulation path. When the flow path is filled with a working fluid, a natural circulation system is ready where fluid circulation can set in automatically following the activation of the heat source under the influence of a driving force, gravity. With both the sink and source conditions held constant, a steady circulation is achieved. The fluid circulation is the result of buoyancy forces, which in turn is the result of the density differences thermally induced by the transport of heat from the source to the sink and the elevation difference between the two. In most cases, the heat sink is located above the source to promote the circulation. Such loops, in which the fluid circulation is caused by the thermally

induced buoyancy force, are also known as natural circulation loops or natural convection loops.

The importance of buoyancy forces in a convection flow can be measured by the ratio of the Grashof and Reynolds numbers. This relationship is shown in Eqn. 3.1:

$$\frac{Gr}{Re^2} = \frac{g\beta\Delta TL}{v^2} \tag{3.1}$$

where Gr ≡ Grashof number

Re ≡ Reynolds number

g ≡ acceleration due to Earth's gravity

β ≡ volumetric thermal expansion coefficient

ΔT ≡ temperature difference

L ≡ length

v ≡ kinematic viscosity

Strong buoyancy force contributions are present when this ratio approaches or exceeds unity. The Reynolds number represents the ratio between inertial and viscous forces. At low Reynolds numbers, viscous forces dominate and tend to damp out all disturbances, which leads to laminar flow. At high Reynolds numbers, the damping in the system is very low giving small disturbances the possibility to grow by nonlinear interactions. If the Reynolds number is high enough, the fluid flow field eventually ends up in the chaotic state of turbulence.

In pure natural circulation, the strength of the buoyancy induced flow is measured by the Rayleigh number as shown in Eqn. 3.2:

$$Ra = \frac{g\beta\Delta TL^3}{v\alpha} \tag{3.2}$$

where Ra ≡ Rayleigh number

α ≡ thermal diffusivity

$$\alpha = \frac{k}{\rho c_p} \tag{3.3}$$

where k ≡ thermal conductivity

ρ ≡ density

c_p ≡ specific heat

Rayleigh numbers less than 10^8 indicate a buoyancy induced laminar flow, with transition to turbulence occurring over the range of $10^8 < Ra < 10^{10}$

Fluid density differences can be created by changes in temperature or by changes in phase. The mass flow rate through the loop is limited by the sum of the resistances in the components and interconnecting piping. This leads to a disadvantage, as described below.

The primary function of a natural circulation loop is to transport heat from a source to a sink. Several advantages and disadvantages are present in the use of natural circulation and are listed in Table 3.1.

Table 3.1. Advantages and Disadvantages to Natural Circulation

Advantages	*Disadvantages*
Reduced cost through simplicity	Lower driving head
Pumps Eliminated	Lower max power per channel
Possibility of improved flow distribution	Potential instabilities
Large thermal inertia	Low critical heat flux

The primary advantage of a natural circulation system is simplicity, in that the heat transport function is achieved without the aid of any fluid moving pumps or other components. Conversely, a low driving head is the primary disadvantage of natural circulation systems. An increase in the vertical spacing between heat

sink and source, or a decrease in fluid resistance is required to increase the mass flow rate at a fixed temperature differential.

3.2 Primary Flow Thermal Hydraulic Analysis

In the chapters to follow a complex convective heat transfer problem is presented along with two computational solution techniques whose results are compared to experimental data. In order to develop a suitable set of governing equations along with correct initial and boundary conditions for their solutions required the joining of two classical areas of applied mechanics: fluid mechanics and heat transfer. This process develops the general forms of the transport equations for single-phase flow in addition to many simplifying assumptions.

The basic assumption is that the working fluid and reactor components are a continuous medium. Temperature, velocity, density and pressure, commonly referred to as field variables, can be discretely calculated at each point in the fluid and surrounding reactor geometry. Differential equations of conservation of mass, momentum and energy are developed and two solution techniques are used to describe the values mentioned above. There are two types of alternative techniques used to express the conservation laws in analytic form. In the first technique, the field variables are evaluated at a fixed spatial location. This technique is called the Eulerian method and equations, primarily focusing of fluid flows. The Lagrangian method and equations focuses on a specific set of fixed material particles, thereby lending it to studies involving solid bodies. The Eulerian method is presented here in the derivation of the conservation equations.

For a continuous medium, the local instantaneous transport equation can be verbally stated as:

{unsteady term} + {convection term} = {diffusion term} + {source term}

Mathematically, the transport equation is shown in Eqn. 3.4: (Todreas and Kazimi 1990)

$$\frac{\partial}{\partial t}[\rho c] + \nabla \cdot [\rho c \vec{v}] = \nabla \cdot \vec{J} + \rho \phi \tag{3.4}$$

where ρ ≡ density

c ≡ specific value of a given extensive property per unit mass

$\vec{v}$ ≡ velocity

$\vec{J}$ ≡ generalized surface source or sink

ϕ ≡ rate of introduction of c per unit mass within the volume

3.2.1 Conservation of Mass

The law of conservation of mass states that the total time rate of change of mass in a fixed region, otherwise known as a control volume (CV) is zero, and can be verbally stated as:

{rate of change of mass in CV} =
{mass flow rate into CV} – {mass flow rate out of CV}

Denoting the three components of the velocity vector $\vec{v}$, the mass equation is expanded in Eqn. 3.5:

$$\frac{\partial \rho}{\partial t} = -\frac{\partial}{\partial x}(\rho v_x) - \frac{\partial}{\partial y}(\rho v_y) - \frac{\partial}{\partial z}(\rho v_z) \tag{3.5}$$

where v_i ≡ x, y and z components of the velocity vector

After rearranging and converting to vector notation, the Eulerian form of the mass conservation equation is:

$$\frac{\partial \rho}{\partial t} + \nabla \cdot (\rho \vec{v}) = 0 \tag{3.6}$$

When the temperature variations in a flow are small, a single-phase fluid can often be assumed incompressible; that is, ρ is constant or nearly constant. This is the case for all liquids under normal conditions and also for gases at low velocities. For constant density, Eqn. 3.6 simplifies to:

$$\nabla \cdot \vec{v} = 0 \tag{3.7}$$

3.2.2 Conservation of Momentum

The law of conservation of linear momentum (or Newton's second law of motion) states that the total time rate of change of linear momentum is equal to the sum of external forces acting on the region, and can be verbally stated as:

{rate of change of momentum in CV} = {momentum flow rate into CV} – {momentum flow rate out of CV} + {net external force on CV}

Gravity, electrical, and/or magnetic body forces, along with three surface forces on each face must be accounted for in evaluating the net external force on the CV. The three surface forces consist of a normal force and two tangential forces that act to elongate and rotate the fluid respectively. Expanding the components of conservation of momentum, as done by Todreas and Kazimi, in the *x*-direction is:

$$\frac{\partial}{\partial t}(\rho v_x) + \frac{\partial}{\partial x}(\rho v_x v_x) + \frac{\partial}{\partial y}(\rho v_x v_y) + \frac{\partial}{\partial z}(\rho v_x v_z) = \frac{\partial \sigma_x}{\partial x} + \frac{\partial \tau_{yx}}{\partial y} + \frac{\partial \tau_{zx}}{\partial z} + \rho f_x \tag{3.8}$$

where σ ≡ normal stress component

τ ≡ shear stress component

f ≡ body force per unit mass

By expanding the normal stress into a pressure component and an internal friction component, as shown in Eqns. 3.9, the 3-D equation of the conservation of momentum in vector form is shown in Eqn. 3.10:

$$\sigma_x = -p + \tau_{xx}$$

$$\sigma_y = -p + \tau_{yy} \tag{3.9}$$

$$\sigma_z = -p + \tau_{zz}$$

$$\frac{\partial}{\partial t}\rho\vec{v} + \nabla \cdot \rho\vec{v}\vec{v} = -\nabla p + \nabla \cdot \bar{\bar{\tau}} + \rho\vec{f} \tag{3.10}$$

where p ≡ pressure

$\bar{\bar{\tau}}$ ≡ shear stress tensor

$$\bar{\bar{\tau}} = \begin{pmatrix} \tau_{xx} & \tau_{xy} & \tau_{xz} \\ \tau_{yx} & \tau_{yy} & \tau_{yz} \\ \tau_{zx} & \tau_{zy} & \tau_{zz} \end{pmatrix} \tag{3.11}$$

Assuming the fluid follows the Newtonian laws of viscosity, and with further development of the internal friction terms, a vector form of the Navier-Stokes equation for momentum balance is given as:

$$\frac{\partial}{\partial t}\rho\vec{v} + \nabla \cdot \rho\vec{v}\vec{v} = -\nabla p + \nabla \mathrm{x}[\mu\nabla \mathrm{x}\vec{v}] + \nabla\left[\frac{4}{3}\mu\nabla \cdot \vec{v}\right] + \rho\vec{f} \tag{3.12}$$

where μ ≡ dynamic viscosity

For an incompressible fluid with constant density, as shown in Eqn. 3.7, and assuming a constant viscosity, the conservation of momentum balance equation is:

$$\rho\frac{\partial\vec{v}}{\partial t} + \rho\vec{v} \cdot \nabla\vec{v} = -\nabla p + \mu\nabla^2\vec{v} + \rho\vec{f} \tag{3.13}$$

A further simplification of Eqn. 3.13 occurs for flow that has negligible viscosity effects, or inviscid flow. In these situations the viscous terms are zeroed out and the resulting inviscid flow equation is:

$$\rho\frac{\partial\vec{v}}{\partial t} + \rho\vec{v} \cdot \nabla\vec{v} = -\nabla p + \rho\vec{f} \tag{3.14}$$

3.2.3 Conservation of Energy

The law of conservation of energy, or the First Law of Thermodynamics, states that the time rate of change of the total internal energy is equal to the sum of the rate of work done by applied forces and the change of heat content per unit time, and can be verbally stated as:

{rate of change of total internal energy in CV} = {rate of heat added to CV}
– {rate of work done} + {rate of energy flow into CV}
– {rate of energy flow out of CV}

Todreas and Kazimi present a straight forward development of the application of the conservation of energy through the evaluation of the stagnation energy, consisting of the internal energy and the kinetic energy. In vector form, this yields:

$$\frac{\partial}{\partial t}\rho u^o = -\nabla\cdot\rho u^o\vec{v} - \nabla\cdot\vec{q}'' + q''' - \nabla\cdot p\vec{v} + \nabla\cdot(\bar{\bar{\tau}}\cdot\vec{v}) + \vec{v}\cdot\rho\vec{f} \qquad (3.15)$$

where u^o ≡ stagnation energy

$\vec{q}''$ ≡ heat flux

q''' ≡ volumetric heat generation rate

The first term on the right represents the net change in the internal energy per unit time due to convection, the second term is the net heat transport rate by conduction and radiation (if present) and the third term is the internal heat generation rate. The fourth, fifth and sixth terms are the work done on the fluid by the pressure, viscous forces and body forces, respectively per unit time.

In a similar fashion, the conservation of energy equation can be formulated in terms of temperature and is shown in Eqn. 3.16:

$$\rho c_p\left(\frac{\partial T}{\partial t} + (\vec{v}\cdot\nabla)\right)T = -(\nabla\cdot\vec{q}'') + \bar{\bar{\tau}}:\bar{\bar{S}} - \frac{T}{\rho}\frac{\partial\rho}{\partial T}\Big|_p\left(\frac{\partial p}{\partial t} + (\vec{v}\cdot\nabla)p\right) + q''' \qquad (3.16)$$

where c_p ≡ specific heat capacity at constant pressure

T ≡ absolute temperature

$\bar{\bar{s}}$ ≡ strain rate tensor

$$\bar{\bar{s}} = \frac{1}{2}(\nabla\vec{v} + (\nabla\vec{v})^T) \tag{3.17}$$

The operation ":" in Eqn. 3.16, denotes a contraction between tensors, sometimes referred to as the double dot product, and is defined in basic terms by Eqn. 3.18:

$$\bar{\bar{a}}:\bar{\bar{b}} = \sum_n \sum_m a_{nm} b_{nm} \tag{3.18}$$

3.2.4 APPROXIMATIONS

As mentioned earlier, in natural circulation, the basic driving force arises from a temperature variation. This temperature variation causes a difference in density, which then results in a buoyancy force due to the presence of a body force. For a gravitational field, the body force is equivalent to:

$$\vec{F} = \rho\vec{g} \tag{3.19}$$

where $\vec{F}$ ≡ force per unit volume

$\vec{g}$ ≡ gravitational acceleration

Accordingly, it is the variation of density with temperature that gives rise to the flow. The temperature field is linked with the flow, and all the preceding conservation equations are coupled through variations in the density. Therefore, these equations have to be solved simultaneously to determine the velocity, pressure, and temperature distributions in space and in time. Due to this complexity in the analysis of the flow, key simplifying approximations are generally made to solve natural circulation problems (Jaluria 1980).

Two of the most important among these are the Boussinesq and the boundary layer approximations. The Boussinesq approximation involves two aspects. As previously mentioned, for incompressible flow, the density variation in the conservation of mass equation is neglected. The derivation and discussion of Eqn. 3.7 provides details of this approximation.

Second, the density difference, which causes the flow, is approximated as a pure temperature effect (i.e., the effect of pressure on the density is neglected). The density varies with temperature according to the relationship:

$$\rho = \rho_0[1 - \beta(T - T_0)] \tag{3.20}$$

where ρ ≡ temperature corrected density

ρ_0 ≡ reference density

β ≡ coefficient of thermal expansion

T_0 ≡ reference temperature

These approximations are employed very extensively for natural circulation, but only as the density variation relates to the calculation of the body force. The density in all other situations is assumed to be that of the reference state (Reddy and Gartling 1994).

An important condition for the validity of these approximations is that $\beta(T - T_0) \ll 1$ (Jaluria 1980). Therefore, the approximations are valid for small temperature differences if the coefficient of thermal expansion is essentially unchanged. However, they are not valid near the density maximum of water at 4°C, where the coefficient is zero and changes sign as the temperature varies across this value (Gebhart 1979). Similarly, for large temperature differences

encountered in fire and combustion systems, these approximations are generally not applicable.

Another approximation made in the governing equations is the extensively employed boundary layer assumption. The basic concepts involved in using the boundary layer approximation in natural circulation are very similar to those in forced flow. The main difference is that the pressure in the region outside the boundary layer is hydrostatic instead of being the externally imposed pressure, as is the case in forced circulation. The velocity outside the layer is only the entrainment velocity due to the motion pressure and is not an imposed free stream velocity. However, the basic treatment and analysis are similar. It is assumed that the flow and the energy, or mass, transfer, from which it arises, are restricted predominantly to a thin region close to the surface. Several experimental studies have corroborated this assumption. As a consequence, the gradients along the surface are assumed to be much smaller than those normal to it (Reddy and Gartling 1994).

3.2.5 GOVERNING EQUATIONS

The conservation equations developed above can be expressed in terms of the velocity, pressure and temperature variables in vector form. The results are summarized below for isotropic, Newtonian, viscous, incompressible fluids with an included buoyancy force:

$$\nabla \cdot \vec{v} = 0 \tag{3.21}$$

$$\rho_0 \left(\frac{\partial \vec{v}}{\partial t} + \vec{v} \cdot \nabla \vec{v}\right) = -\nabla p + \mu \nabla \cdot [(\nabla \vec{v}) + (\nabla \vec{v})^T] + \rho_0 \vec{f} + \rho_0 \vec{g} \beta (T - T_0) \tag{3.22}$$

$$\rho_0 C_v \left(\frac{\partial T}{\partial t} + \vec{v} \cdot \nabla T\right) = \nabla \cdot (k \nabla T) + \bar{\bar{\tau}} : \bar{\bar{s}} + q''' \tag{3.23}$$

Eqns. 3.21 – 3.23 are valid for a fluid region. In the presence of a solid region, annotated with an *s*, the fluid velocity is zero and Eqns. 3.21 and 3.22 are not relevant. The energy equation for the solid region is given by:

$$\rho_s C_s \frac{\partial T}{\partial t} = \nabla \cdot (k_s \nabla T) + q_s''' \tag{3.24}$$

Eqn. 3.24 assumes the solid region is stationary with respect to the coordinate frame, such that the nonlinear part of Eqn. 3.23 need not be considered. As such, Eqns. 3.21 – 3.24 are the theoretical foundation of the thermal hydraulic analysis to follow.

3.2.6 Initial and Boundary Conditions

Suitable initial and boundary conditions are required to complete the description of Eqns. 3.21 – 3.24. For time dependent problems, a set of initial conditions are necessary for the dependent variables. Very often these conditions consist of a solid body at a uniform temperature and a quiescent fluid at a uniform temperature and hydrostatic pressure. Reddy and Gartling propose a second possibility in an initiation of transient motion from an established steady state flow and temperature field. In each case, the dependent variables must be known for all values at the initial time step. They must also satisfy the basic conservation equations, such as the initial fluid velocity field must be divergence free.

Boundary conditions must describe both the fluid mechanics as well as other processes occurring within the volume of concern. From the fluid dynamic perspective, either the velocity components of the total surface stress or traction must be specified on the boundary of the fluid region. In general, boundary

conditions can be classified into two types: Dirichlet or essential boundary conditions and Neumann or natural boundary conditions. Dirichlet boundary conditions, when imposed on an ordinary or a partial differential equation, specify the values a solution needs to take on the boundary of the domain. Neumann boundary conditions, when likewise imposed on a differential equation, specify the values that the derivative of a solution is to take on the boundary of the domain. (Chung 2008) Neumann boundary conditions arise automatically from the finite element or finite volume formulations through integration by parts. This is not the case for finite difference methods. Neumann boundary conditions are common in heat transfer problems in that, for perfectly insulated domains, the derivative at the surface is zero.

Additionally, the Cauchy boundary condition is a “mixed” type of boundary condition that imposes both a Dirichlet and a Neumann boundary condition on a differential equation. These boundary conditions are required for a solution in which both the value of the function and the value of the derivative at a given initial or boundary point are required.

3.3 Finite element Analysis

In general, finite element methods (FEM) are versatile in applications to multi-dimensional complex and irregular geometries. FEM does so by carrying out a generalization of the classical variational and weighted residual methods. These are based on the idea that the solution of a differential equation can be represented as a linear combination of unknown parameters and appropriately selected functions in the entire domain of interest. The parameters are then

determined such that the differential equation is satisfied, often, in a weighted integral sense. The functions, commonly referred to as approximation functions, are selected such that they satisfy the boundary conditions of the problem.

Most complex engineering problems are defined in regions that are geometrically challenging, making them more difficult to generate the approximation functions that satisfy the different types of boundary conditions on the volume of interest. However, if this volume of interest can be subdivided into smaller more manageable subdomains, the approximation functions might be more easily obtained. Then the traditional variational or weighted residual methods can be used to solve the larger problem. This is the basic idea of the FEM approach. The given complex geometry is subdivided into smaller simple geometric shapes, called finite elements, for which it is possible to systematically generate the approximation functions needed for the solution. For a given differential equation, it is possible to develop different finite element approximations, depending on the choice of one of the aforementioned methods. While outside the scope of this research, Becher et al. and Burnett provide a detailed explanation of the theory and applications of FEM.

In general, Reddy and Gartling list the following steps as typical in applying FEM to a problem. These steps will be followed in Chapter 5 in the development of the test facility problem:

1. Discretation of the domain into a set of finite elements (mesh generation).
2. Weighted-integral or weak formulation of the differential equation to be analyzed
3. Development of the finite element model of the problem using its weighted-integral or weak form.

4. Assembly of finite elements to obtain the global system of algebraic equations.
5. Imposition of boundary conditions.
6. Solution of equations.
7. Post-computation of solution and quantities of interest.

While the detailed explanation of the theory of FEM is not included here, a more descriptive view of the weighted integral formulation of the differential equations is explored.

The type of finite element model depends on the weighted integral form used to generate the algebraic equations. Thus if the variational form, also known as the weak form, is chosen, the resulting model will be different from those obtained with a weighted residual form. The weak form of a differential equation is a weighted integral statement that is equivalent to both the governing differential equation as well as the associated natural boundary conditions. In the weighted residual form, the weight function can be any one of several choices.

The weak form exists for and second and higher order equations, because for such equations, it is possible to trade differentiation from the dependent unknown to the weight function and include the natural boundary condition into the weighted integral statement. These observations hold for a linear as well as for nonlinear geometries. (Chung 2008) For example, the Navier-Stokes equations governing the flow of a viscous incompressible fluid do not admit an associated quadratic functional; however, a weak form can be constructed. The methods utilized in this research rely on the weak form for their computational efforts. This idea will be explained in a subsequent chapter.

CHAPTER 4

COMPUTATIONAL METHODS

4.1 METHODOLOGY OVERVIEW

The basic methodology proposed for this research is to model, both in a T-Hs code, TRACE, and a commercially available multi-physics CFD code, COMSOL, a small modular pressurized LWR primary loop. The proposed concept relies on a natural circulation closed loop during both steady-state and transient operations together with integrated passive safety systems. The reactor, the MASLWR, has been tested at the OSU-MASLWR integral test facility, and the experimental data is available for a comparative evaluation with TRACE and COMSOL.

As stated earlier, this test facility was constructed at OSU under a U.S. Department of Energy grant in order to examine the natural circulation phenomena of importance to the MASLWR reactor design, which includes an integrated helical coil SG. A series of tests were conducted at this facility in order to assess the behavior of the MASLWR natural circulation loop and the passive safety systems in both steady-state and transient operations.

This research will model the natural circulation loop of the test facility in both TRACE and COMSOL and conduct numerous computer iterations to mirror the two highly instrumented test cases performed at the OSU-MASLWR facility. A comparative evaluation will be used to compare the results of the code output

to the experimental data to identify deviations and inaccuracies. Additionally, a sensitivity analysis will be performed on the COMSOL model to evaluate the effects on several phenomena and parameters relevant to natural circulation in a closed loop. These include, but are not limited to the heat transfer coefficient, critical heat flux, flow rates (both primary and FW loops), density, temperature and pressure changes. These parameters will be described later in detail.

4.2 Computational Code Overview

Advanced computing is a key component to the design, licensing and operation of nuclear power plants. The modern plants operate at a level of sophistication where a system's operation and response to changes cannot fully be represented by simple models. The NRC uses advanced codes to model and evaluate various plant specifics including reactor kinetics, severe accident progression, fuel behavior, time-dependent design-basis accidents, and thermal hydraulics. The code results support a risk-informed decision making process and ultimately improve the understanding of plant and component operation.

4.2.1 TRACE Overview

The NRC uses TRACE, a modernized T-Hs code, to consolidate and extend the capabilities of three legacy safety codes: RELAP, TRAC-P and TRAC-B. TRACE is supported by the symbolic nuclear analysis package (SNAP), which assists users in developing TRACE input decks and running the code.

TRACE has been designed to perform best-estimate analyses of loss-of-coolant accidents (LOCAs), operational transients, and other accident scenarios

in both PWRs and BWRs. It can also model phenomena occurring in experimental facilities designed to simulate transients in reactor systems. Models used include multi-dimensional two-phase flow, non-equilibrium thermodynamics, generalized heat transfer, level tracking and reactor kinetics. Automatic steady-state and dump/restart capabilities are also provided.

The partial differential equations that describe two-phase flow and heat transfer are solved using finite volume numerical methods. The heat-transfer equations are evaluated using a semi-implicit time-differencing technique. The fluid-dynamics equations in the spatial 1-D and 3-D components use, by default, a multi-step time-differencing procedure that allows the material Courant-limit condition to be exceeded. A more straightforward semi-implicit time-differencing method is also available. The finite difference equations for hydrodynamic phenomena form a system of coupled, nonlinear equations that are solved by the Newton-Raphson iteration method. The resulting linearized equations are solved by direct matrix inversion.

TRACE takes a component-based approach to modeling a reactor system. Each physical piece of equipment in a flow loop can be represented as some type of component, and each component can be further nodalized into some number of physical volumes or cells over which the fluid, conduction, and kinetics equations are averaged. The number of reactor components in the problem and the manner in which they are coupled is arbitrary. There is no built-in limit for the number of components or volumes that can be modeled; the size

of a problem is theoretically only limited by the available computer memory. (TRACE V5.0 2008)

TRACE can be executed in either steady-state of transient mode. The steady-state execution requires a zero rate of change of various parameters, at which point the run is terminated. Steady-state input models are generally not allowed to perform actions that would explicitly lead to changes in the time derivative terms in the basic equations. More specifically, at every fifth time-step, the maximum fractional change per second of seven key parameters, total pressure, liquid and steam velocities, steam volume fraction, liquid and steam temperatures and non-condensable gas pressure, over the entire TH model. Then TRACE requires that all seven maximum rate of change values be less than or equal to a user defined convergence criteria.

As a general rule, computational codes like TRACE are really only applicable within their assessment range. TRACE has been qualified to analyze the ESBWR design as well as conventional PWR and BWR large and small break LOCAs. The TRACE code is not appropriate for modeling situations in which transfer of momentum plays an important role at a localized level. For example, TRACE makes no attempt to capture, in detail, the fluid dynamics in a pipe branch or plenum, or flows in which the radial velocity profile across the pipe is not flat.

According to the TRACE User's Manual, the TRACE field equations have been derived assuming that viscous shear stresses are negligible (to a first-order approximation) and explicit turbulence modeling is not coupled to the

conservation equations (although turbulence effects can be accounted for with specialized engineering models for specific situations). Thus, it is suggested the TRACE code should not be employed to model those scenarios where the viscous stresses are comparable to, or larger than, the wall (and/or interfacial, if applicable) shear stresses, as is the case with natural circulation. For example, TRACE is incapable of modeling circulation patterns within a large open region, regardless of the choice of mesh size. Hence, the motivation to further understand these phenomena with a more robust CFD analysis is fully appreciated.

4.2.2 COMSOL OVERVIEW

COMSOL is a multi-physics modular interactive computer simulation for modeling and solving various scientific and engineering problems based on partial differential equations (PDEs). COMSOL uses proven finite element methods when solving these models. The code runs the finite element analysis together with adaptive meshing and error control using a variety of numerical solvers. The multi-physics coupling of various modules makes the code attractable for advanced engineering designs.

As stated in the COMSOL user's guide, the CFD module is the premier tool in the COMSOL product suite for sophisticated fluid flow simulations. Compressible as well as incompressible flows can be combined with advanced turbulence models and forced and natural convection. An important characteristic of the CFD module is its capability of precise multi-physics flow simulations such as conjugate heat transfer with non-isothermal flow, fluid-

structure interactions, non-Newtonian flow with viscous heating, and fluids with concentration-dependent viscosity. Porous media flow user interfaces allow for isotropic or anisotropic media, as well as automatically combined free flow and porous domains.

The CFD module's interfaces for homogeneous two-phase flow include a mixture model for fine particle suspensions and a bubbly flow model for macroscopic gas bubble flow. For interface tracking two-phase flow, formulations are provided using the level-set and phase-field methods.

An important feature of COMSOL is the ability to model large-scale problems, like the one proposed, and tune solver settings and use symmetry to reach a solution. Computational memory usage does not scale linearly, but rather as a polynomial. Therefore the model needs less than half the memory if a symmetric plane can cut the geometry size by half. To take full advantage of the symmetry, a proposed half or quarter geometry model will be utilized in the COMSOL evaluation. (COMSOL V4.2a 2008)

4.3 Numerical Techniques and Computing Resources

TRACE uses a finite volume method (FVM) compared to the FEM method explored in detail in Chapter 3. The FVM is a discretization method which is well suited for the numerical simulation of various types (elliptic, parabolic or hyperbolic, for instance) of conservation laws. It has been extensively used in several engineering fields, such as fluid dynamics, heat and mass transfer and nuclear engineering. Some of the important features of the finite volume method are similar to those of FEM. (Oden 1991) It may be used on arbitrary

geometries, using structured or unstructured meshes, and it leads to robust schemes. An additional feature is the local conservation of the numerical flux, which is conserved from one discretized cell to its adjoining one. This last feature makes the FVM quite attractive when modeling problems for which the flux is of importance, such as in fluid dynamics. The FVM is locally conservative because it is based on a "balance" approach: a local balance is written on each discretization cell which is often called "control volume"; by the divergence formula, an integral formulation of the fluxes over the boundary of the control volume is then obtained. The fluxes on the boundary are discretized with respect to the discrete unknowns. As was discussed in Chapter 3, COMSOL utilizes the FEM method.

Computing resources vary greatly with the complexity of the problem, inclusion of liquids and gases and the fineness of the mesh generated. TRACE and COMSOL feature varying methods for maximizing the computing resources and those are discussed below.

4.3.1 TRACE

TRACE execution time is highly dependent and is a function of the total number of mesh cells, the maximum allowable time step size and the rate of change of the neutronic and TH problem being evaluated. The stability enhancing two-step numeric in hydraulic components allows the material Courant limit to be exceeded. This allows very large time steps to be used in slow transients. Significant speedups in simulations of slow developing accidents and operational transients are therefore possible.

Additionally, TRACE does not solve the governing equations in the form presented in Chapter 3. To eliminate complexity and improve computational effort, the fully conservative forms of the energy and the momentum equations are rearranged to provide internal energy and motion equations. The TRACE Theory Manual (TRACE V5.0 2008) provides a robust overview of the development of these equations.

4.3.2 COMSOL

COMSOL execution time is also highly dependent on model complexity and geometry. To aid in this, COMSOL permits user adjustment of solver settings and the use symmetries and other model properties to reach a solution. The use of symmetry in the model allows for the reduction of its size by one-half or more, making this an efficient tool for solving large problems. This applies to the cases where the geometries and modeling assumptions include symmetries. This technique is used in the development of the COMSOL model for the test facility presented in Chapter 5.

To take advantage of symmetry planes and symmetry lines, all of the geometry, material properties, and boundary conditions must be symmetric, and any loads or sources must be symmetric. A model can be built of a specific portion, which can be half, a quarter, or an eighth of the full geometry, and apply the appropriate symmetric boundary conditions.

COMSOL is capable of running in parallel which allows the user to drastically improve computational time. As is the case with the test facility modeled in this research, extensive memory usage dictates some extra

precautions. The choice of which solver to use is paramount as this will dictate the computation time. COMSOL makes use of a default choice when presented with a multi-physics based model. In some situations, though, it might be necessary to make additional changes to the solver settings and the model, and these will be discussed further in Chapter 5.

CHAPTER 5

EXPERIMENTAL DESIGN AND SIMULATION

5.1 MULTI-APPLICATION SMALL LIGHT WATER REACTOR OVERVIEW

The MASLWR is a modular design and consists of an integral reactor and SG, enclosed in a vessel that is located within a steel cylindrical containment, as seen in Figure 5.1. The entire module is 4.3 m in diameter and 18.3 m long. The free space within the containment is partially occupied with water, and the integral vessel is submerged in liquid to a level just below the FW nozzles. A sump makeup system connects the containment with the lower vessel region, and an ADS provides pressure suppression and primary system venting, thereby permitting makeup liquid from the containment to enter the vessel in the event of an accident scenario.

The containment is submerged in a pool of water. Cooling of the containment during normal and abnormal conditions is accomplished by steam condensation on and heat conduction through the containment steel walls to this pool of water. Heat from the pool is removed through a closed loop circulating system and rejected into the atmosphere in a cooling tower designed to maintain a pool temperature below 311 K. For the most severe postulated accident, the volume of water in the cavity provides a passive ultimate heat sink for three or more days, permitting time for restoration of the active heat removal systems.

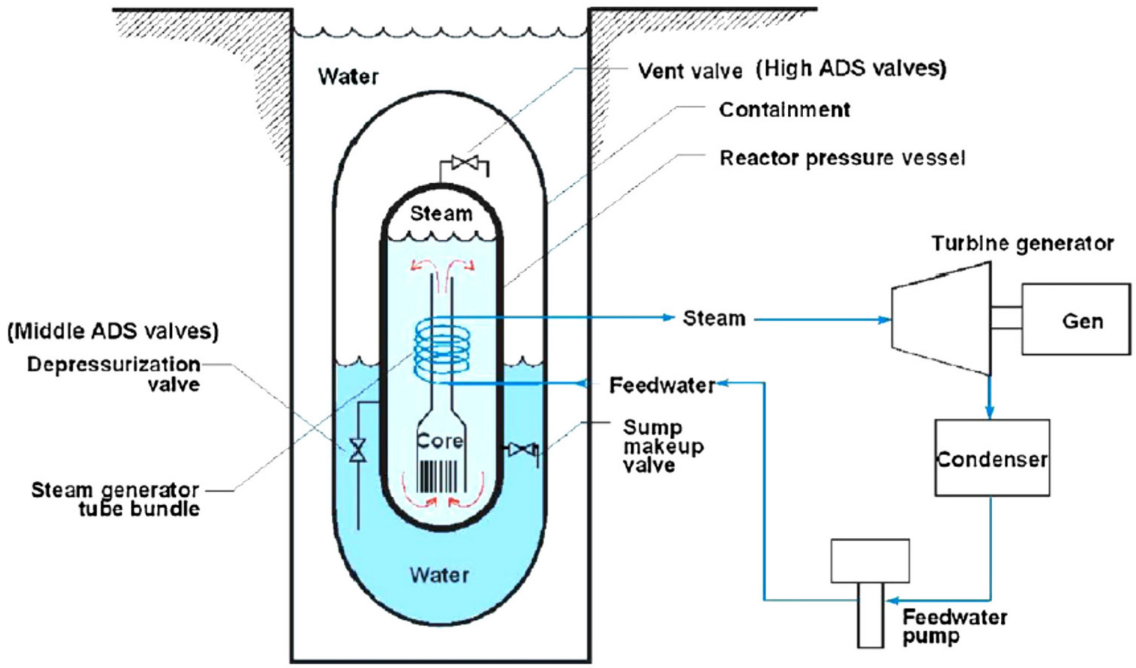

Figure 5.1. Simplified MASLWR Diagram

The nuclear steam supply system (NSSS) is a “self-contained” assembly of reactor core and SG within a single pressure vessel. The nuclear core is located in the lower part of the vessel, with the SG above it. To effectively use natural circulation, the core is connected directly to the space above the heat exchanger via a large-diameter tube, or riser, which is an upper extension of the core barrel. The primary liquid flow path is upward through the riser, then downward around the heat exchanger tubes, returning to the bottom of the core via an annular space.

The SG is a helical-tube, once-through heat exchanger, located above the reactor. The heat exchanger consists of approximately 1000 tubes, arranged in an upwardly spiraling pattern. Cold FW enters the tubes at the bottom, and slightly superheated steam is produced and exits at the top. This steam ultimately drives a turbine generator to produce electricity.

The core consists of standard PWR assemblies, with an active fuel height of approximately 1 m. The fuel consists of cylindrical pins with a cladding outer diameter of 9.5 mm, and a pitch-to-diameter ratio (P/D) of 1.33. The fuel pellets are UO_2 or ThO_2- UO_2, enriched to less than 20% ^{235}U.

The steady-state operating conditions for the MASLWR are summarized in Table 5.1. (Modro et al. 2003)

Table 5.1. MASLWR Steady-State Operating Conditions

Parameter (units)	*Value*
Primary Side	
Reactor Thermal Power (MWt)	150
Primary Pressure (MPa)	7.60
Fuel	UO_2 (<20% enriched)
Fuel Design	24 Assemblies (17 x 17)
Cladding	Zircoloy-4
Life Cycle (years)	60
Refueling Intervals (years)	5
Coolant Mass Flow Rate (kg/s)	597
Inlet Temperature (K)	491.9
Outlet Temperature (K)	544.3
Saturation Temperature (K)	565
Average Power Density (kW/L)	100
Secondary Side	
Steam Pressure (MPa)	1.50
Steam Temperature (K)	481.4
Saturation Temperature (K)	471.6
FW Temperature (K) 310	
FW Flow Rate (kg/s) 56.10	

5.2 OSU-MASLWR OVERVIEW

The OSU MASLWR test facility illustrated in Figure 5.2, models the MASLWR conceptual design including a RPV cavity and a containment structure. It is a 1:3 length, 1:254 volume and 1:1 time scale integral facility constructed entirely of stainless steel. It is designed for full reactor pressure replication at a

maximum pressure of 11.4 MPa and a maximum temperature of 590K. (Galvin 2007)

Figure 5.2. Photograph of OSU-MASLWR Facility (Modro et al. 2003)

The remainder of this section provides a brief overview of the OSU-MASLWR test facility, including the major systems: primary systems, secondary systems, containment and cooling, and the automatic depressurization system. Detailed descriptions of specific physical structures, geometric data, and instrumentation locations necessary for modeling the facility and comparing the computational data to the experimental test results are provided in subsequent sections. The majority of this description is in Section 5.4, as the TRACE model

follows the geometric layout of the test facility in a very logical manner. Changes to these descriptions in regards to the COMSOL model will be highlighted in Section 5.5.

5.2.1 Primary Circuit

The primary circuit of the test facility models the self-contained integrated reactor core and steam generator system. The core is comprised of electric heaters. The steam generator is comprised of helical coils that are located in the vessel, above the core and outside of the hot leg chimney. This relative placement of core and steam generator allows for sufficient natural circulation flow under normal steady state and transient operating conditions. As previously mentioned, the primary circuit of the test facility has been designed with limits for operation at a primary side pressure of 11.4 MPa and a primary side temperature of 590K.

Primary coolant flow is upwards through the core and hot leg riser. This hot fluid is then cooled by the steam generator in the upper portion of the vessel. The cooler fluid flows downward around the outside of the hot leg riser into the lower plenum. From the lower plenum the fluid is drawn back into the core and heated once more. Figure 5.3 illustrates the significant test facility primary circuit components.

The test facility core consists of 56 electric heaters distributed in a square array with a maximum core power of 398 kW. The core geometry and thermal characteristics (flow areas, hydraulic diameters and local heat flux) have been preserved on a scaled basis.

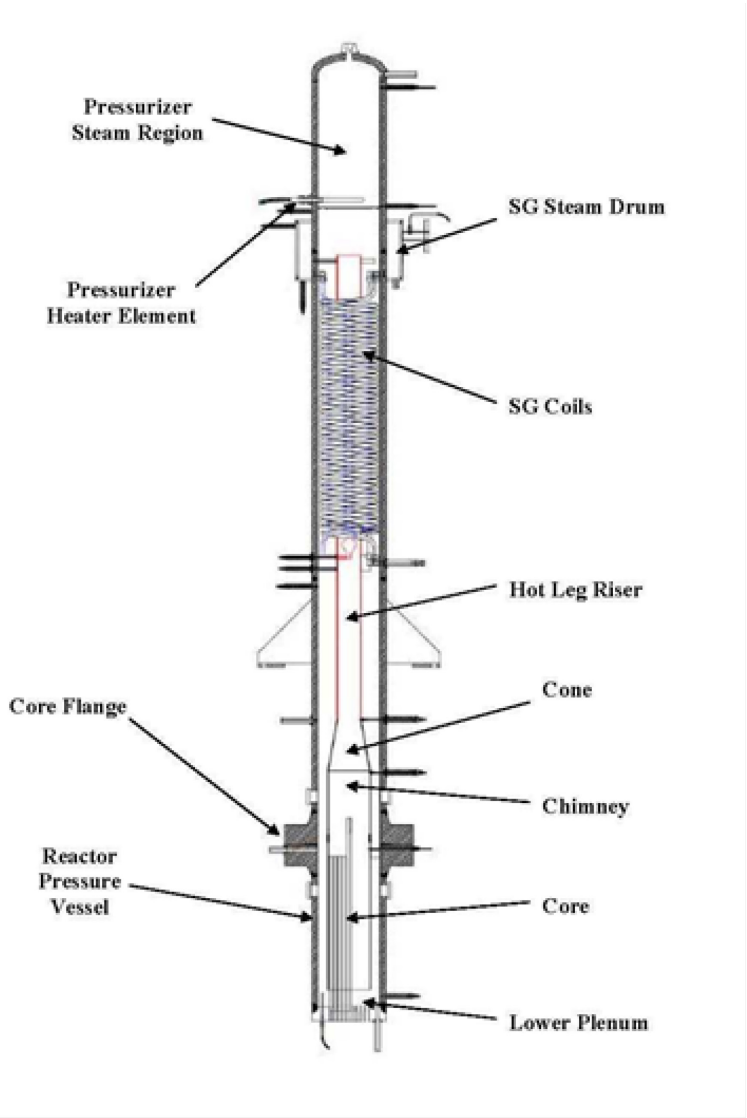

Figure 5.3. Primary System Key Structures (Galvin 2007)

5.2.2 SECONDARY CIRCUIT

The SG is a helical coil, once through heat exchanger located within the pressure vessel in the annular space between the hot leg riser and the inside surface of the pressure vessel shell. FW is provided from the city water supply and, after de-ionization and chemical treatment, is pumped into the SG from a FW storage tank by a positive displacement pump. This pump uses a

variable speed controller to allow for precise control of the FW mass flow rate. The steam produced is vented to atmosphere.

The SG consists of three separate parallel helical coil tube sections. The outer and middle coils consist of five tubes each while the inner coil consists of four tubes. Each coil is separate from the others, but the tubes within a coil are joined at a common inlet header to ensure pressure equilibrium. Cold FW enters at the bottom of the SG and boils off after traveling a certain length in the SG tubes. This boil off length is a function of both core power and FW flow rate. Nominally, this boil off length is approximately 40% shorter than the actual length of the steam generator tubes so the steam will leave the SG superheated. Each SG coil exhausts the superheated steam into a common steam drum from where it is subsequently exhausted to atmosphere.

5.2.3 Containment and Cooling

The MASLWR containment vessel and the surrounding containment pool are modeled in the OSU MASLWR test facility as two separate vessels. One vessel models the suppression pool volume, vapor bubble volume and the condensation surface inside of the containment vessel. The second vessel models the heat capacity of the water pool within which the containment vessel is held. The two vessels are separated by a stainless steel plate. This plate models the scaled heat transfer surface between the containment vessel and the surrounding vessel pool. Figure 5.4 is a photograph of the test facility containment, taken during facility construction, which identifies these two vessels.

The containment vessel is connected to the RPV by six independent automatic depressurization system lines. There are two blowdown lines, two vent lines and two sump recirculation (core makeup) lines.

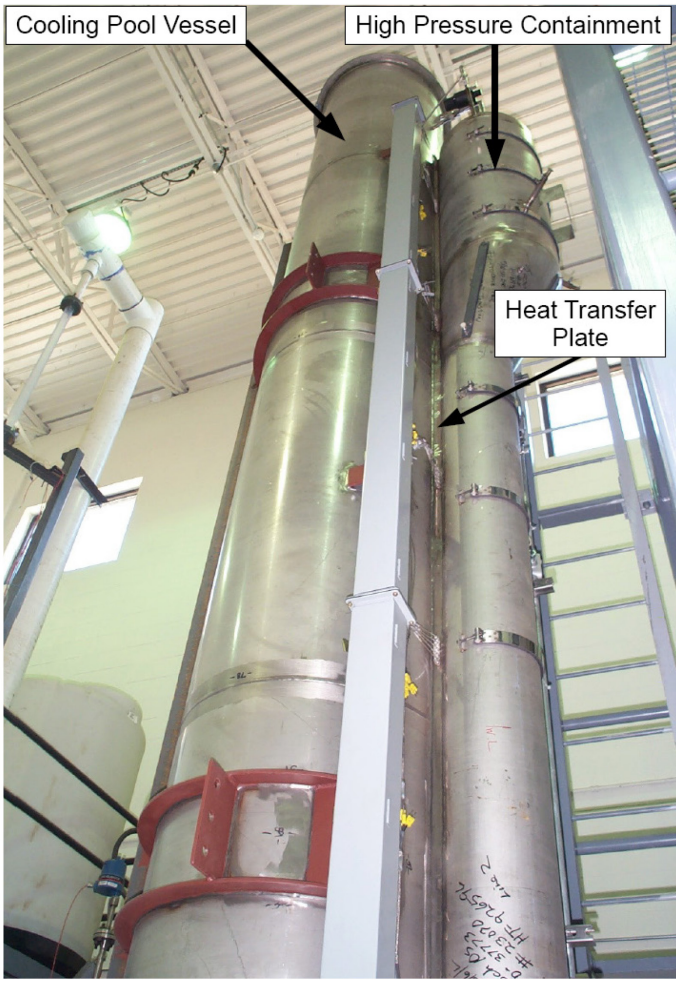

Figure 5.4. High Pressure Containment and Cooling Pool (Galvin 2007)

Flow through each of these lines is via an independent automatically operated valve controlled through the test facility control system. The containment vessel is capable of prolonged operation at 2.07 MPa and 477.6K.

5.2.4. Data Acquisition, Instrumentation and Control System

The OSU-MASLWR test facility is instrumented to capture the behavior of the facility during steady-state and transient operation. In general, the following information can be obtained by the test facility data acquisition system:

- FW—mass flow rate and temperature
- FW through each SG coil—mass flow rate, temperature and pressure
- Main steam—volumetric flow rate and pressure
- Differential pressure—across core, hot leg chimney, SG, and annulus below SG,
- PZR—coolant level, pressure and temperature,
- Temperatures—core inlet, core exit, primary loop at SG

Table 5.2 lists and Figure 5.5 illustrates selected instrumentation tags and a description of the installed instrumentation for the OSU-MASLWR. These tags will be used to identify the experimental data presented in ensuing sections and chapters.

In conjunction with the instrumentation and data acquisition, the test facility control system accomplishes two tasks. The first is to process input signals from the various facility instrumentation (thermocouples, pressure meters, flow meters, valve and relay positions). The second is to generate control signals determined by the system logic (valve and relay control signals, heater and pump control signals). (Woods, Galvin and Bowser 2010) The following systems can be regulated by the test facility control system:

- Core heaters (including decay power modeling)
- Main FW pump,
- Pressurizer heaters
- FW storage tank level
- PZR water level (draining during system heat-up only)

Containment heaters (used to maintain an adiabatic boundary condition on all walls of containment except for the prescribed condensation wall ensuring that heat transfer only takes place between the containment pool vessel and the high pressure containment vessel)

Table 5.2. OSU-MASLWR Test Facility Instrumentation

Tag	*Description*
FMM-501	FW mass flow rate
TF-501	FW temperature
PT-602	Main steam pressure
FVM-602-P	Main steam pressure
FVM-602-T	Main steam temperature
FVM-602-M	Main steam mass flow rate
TF-611 – TF-615	Thermocouples inside the outer coil pipe of the SG
TF-621 – TF-625	Thermocouples inside the middle coil pipe of the SG
TF-631 – TF-634	Thermocouples inside the inner coil pipe of the SG
TF-101 – TF-106	Center of core thermocouples-spaced six inches apart
TH-141 – TH-146	Core heater rod temperatures
TF-121 – TF-124	Core inlet temperatures
TF-131, 133, 134	Primary coolant downcomer temperatures after SG
TF-132	Primary coolant hot leg riser temperatures below SG
TF-111	Primary coolant temperature at top of hot leg chimney
TF-301	Steam temperature in PZR
PT-301	Steam pressure in PZR
DP-101	Pressure loss in the core
DP-102	Pressure loss between core top and hot leg riser cone
DP-103	Pressure loss in the riser cone
DP-104	Pressure loss in the hot leg riser chimney
DP-105	Pressure loss across the SG
DP-106	Pressure loss in the annulus below the SG
FDP-131	Differential pressure in hot leg riser V-cone
LDP-106	Primary coolant water level
TF-871 – TF-873	Water temperatures of ADS lines inside the HPC
PT-801	HPC pressure
LDP-801	HPC level
TF-882	CPV water temperatures
LDP-901	CPV level

- .

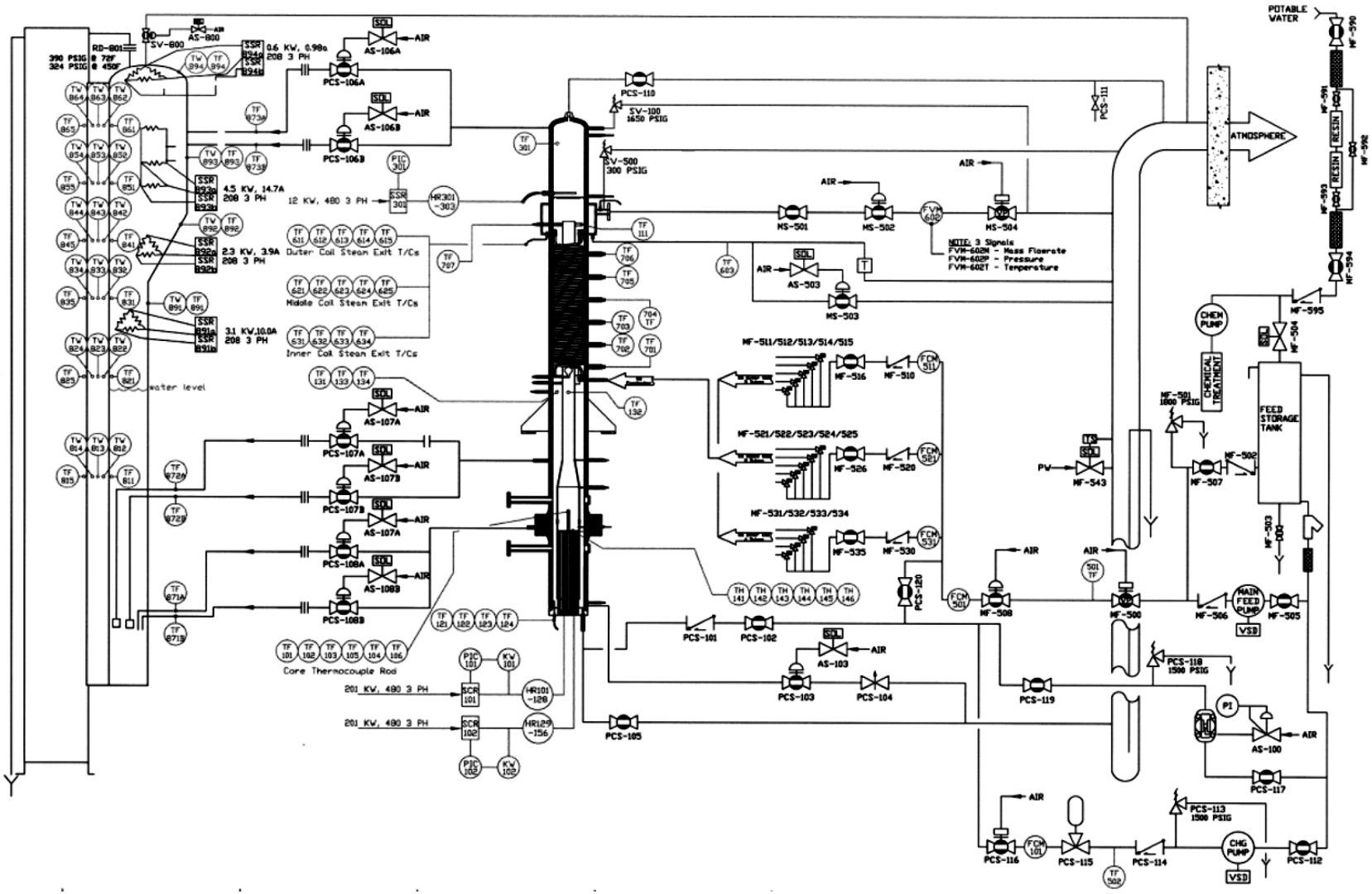

Figure 5.5. OSU-MASLWR Instrumentation Diagram (Galvin 2007)

5.3 Test Case Description

Two test case computer models were designed in order to compare available experimental data to the TH and CFD computer models. TRACE and COMSOL models were developed and then executed with the proper initial and boundary conditions to replicate the two test cases described in detail below. A comparative evaluation of the experimental data, the TH code results and the CFD code results was then conducted. As seen in Chapters 6 and 7, this evaluation provides an opportunity to validate the best-estimate thermal hydraulic code's treatment of a natural circulation loop and provide insights into expanded use of the CFD code in future designs and operations. In addition, a sensitivity analysis was conducted to identify several parameters that most effect the steady state operation of the test facility during normal operating conditions. Sections 5.3.1 through 5.3.3 provide a detailed description of the two test cases and the sensitivity analysis.

5.3.1 Test Case One

Test case one characterizes the steady-state natural circulation in the primary side during various core power inputs. As outlined in the original facility test plan, this was accomplished by configuring the OSU-MASLWR test facility in a natural circulation state and varying the power inputs of the core heaters. Power inputs of the core heaters were increased step by step from 10 percent of full power to 80 percent of full power, with a 10 percent increment at each step. For each power input, the primary side flow rate, hot leg and cold leg temperatures were monitored to determine whether the flow stabilization was

achieved. The primary side and steam generator pressures were maintained at 8.72 MPa gage and 1.44 MPa gauge, respectively, for all power inputs.

By procedure, the OSU-MASLWR test facility was allowed to reach steady state prior to increasing the core power and moving on to the next step. The following three parameters were used to determine whether the OSU-MASLWR test facility had reached steady state conditions or not:

1. Constant hot leg temperature as indicated by TF-106 (± 2.8 °C),
2. Constant cold leg temperature as indicated by TF-131 (± 2.8 °C),
3. Constant primary mass flow rate as indicated by FDP-131 (± 5%).

Table 5.3 lists the initial conditions for test case one. (Mai and Ascherl 2012) The values presented in Table 5.3 represent the average of the specified instruments over the two-minute data collection time for the initial power level (40 kW) for the test.

Table 5.3. Test Case One Initial Conditions

Parameter (units)	*Tag*	*Experimental Value*
PZR pressure (MPa)	PT-301	8.72
PZR level (m)	LDP-301	0.3574
Power to heater rods (kW)	KW-101/102	40.0
FW temperature (°C)	TF-501	31.49
Steam temperature (°C)	FVM-602-T	205.44
Steam pressure (MPa)	FVM-602-P	1.446
Primary flow at core outlet (kg/s)	FDP-131	0.68
Primary coolant temp at core inlet (°C)	TF-121-124	250.0
Primary coolant temp at core outlet (°C)	TF-106	263.0
FW flow (kg/s)	FMM-501	0.010
Ambient temperature (°C)	n/a	22.0

Table 5.4 lists the sequence of the major events that occurred while running test one. Table 5.5 lists the boundary conditions for the test—core power, FW flow rate, and FW temperature. A constant secondary side pressure was maintained

at 1.44 MPa. It is assumed that the ambient temperature during test one, while not specifically measured, was between 20 – 24 °C.

Table 5.4. Test Case One Sequence of Events

Event	*Test Time (sec)*
Beginning of test	-180
Initiate core power increase to 40 kW	-180
Steady-state achieved at 40kW	-120
Begin data collection at 40 kW	0
Initiate core power increase to 80 kW	180
Initiate core power increase to 120 kW	1060
Initiate core power increase to 160 kW	1830
Initiate core power increase to 200 kW	2367
Initiate core power increase to 240 kW	4195
Initiate core power increase to 280 kW	4687
Initiate core power increase to 320 kW	5286
End of test	6347

Table 5.5. Test Case One Boundary Conditions

Time (s)	*KW-101/2 (kW)*	*FCM-511 (kg/s)*	*FCM-521 (kg/s)*	*FCM-531 (kg/s)*	*TF-501 (°C)*	*FVM-602-T (°C)*
190	21.1	0.0034	0.0032	0.0036	31.5	205.8
1060	39.6	0.0134	0.0157	0.0144	26.9	241.7
1830	59.1	0.0128	0.0148	0.0131	26.1	249.3
2367	79.2	0.0182	0.0195	0.0177	25.4	253.8
4195	98.9	0.0240	0.0268	0.0224	23.1	208.8
4687	119.5	0.0291	0.0327	0.0271	22.2	205.3
5286	140.4	0.0332	0.0375	0.0310	21.6	206.3

5.3.2 TEST CASE TWO

The second test case replicates the thermo-hydraulic coupling between the primary system and the high-pressure containment (HPC) system. The purpose of this test, a design basis accident for the MASLWR concept design, is to determine the behavior of the RPV and containment pressures and core inlet and outlet temperatures following an actuation of an ADS vent valve and subsequent blowdown.

More specifically, test case two simulates the loss of FW, activation of safety systems and the long term cooling of the OSU-MASLWR test facility to determine the progression of a loss of FW transient. The test begins by bringing the OSU-MASLWR test facility to steady state at 75% power with a primary pressure of 8.72 MPa(g) and the main feed pump running on the secondary side.

Once the initial conditions are reached the test is initiated by stopping the main feed pump thus cutting off flow to the SG. With the subsequent loss of the reactor heat sink the primary pressure will begin to rise. When the PZR pressure reaches 8.963 MPa(g) the OSU-MASLWR core heaters will be set to decay power and the one line of the ADS vent system opens on a pressure reading of 9.064 MPa(g). This causes the primary system under rising pressure to vent into the high-pressure containment. The ADS blowdown system operates in automatic mode to vent the primary system to the high-pressure containment while at the same time preventing the high pressure containment from exceeding its maximum operating pressure of 2.068 MPa(g). When the difference between RPV pressure and HPC pressure is less than 0.034 MPa, the remaining ADS vent valves and ADS sump values open and long-term cooling is started. Test case two continues until the PZR pressure drops below 0.517 MPa(g) or five hours have elapsed since commencing the procedure.

Table 5.6 lists the initial conditions for test case two. (Mai and Ascherl 2011) The values listed in Table 5.6 represent the last measurement before the main feed pump was stopped—effectively starting the transient. Table 5.7 lists the sequence of the major events that occur during the conduct of test case two.

Table 5.8 lists the boundary conditions for the transient at the OSU-MASLWR test facility.

Table 5.6. Test Case Two Initial Conditions

Parameter (units)	*Tag*	*Experimental Value*
PZR pressure (MPa)	PT-301	8.718
PZR level (m)	LDP-301	0.3606
Power to heater rods (kW)	KW-101/102	297.4
FW temperature (°C)	TF-5-1	21.2
Steam temperature (°C)	FVM-602-T	205.4
Steam pressure (MPa)	FVM-602-P	1.411
Primary flow at core outlet (kg/s)	FDP-131	1.82
Primary coolant temp at core inlet (°C)	TF-121-124	215.1
Primary coolant temp at core outlet (°C)	TF-106	251.5
FW flow (kg/s)	FMM-501	0.106
Ambient temperature (°C)	n/a	25.0

Table 5.7. Test Case Two Sequence of Events

Event	*Test Time (sec)*
Beginning of test	-600
Initiate core power increase to 297.4 kW	-600
Steady-state achieved at 40kW	-300
Begin data collection	0
Stop main FW pump	0
PZR pressure (PT-301) reaches 9.064 MPa	30
Enter decay power mode	30
Open ADS vent valve (PT-106A)	48
Long-term cooling established	4114
End of test	15822

Following the ADS actuation, the blowdown of the primary system takes place as seen in Figure 5.6. A sub-cooled blowdown characterized by a fast RPV depressurization takes place after the start of the transient. A multi-phase blowdown occurs when the differential pressure, at the break location, results in fluid flashing. When the PZR pressure reaches saturation, single-phase blowdown occurs, and the depressurization rate increases.

Table 5.8. Test Case Two Boundary Conditions

Time (s)	*KW-101 (kW)*	*KW-102 (kW)*
0.0	149.5	147.9
100.0	14.5	14.1
200.0	12.1	11.5
300.0	10.7	10.0
400.0	9.7	9.0
500.0	9.0	8.3
600.0	8.4	7.6
700.0	7.9	7.1
800.0	7.5	6.7
900.0	7.1	6.4
1000.0	6.8	6.1
2000.0	5.2	4.3
3000.0	4.2	3.4
4000.0	3.7	2.8
5000.0	3.3	2.3
6000.0	3.0	2.0
7000.0	2.7	1.8
8000.0	2.5	1.6
9000.0	2.3	1.5
10000.0	2.2	1.3
11000.0	2.1	1.2
12000.0	1.9	1.1
13000.0	1.9	0.9
14000.0	1.7	0.9
15000.0	1.6	0.8

During the saturated blowdown period, the inlet and the outlet temperature of the core are equal to each other assuming the saturation temperature value. However, as seen in Figure 5.7, a core reverse flow and a core coolant boiling off at saturation are present in the facility during this period. When the refill takes place, the core flow normal flow direction is restarted and a core temperature difference is observed depending on the refill rate and core power. (Mascari et al. 2012)

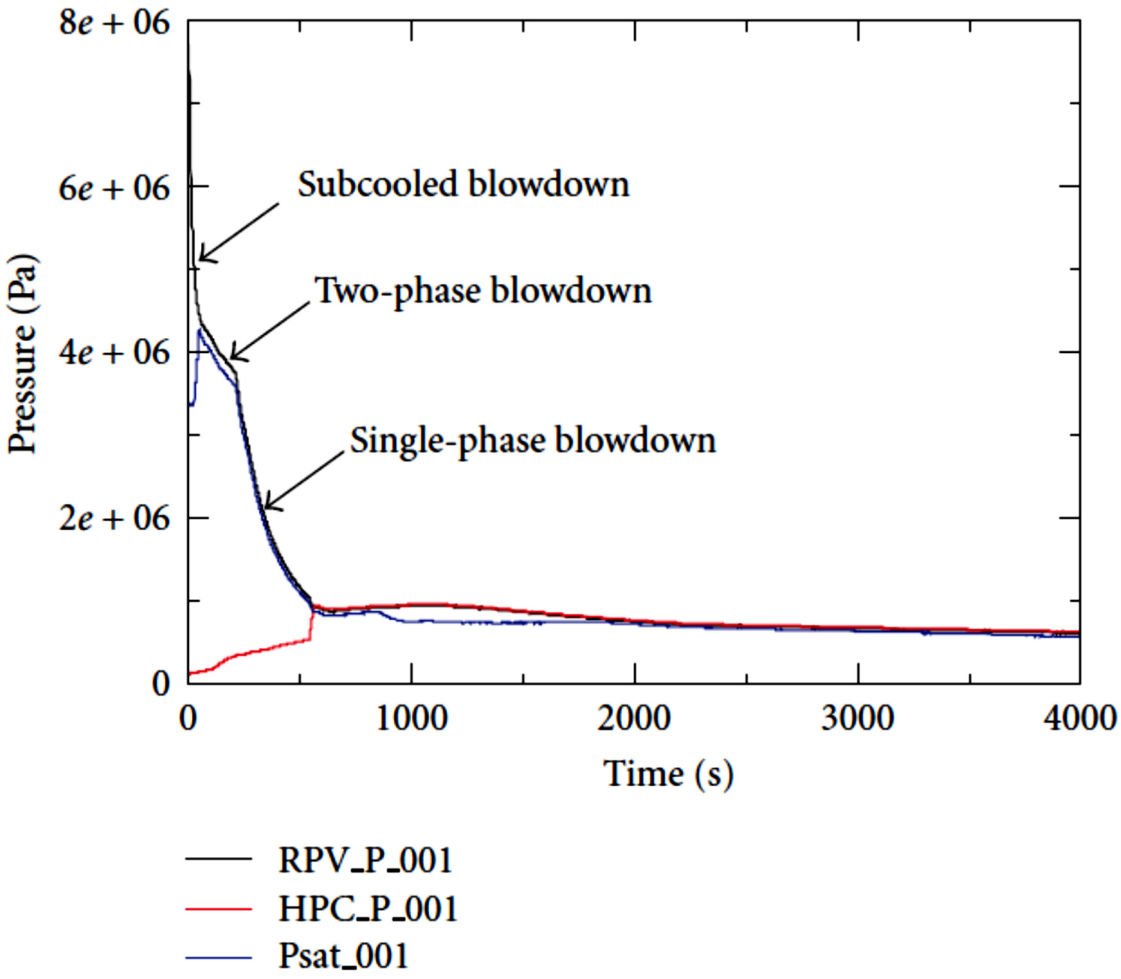

Figure 5.6. RPV and HPC Pressure Behavior

Accurately predicting these temperature values is the main purpose of this test case. As before, experimental data including highly instrumental RPV pressures, mass flow rates and various location temperatures will be compared to the two code simulation results and any deviations will be further explored.

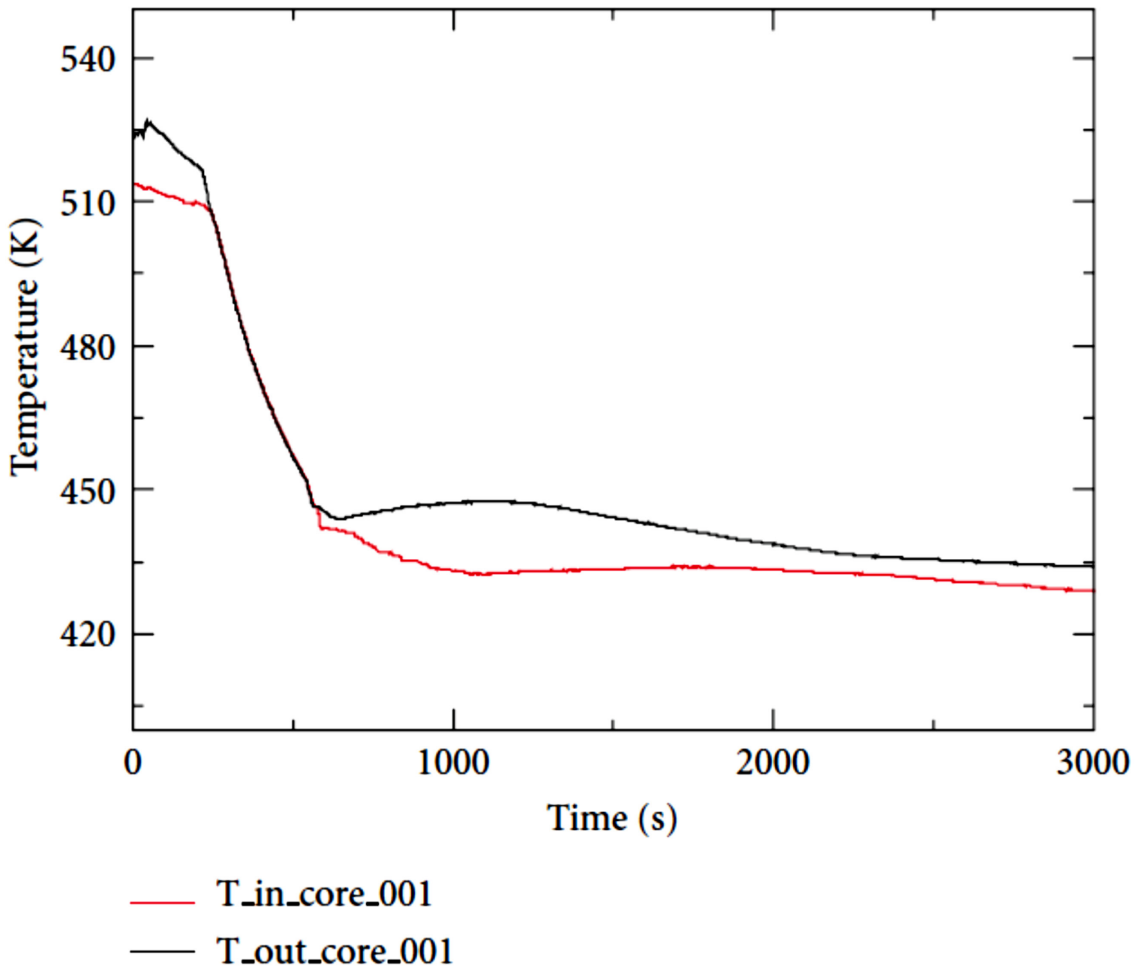

Figure 5.7. Inlet and Outlet Core Temperature Behavior

5.3.3 Sensitivity Analysis

A comparative evaluation of the experimental data, the thermal hydraulic code results and the CFD code results was completed. This assessment provides an opportunity to validate the best-estimate thermal hydraulic code's treatment of a natural circulation loop and provide insights into expanded use of the CFD code in future designs and operations through the exploration of these two test cases.

Additionally, a sensitivity analysis was conducted to determine those parameters that have the most impact on the CFD code results. The sensitivity

analysis was completed on test case one to gain a better understanding of the natural circulation flows in the reactor coolant system and the parameters that can impact them during steady-state operations at various power levels.

An altered set of test case one computer runs was completed with the initial and boundary conditions found in Tables 5.3 and 5.5. Table 5.9 lists those parameters that were altered and the target of the sensitivity analysis. A more detailed discussion of the sensitivity analysis is explored in the COMSOL model development contained in Section 5.5.3. The results of the sensitivity analysis are presented in later chapters.

Table 5.9. Sensitivity Analysis Parameters

Value	*Variation from Reference Calculation*	*Sensitivity Analysis Target*
REF	Reference calculation	
SEN1	Decrease FW mass flow rate	Show the effect of the initial condition on the steady-state values
SEN2	Increase FW mass flow rate	Show the effect of the initial condition on the steady-state values
SEN3	Decrease the thermal conductivity of the hot leg riser around the SG	Show the effect of the heat transfer properties on the steady-state values
SEN4	Increase the thermal conductivity of the hot leg riser around the SG	Show the effect of the heat transfer properties on the steady-state values

As is discussed in Chapters 6 and 7, this analysis could lead to an alteration of the initial and boundary conditions for the T-H code assessment. Furthermore, this analysis could lead to changes in the T-H modeling approach to more accurately account for the effects of the CFD 3-D analysis.

5.4 TRACE Model Design

TRACE Version 3.2.7 was used, in conjunction with the Symbolic Nuclear Analysis Package (SNAP) Version 2.2.3, to construct a model of the OSU-MASLWR test facility. SNAP is a graphical user interface tool that aids in modeling the nodalization and control features of TRACE. It was used exclusively to develop the TRACE input files used in both test cases and the sensitivity analysis.

TRACE input data must be specified either in a fixed-format way or a free-format way. The term fixed-format implies that numerical values must lie in specific columns, while free-format does not have these restrictions. In addition to the obvious convenience of not having to count columns, free-format input also allows greater flexibility in using comments to document the input data. The model presented here utilizes the free-format option.

As per the TRACE Version 3.2.7 manual, the data in an input file is divided into eleven major sections which must appear in the following order:

1. Main Data
2. Countercurrent Flow Limitation Data
3. Material Properties Data
4. Hydraulic-Path, Steady-State Initialization Data
5. Constrained Steady-State (CSS) Controller Data
6. Signal Variable Data
7. Control Block Data
8. Trip Data
9. General Table Data
10. Component Data
11. Time step Data

Each of these sections has its own specific rules regarding how the data is formatted in an input file. (TRACE Version 3.2.7) A select few will be explored here in detail as they pertain to the OSU-MASLWR model.

The NAMELIST capability, which is contained in the Main Data section, is an extremely useful feature of Fortran that can be used to load values directly into variables named within the program. TRACE uses this feature as a means of setting global parameters and flags that govern overall behavior of the code during the run. Changes to the default variable values, found in the TRACE Version 3.2.7 manual, are listed in Table 5.10.

Table 5.10. Changes to NAMELIST Default Variable Values

Variable	*Value*	*Description*
icflow	1	Choked-flow enabled at BREAK components
ielv	1	Reference zero elevation method
ikfac	1	K factors will be input for each component
ioinp	0	SI units used for reading input data
noair	0	Non-condensable gas partial pressures solved
use_iapws_st	true	Use steam tables based on IF97 standard
usesjc	3	Single junction components can be made
numgentbl	3	Number of general tables to be read
npower	1	Number of power components used to power HTSTR components
nhtstr	5	Number of heat structure components

There are three methods for establishing the elevation and/or vertical orientation of components and cell volumes in TRACE. The IELV NAMELIST option controls which method the model will use for calculations. The OSU-MASLWR model presented here utilizes the cell-centered reference zero elevation method for calculating elevations. This method requires the elevation of each cell center directly. Conceptually, this is the most straightforward approach and is generally recommended when developing new system models.

(TRACE Version 3.2.7) To engage this method, the NAMELIST IELV variable is set equal to one. The choice in a reference zero elevation point is entirely arbitrary, as all other elevation values supplied in the input model are referenced from this same point. Table 5.11 lists the reference zero elevation point and several other key elevations in the model.

Table 5.11. Select Model Elevation Values

Position	*Elevation (m)*
Top of core	0.0
Bottom of vessel	-0.69
Bottom of HPC	-0.94
Bottom of containment pool	-1.13
HPC water level	1.29
Top of vessel	3.74
Top of HPC	4.70
Top of cooling pool	5.63

The component data section is the main body of the input-data file. This section contains a detailed description of every hydraulic and heat-transfer component in the system model. The components are assembled one following another in the component data section of the input file. The hydrodynamic components of the OSU-MASLWR model consist of the primary system, the secondary system, the automatic depressurization system (ADS), the high pressure containment (HPC) and the cooling pool vessel (CPV). The following sections detail the modeling effort of each of these component areas.

5.4.1 PRIMARY SYSTEM

As per Woods, a sliced nodalization approach was applied to the RPV because of the combination of low mass flow rates and the free convection natural circulation circuit. Figure 5.8 illustrates the base nodalization model for

the OSU-MASLWR test facility TRACE model. A total of 15 PIPE components were used to model both the cold and hot legs with matching axial lengths to set up the cross-over heat transfer modeling through the hot leg riser metal mass to the cold leg. As per the TRACE Version 3.2.7 manual, component cell lengths should be shorter where the T-H conditions are expected to vary more per unit length. That generally results in 0.1 m to 3.0 m long cells. However, the 1-D flow equations are constructed by averaging across the width of the flow channel. This means that selection of a cell length less than the hydraulic diameter of the flow channel does not normally make sense and will be taken into consideration when deciding which components should have more axial cells. Accordingly, components 106 and 113 were broken into eight cells to allow more refinement in the cold and hot leg regions in contact with and containing the SG.

Cross-flow PIPE components were used to model the lower and upper plenums to complete the natural circulation circuit. Above the upper plenum, the PZR is modeled with two PIPE components and the uppermost fluid volume in the RPV is also a PIPE component where the upper ADS vent line junctions connect to the RPV. Specific geometric data for all primary system TRACE components is listed in Table 5.12. The OSU-MASLWR region(s) corresponding to each component are indicated, and these regions are detailed as illustrated in Figure 5.10. The vertical angle column indicates the orientation of the mass flow: 90.0° indicates flow in the positive z-direction (against gravity), -90.0° indicates flow in the negative z-direction (with gravity) and 0.0°

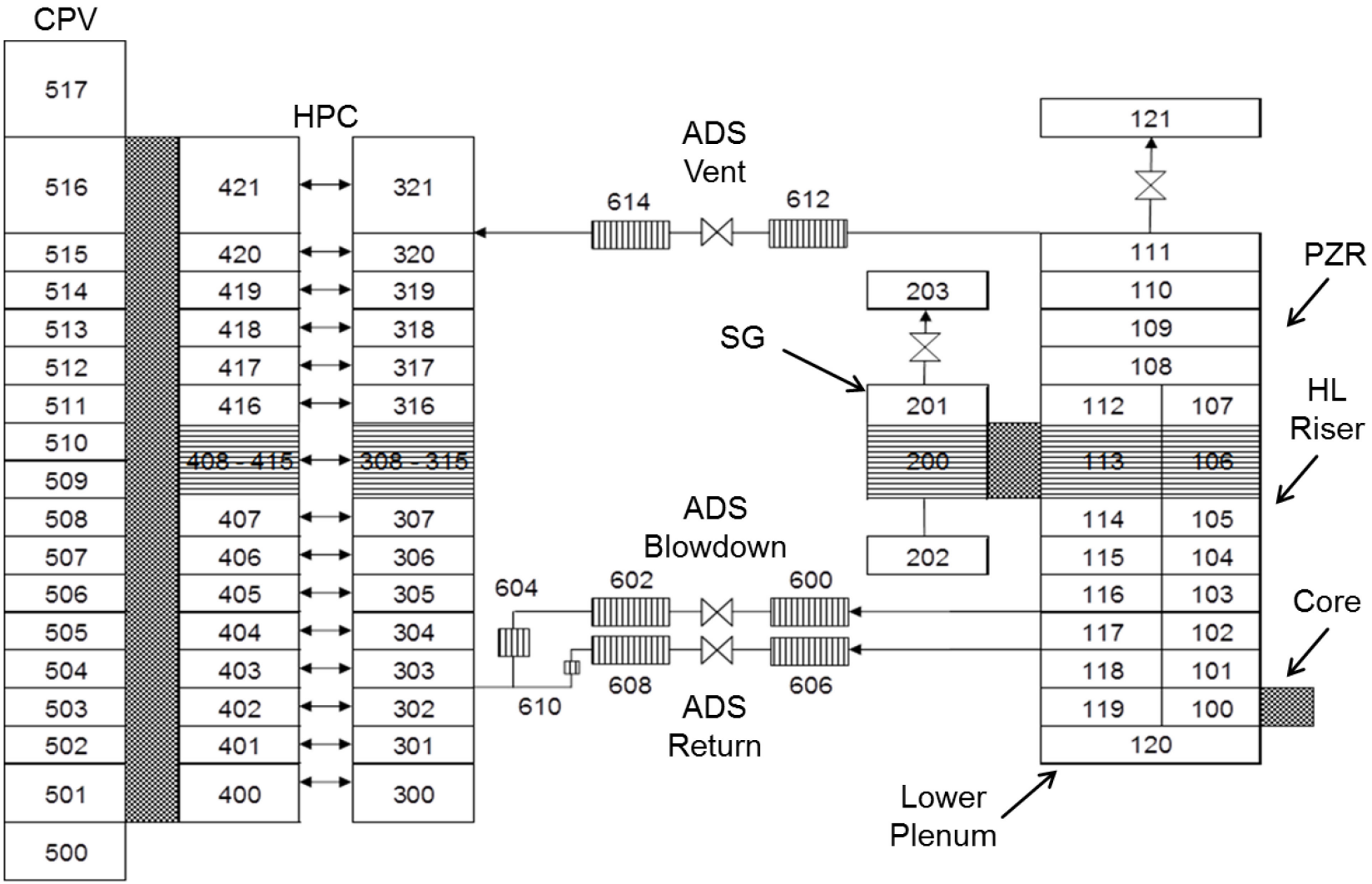

Figure 5.8. OSU-MASLWR Test Facility TRACE Nodalization Model

indicates cross-flow in the x-direction (gravity neutral). All geometric data used in both the TRACE and COMSOL models was obtained from Galvin, 2007.

The OSU-MASLWR test facility PZR heaters are not modeled as part of the TRACE or COMSOL models. As seen in Figure 5.9, the experimental data illustrates that the PZR pressure maintains a very narrow band about the pressure set-point for the test facility. This experimental data indicates that the PZR heaters are cycling to make up for losses from the PZR water and steam space to the environment, and primary coolant surges to/from the PZR have little effect on their cycling frequency or magnitude. Lastly, since the primary coolant remains sub-cooled throughout all normal operations, it is assumed negligible error is introduced by using the nominal pressure in thermodynamic property calculations.

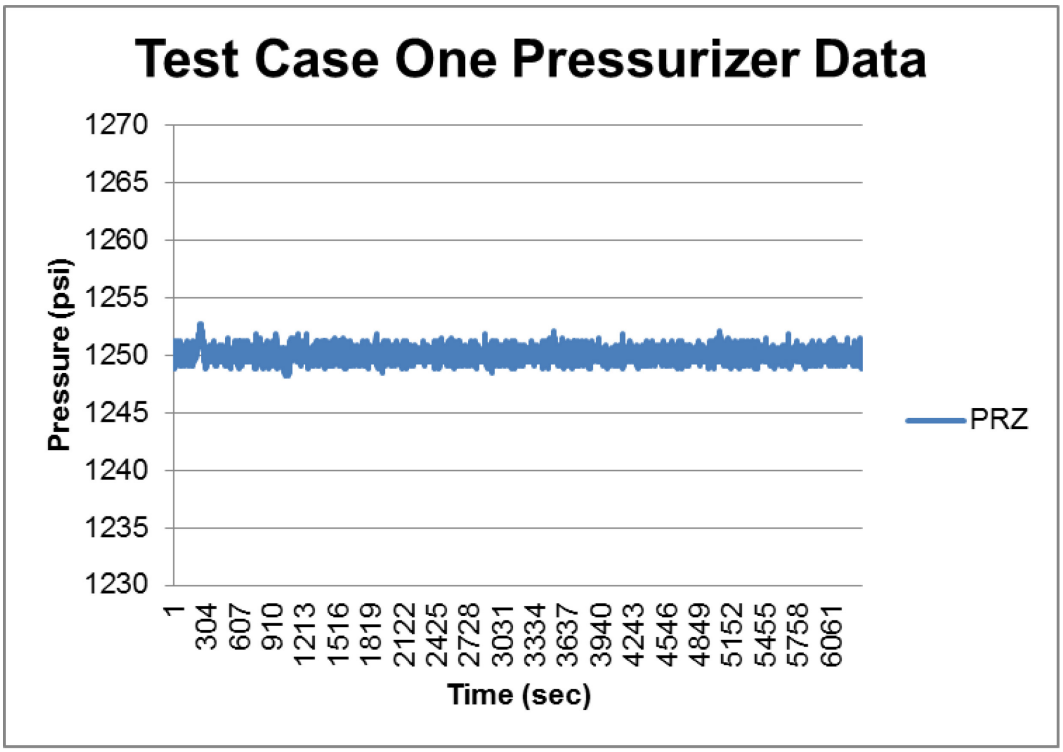

Figure 5.9. Test Case One Pressurizer Experimental Data

Table 5.12. Primary System Geometric Data

TRACE Component	*Component Type*	*Test Facility Region*	*Length (m)*	*Flow Area (m^2)*	*Vertical Angle(°)*	*Hydraulic Diam.(m)*
100	PIPE	2,3,4,5,6	0.6301	0.00842	90.0	0.0096
101	PIPE	7,8	0.4192	0.0305	90.0	0.194
102	PIPE	9	0.2446	0.0188	90.0	0.153
103	PIPE	10	0.8699	0.00821	90.0	0.103
104	PIPE	11	0.1111	0.00821	90.0	0.103
105	PIPE	12	0.0500	0.00821	90.0	0.103
106	PIPE	12	0.9800	0.00821	90.0	0.103
107	PIPE	12	0.2000	0.00821	90.0	0.103
108	PIPE	13	0.1047	0.0670	90.0	0.292
109	PIPE	13	0.1047	0.0670	90.0	0.292
110	PIPE	PZR	0.3207	0.0670	90.0	0.292
111	PIPE	PZR	0.3207	0.0670	90.0	0.292
112	PIPE	17,18	0.2000	0.0568	-90.0	0.178
113	PIPE	19	0.9800	0.0568	-90.0	0.178
114	PIPE	20	0.0500	0.0568	-90.0	0.178
115	PIPE	21,22	0.1111	0.0568	-90.0	0.178
116	PIPE	23	0.8699	0.0568	-90.0	0.178
117	PIPE	24-28	0.2449	0.0467	-90.0	0.132
118	PIPE	29-33	0.4192	0.0346	-90.0	0.0887
119	PIPE	34,35	0.6301	0.0346	-90.0	0.0887
120	PIPE	36	0.0620	0.067	90.0	0.292

The hydraulic diameters listed in Table 5.12 were calculated using Eqn. 5.1:

$$D_H = \frac{4A_c}{P_w} \tag{5.1}$$

where D_H ≡ hydraulic diameter

A_c ≡ cross-sectional area

P_w ≡ wetted perimeter

The heat structures contained in the primary system include the electric heater rods, ambient heat loss and the core barrel. The core consists of 57 heater rods with a diameter of 0.0159 m and a heated length of 0.597 m. The nominal power of each heater rod is 7.1 kW resulting in a maximum core power

of 398 kW. The core heater rods are modeled in TRACE as a heat structure (HTSTR) with a radial geometry, a radius of 0.00625 m and a total heated length of 34.03 m (57 rods x 0.597 m per rod). The HTSTR component in TRACE evaluates the dynamics of conduction, convection and gap-gas radiation heat transfer in a fuel rod or structure hardware component. The core rods are modeled with the default stainless steel properties contained in TRACE and with the default convection boundary condition at the rod surface in contact with PIPE 100.

The ambient heat loss from all of the exterior primary system components (with the exception of the PZR) are also modeled in TRACE as a HTSTR. The ambient heat loss was modeled using a radial geometry with an inner vessel radius of 0.146 m, an outer vessel radius of 0.178 m and an outer insulation radius of 0.280 m, as specified in Galvin, 2007. The vessel wall is modeled as stainless steel and the insulation properties were entered into TRACE as a user-defined material. Thermo-12 Gold, a hydrous calcium silicate, is the insulation used in the OSU-MASLWR. The insulation material properties are listed in Table 5.13.

The HSTRT is connected along the entire length of the exterior primary system, including PIPE components 109, 108 and 113 thru 120. The default convection boundary condition is used on the interior boundary while a constant temperature boundary condition of 300 K is used on the exterior boundary.

Table 5.13. Thermo-12 Gold Properties

Physical Property	*T* (K)	*k* $\left(\frac{W}{m \cdot K}\right)$
Specific Heat Capacity	311	1.089
	616	1.089
	811	1.005
Thermal Conductivity	312	0.058
	366	0.059
	422	0.065
	477	0.072
	533	0.079
	589	0.086
	644	0.094

As previously mentioned, the heat transfer through the core barrel between the hot leg riser and the downcomer is of particular concern when evaluating the natural circulation system. The HTSTR is modeled in TRACE using a radial geometry with an inner radius ranging from 0.09855 m to 0.0541 m and an outer radius ranging from 0.1016 m to 0.05715 m. As before, the structure makes use of the default TRACE values for stainless steel. The lengths of 15 axial cells are listed in Table 5.12 and are illustrated in Figure 5.8. The default convection boundary condition is used on both the interior and exterior boundaries of the structure.

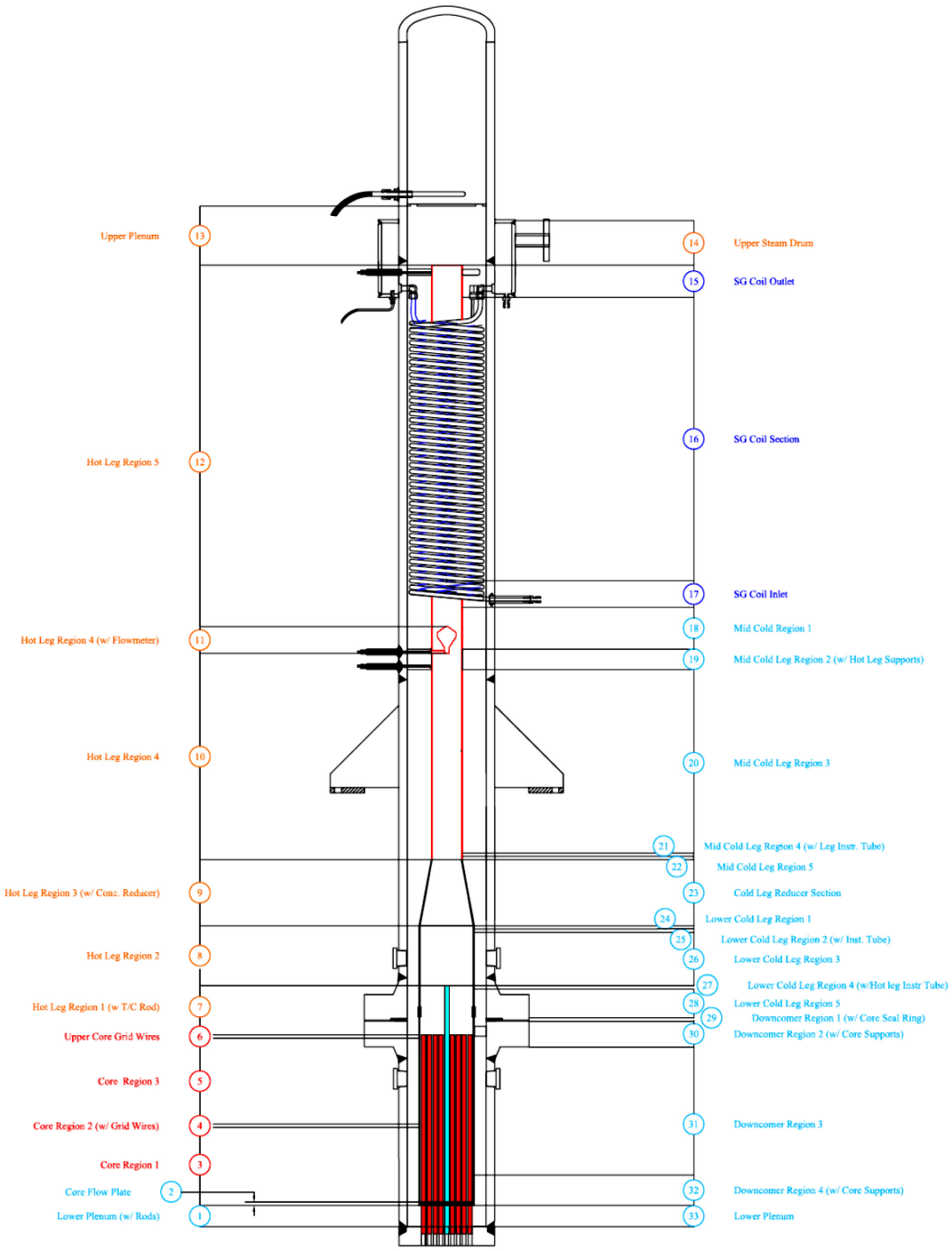

Figure 5.10. OSU-MASLWR Primary System Regions

5.4.2 Secondary System

As seen in Figure 5.8, the secondary system of the OSU-MASLWR is modeled as a PUMP component, a series of PIPEs and a BREAK component.

As mentioned previously, there are three separate parallel sections (coils) of stainless steel tubes. The outer and middle coils consist of five tubes each, while the inner coil consists of four tubes. Each coil is separate from the others and joined at a common inlet header to ensure pressure equilibrium within the coil. In total there are 14 SG tubes with an inner tube radius of 0.0063 m and an outer tube radius of 0.00795 m. Specific geometric data for the SG is listed in Table 5.14.

Table 5.14. Steam Generator Bundle Geometric Data

Bank	*Inner*	*Middle*	*Outer*
Tube Wrap Direction	cw	ccw	cw
Number of tubes in bank	4	5	5
Number of rotations in bank	13	9.5	7.5
Tube spacing (m)	0.0198	0.0211	0.0262
Average tube length of bank (m)	6.05	6.15	6.21
Total bank length (m)	24.20	30.75	31.05
Total tube bank surface area (m^2)	1.209	1.535	1.551

The SG is modeled in TRACE as a HTSTR with a radial geometry, 8 axial nodes and a total length of 86.0 m. It is modeled as stainless steel with convection boundary conditions at the inner surface, PIPE 200, and the outer surface, PIPE 113, as listed in Table 5.15. The boundary conditions at each axial node of the SG utilize the hydro component setting which defines a heat-transfer surface coupled to hydraulic-component cells that are input specified. The heat transfer coefficients and temperatures are evaluated by the TRACE hydrodynamic solution for the gas- and liquid-coolant phases that are heat-transfer coupled to the inner or outer surface.

The OSU-MASLWR main FW pump has a maximum rated flow of 15.9 liters per minute at 1750 RPMs. The maximum discharge pressure is 1500 psig,

and the speed is controlled by a variable speed controller that is adjustable from 0 – 100% rated flow. The main FW pump is modeled as a single junction PUMP component in TRACE. This type of component utilizes a control block to set the value of the liquid and vapor mass flow rates depending on the values from an input table. The control block input function tables are created to simulate the specifics of main FW flow rates in both test cases and the sensitivity analysis. These control blocks utilize the transient time as the input source. A mass flow rate in kilograms per second function is generated based on the transient time.

Table 5.15. Steam Generator Heat Structure Boundary Conditions

Axial Cell	*Inner Surface Boundary Conditions*	*Outer Surface Boundary Conditions*
1	PIPE: 200 CELL: 1	PIPE: 113 CELL: 8
2	PIPE: 200 CELL: 2	PIPE: 113 CELL: 7
3	PIPE: 200 CELL: 3	PIPE: 113 CELL: 6
4	PIPE: 200 CELL: 4	PIPE: 113 CELL: 5
5	PIPE: 200 CELL: 5	PIPE: 113 CELL: 4
6	PIPE: 200 CELL: 6	PIPE: 113 CELL: 3
7	PIPE: 200 CELL: 7	PIPE: 113 CELL: 2
8	PIPE: 200 CELL: 8	PIPE: 113 CELL: 1

The main FW water supply system and the main steam system are modeled in TRACE as BREAK components. The input for the single junction PUMP component is a BREAK component simulating the availability of FW. Similarly, the output for the SG PIPE component serves as the input for the main steam system BREAK component. These BREAK components have initial temperature and pressure conditions that vary with transient time. A user-defined input data interpolation table governs how the pressure, temperature, void fraction and non-condensable gas pressure behave with time. These tables are known as ’component-action tables’ in TRACE. (TRACE Version 3.2.7)

5.4.3 AUTOMATIC DEPRESSURIZATION SYSTEM

The principal facility characteristics of the ADS lines are the multiple elbows, small area to length ratios, and the outlets which provide the appropriate scaled area for the interaction between the RPV and HPC. All of the ADS lines are modeled in TRACE utilizing numerous PIPE and VALVE components. Specific geometric data for all ADS TRACE components is listed in Table 5.16.

Table 5.16. Automatic Depressurization System Geometric Data

TRACE Component	*Component Type*	*Test Facility Region*	*Length (m)*	*Flow Area (m^2)*	*Vertical Angle(°)*	*Hydraulic Diam.(m)*
600-01 to 05	PIPE	From RPV	0.10	9.61×10^{-5}	0.0	0.0111
600-06 to 09	PIPE	ADS Line	0.08	1.39×10^{-4}	0.0	0.0094
601	VALVE	ADS Valve	n/a	1.39×10^{-4}		
602-01 to 04	PIPE	ADS Line	0.08	1.39×10^{-4}	0.0	0.0094
602-05 to 14	PIPE	ADS Line	2.79	9.61×10^{-5}	0.0	0.0111
604	PIPE	Into HPC	0.67	9.61×10^{-5}	-90.0	0.0111
606-01 to 05	PIPE	From RPV	0.10	9.61×10^{-5}	0.0	0.0111
606-06 to 09	PIPE	Sump Line	0.08	1.39×10^{-4}	0.0	0.0094
607	VALVE	Sump Valve	n/a	1.39×10^{-4}		
608-01 to 04	PIPE	Sump Line	0.08	1.39×10^{-4}	0.0	0.0094
608-05 to 14	PIPE	Sump Line	2.80	9.61×10^{-5}	0.0	0.0111
604	PIPE	Into HPC	0.43	9.61×10^{-5}	-90.0	0.0111
612-01 to 05	PIPE	From RPV	0.10	9.61×10^{-5}	0.0	0.0111
612-06 to 09	PIPE	Vent Line	0.08	1.39×10^{-4}	0.0	0.0094
613	VALVE	Vent Valve	n/a	1.39×10^{-4}		
614-01 to 04	PIPE	Vent Line	0.08	1.39×10^{-4}	0.0	0.0094
614-05 to 14	PIPE	Vent Line	1.94	9.61×10^{-5}	0.0	0.0111

Although not utilized in test case one and the sensitivity analysis, the ADS system was modeled in TRACE and was included in all computer runs. The test case two blowdown is simulated by a single ADS vent valve and was experimentally set-up to open at 200 psig after the initial event and always close at 250 psig. This was accomplished in TRACE by a series of control variables

that culminated in open and close logical trips. These trips were used to open and close VALVE 601, thereby simulating the ADS vent valve. The other ADS valves were simulated with trip valves that open once the pressure difference between the HPC and CPV drops below 5 psig.

5.4.4. HIGH PRESSURE CONTAINMENT VESSEL

The HPC vessel was modeled with a single stack of 22 fluid volumes including those initially filled with liquid and the upper fluid volumes which initially contained air. All of the fluid volumes are modeled as PIPE components, including the upper and lower ADS valve connection volumes which are modeled with a cross-flow connection. Many of the PIPE axial lengths were dictated by the location of the heat transfer plate thermocouple banks. Cell lengths were calculated so as to have their midpoint elevation the same as the location of HPC thermocouples. This enabled the comparisons between heat structure mesh points and the wall temperatures. Specific geometric data for all HPC TRACE components is listed in Table 5.17.

As seen in Figure 5.8, the HPC system is made up of two vertically parallel banks of fluid volumes. This intentional modeling technique was done to allow for cross-flow within the HPC during the blowdown phase of test case two. This is accomplished by setting the NAMELIST variable USESJC equal to 3, thereby permitting the use of 22 single junction components that allow for side junction mass flow. Given the appropriate conditions, the use of this technique allows for the establishment of a natural circulation and/or convection phenomena inside the HPC.

Table 5.17. High Pressure Containment System Geometric Data

TRACE Component	*Component Type*	*Test Facility Region*	*Length (m)*	*Flow Area (m^2)*	*Vertical Angle(°)*	*Hydraulic Diam.(m)*
300	PIPE	lower contain	0.25	0.0273	90.0	0.264
301	PIPE	lower contain	0.07	0.0273	90.0	0.264
302	PIPE	lower contain	0.62	0.0273	90.0	0.264
303	PIPE	lower contain	0.43	0.0273	90.0	0.264
304	PIPE	lower contain	0.24	0.0273	90.0	0.264
305	PIPE	lower contain	0.86	0.0273	90.0	0.264
306	PIPE	lower contain	0.11	0.0273	90.0	0.264
307	PIPE	lower contain	0.05	0.0273	90.0	0.264
308-315	PIPE	lower contain	0.98	0.0273	90.0	0.264
316	PIPE	lower contain	0.20	0.0273	90.0	0.264
317	PIPE	lower contain	0.07	0.0273	90.0	0.264
318	PIPE	cone	0.15	0.0566	90.0	0.379
319	PIPE	cone	0.36	0.0566	90.0	0.379
320	PIPE	upper contain	0.30	0.0976	90.0	0.498
321	PIPE	upper contain	0.95	0.0976	90.0	0.498
400	PIPE	lower contain	0.25	0.0273	90.0	0.264
401	PIPE	lower contain	0.07	0.0273	90.0	0.264
402	PIPE	lower contain	0.62	0.0273	90.0	0.264
403	PIPE	lower contain	0.43	0.0273	90.0	0.264
404	PIPE	lower contain	0.24	0.0273	90.0	0.264
405	PIPE	lower contain	0.86	0.0273	90.0	0.264
406	PIPE	lower contain	0.11	0.0273	90.0	0.264
407	PIPE	lower contain	0.05	0.0273	90.0	0.264
408-415	PIPE	lower contain	0.98	0.0273	90.0	0.264
416	PIPE	lower contain	0.20	0.0273	90.0	0.264
417	PIPE	lower contain	0.07	0.0273	90.0	0.264
418	PIPE	cone	0.15	0.0566	90.0	0.379
419	PIPE	cone	0.36	0.0566	90.0	0.379
420	PIPE	upper contain	0.30	0.0976	90.0	0.498
421	PIPE	upper contain	0.95	0.0976	90.0	0.498

The HTSTR attached to the HPC fluid volumes is a heat transfer plate that allows for thermal conduction between the HPC and CPV. The containment condensation plate is modeled between the HPC and the containment cooling pool. The TRACE HTSTR consists of 22 nodes with axial lengths corresponding to the axial lengths and surface areas listed in Table 5.18. The heat transfer

place width is 0.168 m and the thickness is 0.0381 m. It is stainless steel and is modeled in TRACE with a “slab” geometry. As before, the boundary conditions at each axial node of the heat transfer plate utilize the hydro component setting which defines a heat-transfer surface coupled to hydraulic-component cells that are input specified. The heat transfer surface areas are calculated using the width of the plate and the height of the adjacent axial cell.

Table 5.18. High Pressure Containment Heat Structure Boundary Conditions

Axial Cell	*Inner Surface Boundary Conditions*	*Outer Surface Boundary Conditions*	*Length (m)*	*Area (m^2)*
1	PIPE: 300	PIPE: 400	0.25	0.042
2	PIPE: 301	PIPE: 401	0.07	0.0118
3	PIPE: 302	PIPE: 402	0.62	0.0104
4	PIPE: 303	PIPE: 403	0.43	0.0722
5	PIPE: 304	PIPE: 404	0.23	0.0403
6	PIPE: 305	PIPE: 405	0.86	0.144
7	PIPE: 306	PIPE: 406	0.11	0.0185
8	PIPE: 307	PIPE: 407	0.05	0.0084
9	PIPE: 308	PIPE: 408	0.1225	0.0206
10	PIPE: 309	PIPE: 409	0.1225	0.0206
11	PIPE: 310	PIPE: 410	0.1225	0.0206
12	PIPE: 311	PIPE: 411	0.1225	0.0206
13	PIPE: 312	PIPE: 412	0.1225	0.0206
14	PIPE: 313	PIPE: 413	0.1225	0.0206
15	PIPE: 314	PIPE: 414	0.1225	0.0206
16	PIPE: 315	PIPE: 415	0.1225	0.0206
17	PIPE: 316	PIPE: 416	0.20	0.0336
18	PIPE: 317	PIPE: 417	0.07	0.0118
19	PIPE: 318	PIPE: 418	0.15	0.0252
20	PIPE: 319	PIPE: 419	0.36	0.0605
21	PIPE: 320	PIPE: 420	0.30	0.0504
22	PIPE: 321	PIPE: 421	0.95	0.160

5.4.5 COOLING POOL VESSEL

The CPV is modeled in TRACE with PIPE components with axial lengths set up to match their HPC counterparts via the heat transfer plate. The two exceptions are the water volume that extends below the HPC and the air volume

above the HPC. Specific geometric data for all CPV TRACE components is listed in Table 5.19.

Table 5.19. Cooling Pool Vessel Geometric Data

TRACE Component	*Component Type*	*Test Facility Region*	*Length (m)*	*Flow Area (m^2)*	*Vertical Angle(°)*	*Hydraulic Diam.(m)*
500	PIPE	cooling pool	0.19	0.441	90.0	0.749
500	PIPE	cooling pool	0.25	0.441	90.0	0.749
501	PIPE	cooling pool	0.07	0.441	90.0	0.749
502	PIPE	cooling pool	0.62	0.441	90.0	0.749
503	PIPE	cooling pool	0.43	0.441	90.0	0.749
504	PIPE	cooling pool	0.24	0.441	90.0	0.749
505	PIPE	cooling pool	0.86	0.441	90.0	0.749
506	PIPE	cooling pool	0.11	0.441	90.0	0.749
507	PIPE	cooling pool	0.05	0.441	90.0	0.749
508	PIPE	cooling pool	0.98	0.441	90.0	0.749
509	PIPE	cooling pool	0.49	0.441	90.0	0.749
510	PIPE	cooling pool	0.49	0.441	90.0	0.749
511	PIPE	cooling pool	0.20	0.441	90.0	0.749
512	PIPE	cooling pool	0.07	0.441	90.0	0.749
513	PIPE	cooling pool	0.15	0.441	90.0	0.749
514	PIPE	cooling pool	0.36	0.441	90.0	0.749
515	PIPE	cooling pool	0.30	0.441	90.0	0.749
516	PIPE	cooling pool	0.95	0.441	90.0	0.749
517	PIPE	cooling pool	0.93	0.441	90.0	0.749

5.5 COMSOL MODEL DESIGN

COMSOL Version 4.2a was used to construct a model of the OSU-MASLWR test facility. More specifically, this work uses the CFD module with a multi-physics coupling to the heat transfer module to model the test cases outlined earlier. According to the COMSOL Version 4.2a documentation, the CFD module is the premier tool in the COMSOL product suite for sophisticated fluid flow simulations. It states that compressible as well as incompressible flows can be combined with advanced turbulence models and forced and natural convection. Also noted as an important characteristic of the CFD module is its

capability of precisely modeling multi-physics flow simulations such as conjugate heat transfer with non-isothermal flow, fluid-structure interactions, non-Newtonian flow with viscous heating and fluids with concentration-dependent viscosity. Porous-media flow user interfaces allow for isotropic or anisotropic media, as well as automatically combined free flow and porous domains. Additionally, COMSOL features tools for the modeling of complex geometries in both 2D and 3D flows scenarios.

COMSOL, much like TRACE, follows a certain protocol for constructing a model. To begin with, all of the specifications of the model, including the dimensions of the geometry, the properties of the materials, the boundary conditions and initial conditions and any other information that the solver will need to carry out the simulation is provided. A model “wizard” is the user interface and a step-by-step guide aids in the input of the problem specification.

The main “wizard” interface is the model builder. The model builder is the tool where the model is defined, the solver is configured and the results and analysis are specified. This is accomplished by building a model tree. The model tree starts with a default model and additional nodes and node setting are entered based on the problem specification.

A model tree always has a root node, a global definitions node and a results node. The root node has basic settings for the author’s name, default unit settings and other basic information. The global definitions node defines parameters, variables, functions and any other computations that will be used in the model tree. The results node accesses the solution after performing a

computer run and contains tools for post-processing data. The results node initially has five sub-nodes:

1. Data sets: contains a list of the solutions
2. Derived values: defines values to be derived from the solution using a number of post-processing tools
3. Tables: a convenient destination for the derived values, or for results generated by probes that monitor the solution in real-time while the simulation is running
4. Export: defines numerical data, images and animations to be exported
5. Reports: contains automatically generated or custom reports about the model in various programming formats.

Plot sub-nodes are added, as necessary, to define graphs available in the graphics window or for export to plot applications.

In addition to the three nodes just described, two other top-level node types are evident in most models. These include the model and study nodes. These are usually created by the "wizard" when a new model is created. After specifying the type of multi-physics modules are involved (e.g. heat transfer and fluid dynamics) and what type of study is used (e.g. steady-state or time-dependent), the "wizard" automatically creates one node of each type.

Two distinct COMSOL models have been developed that accurately model the test cases; focusing on the material and geometric components directly related to the problem solution. Each test case has its own set of initial and boundary conditions and they will be explained in detail as they pertain to each case. The OSU-MASLWR model was constructed using the computational fluid dynamics module coupled to the conjugate heat transfer module and features non-isothermal laminar flow in test case one and the sensitivity analysis. Test case two is more complicated as it features multi-phase flow. The

techniques used in the model will be further developed in Section 5.5.2. The following sections detail the COMSOL modeling effort of each of the test cases.

5.5.1 Test Case One

As outlined in Section 5.3.1, test case one characterizes the steady-state natural circulation in the primary side during various core power inputs. This is accomplished by configuring the OSU-MASLWR test facility in a natural circulation state and varying the power inputs of the core heaters. Power inputs of the core heaters are increased step by step from 10 percent of full power to 80 percent of full power, with a 10 percent increment at each step. For each power input, the primary side flow rate, hot leg and cold leg temperatures are monitored to determine whether the flow stabilization was achieved. This is accomplished in COMSOL by running a steady-state problem and taking a snapshot of the aforementioned values. Once all data has been collected for a steady-state power level solution, the COMSOL model is altered to replicate the new power level. This is accomplished by changing the heat transfer properties of the core heaters. A full steady-state computer run is done at the new power level and a new set of data collection occurs. This process continued through all the test case one power levels and the results are contained in Section 6.1.

As previously mentioned, the COMSOL CFD module was used to model test case one. The CFD module's general capabilities include stationary and time-dependent flows in 2-D and 3-D spaces. Formulations of different types of flow are predefined in a number of user interfaces, referred to as fluid flow interfaces. The fluid flow interfaces use physical quantities, such as pressure

and flow rate, and physical properties, such as viscosity and density, to define a fluid flow problem. These will be explained below as they pertain to test case one. There are different fluid flow interfaces that cover a wide range of flows: for example, laminar flow, turbulent flow, single-phase flow and multiphase flow.

5.5.1.1 Model Set-Up and Material Properties

According to the COMSOL Version 4.2a manual, the non-isothermal flow branch included with the CFD module license has a number of options to describe momentum transport. One or more of them are added, either singularly or in combination with other interfaces such as mass and energy transfer. Since COMSOL features a multi-physics interface, the physics for modeling fluid flow, which can be laminar or turbulent, as well as heat transfer are included. Test case one features steady-state single-phase non-isothermal flow coupled with heat transfer.

The test case one COMSOL model utilizes the non-isothermal laminar flow interface along with a 3-D space dimension in building the geometry. This interface models slow-moving flow in environments where energy transport is also an important part of the system and application, and must coupled or connected to the flow in some way. The COMSOL Version 4.2 manual states that processes where natural convection are an important component are classic areas for such modeling. This interface solves the Navier-Stokes equations, developed in Chapter 3, together with an energy balance assuming heat flux through convection and conduction. The dependent variables chosen as global variables include the velocity field,$\vec{v}$, pressure, p and temperature, T.

Materials used in the conduct of test one include SA312 TP304 Schedule 140 stainless steel and water; both of which are included in a built-in selection of materials within COMSOL. Table 5.20 lists the material properties for these two built-in selections:

Table 5.20. Test Case One Material Properties

Property (units)	*Stainless Steel*	*Water*
Heat capacity (J/kg·K)	475	C_p
Thermal conductivity (W/m·K)	44.5	k
Density (kg/m^3)	7850	ρ
Dynamic viscosity (Pa·s)	n/a	μ

where C_p is temperature dependent and is shown in Eqn. 5.2:

$$C_p = 12010.15 - 80.41T + 0.31T^2 - 5.38x10^{-4}T^3 + 3.63x10^{-7}T^4 \quad (5.2)$$

where T ≡ temperature (K)

k is temperature dependent and is shown in Eqn. 5.3:

$$k = -0.87 + 0.0089T - 1.58x10^{-5}T^2 + 7.98x10^{-9}T^3 \quad (5.3)$$

ρ is temperature dependent and is shown in Eqn. 5.4:

$$\rho = 838.47 + 1.4T - 0.003T^2 + 3.72x10^{-7}T^3 \quad (5.4)$$

μ is temperature dependent and is shown in Eqn. 5.5:

$$\mu = 1.3799 - 0.021T + 1.36x10^{-4}T^2 - 4.65x10^{-7}T^3 + 8.9x10^{-10}T^4 \quad (5.5)$$

5.5.1.2 GEOMETRY

The COMSOL test case one model includes the RPV, the core, the HL riser, the upper plenum, the SG, and the cold leg downcomer. The following sections describe the development of these model parts in COMSOL.

From Galvin, the RPV shell consists of four sections: lower shell, exchanger section, coil section, and PZR section. The lower surface of the

cylindrical lower shell is planar, the exchanger and coil sections are right circular cylinders, and the upper head of the cylindrical PZR section is hemispherical. Nominal 14” SA312 TP304 Schedule 140 stainless steel (SS) pipe with an outside diameter (OD) of 35.56 cm, an inside diameter (ID) of 29.21 cm, and a wall thickness of 3.175 cm is used to construct all sections. Thermo-12 hydrous calcium silicate insulation, with a 10.2 cm thickness, surrounds the RPV shell. Contrary to the TRACE model, the COMSOL model does not contain the insulation as part of the geometry. Section 5.5.1.4 describes the specific initial and boundary conditions present at the RPV and insulation boundary. The core seal ring at the joint between the lower shell and the exchanger section defines the zero reference level for elevation measurements, and this reference location is 167 cm above the facility floor. The RPV shell has penetrations for the steam generator, PZR heaters, over-pressure safety valve, automatic depressurization system (ADS) vent lines, ADS blowdown lines, ADS sump recirculation lines, vessel fill and drain lines, core heater elements, and instrumentation. However, the test protocol of test case one does not include the use of the ADS, HPC and CPV. Consequently, they are not included in the COMSOL model geometry.

The COMSOL model of the RPV consists of a single right circular cylinder constructed of stainless steel and 3.7783 m in height and 3.175 cm in thickness on the bottom and shell of the cylinder. The top of the cylinder is modeled with no thickness. The PZR section is a hemisphere, also constructed of stainless steel, with a height of 0.6414 m, and it sits centered on the top of the right

circular cylinder. Figure 5.11 illustrates the RPV COMSOL geometry (all measurements are in meters):

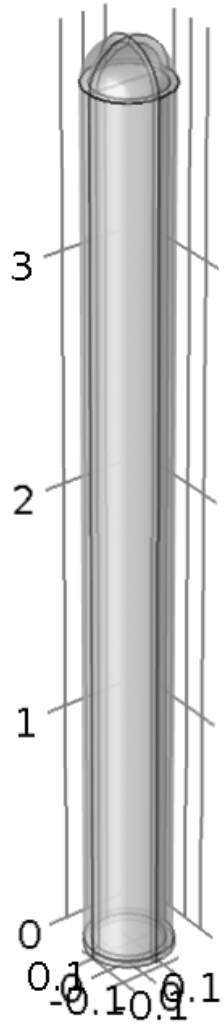

Figure 5.11. Reactor Pressure Vessel COMSOL Geometry

The RPV houses the core, and the model contains 57 cylindrical rods distributed in a 1.86 cm pitch square array with a 1.33 pitch to diameter ratio. The core rods are SA312 TP304 SS watertight penetrations via the lower core plate of the RPV lower shell, into which either an electric heater (one of 56) or a thermocouple array (center rod only) is inserted. From Galvin, each core heater

rod is 73.7 cm long with an external diameter of 1.59 cm and a heated length of 57.5 cm. The nominal power of each heater rod is 7.1 kW that yields a 398 kW maximum power.

The core is shrouded to separate the downcomer region from the core region and ensure all flow enters the core via the lower plenum and travels the entire heated length of the rods. More specifically, the flow exits the unrodded lower plenum region below the downcomer radially inward into the rodded (but unheated) lower plenum region, then upward into bottom of the core via the 20.3 cm diameter and 1.27 cm thick lower core plate. The rodded lower core flow plate holes are oversized at 1.72 cm diameter to create a flow annulus between the flow plate and the heater rods. In addition to the 57 core rod flow holes, the lower flow plate contains 76 auxiliary flow holes with a 0.635 cm diameter each and arranged at the same 1.86 cm square pitch. Table 5.21 lists the lower core plate geometric data.

Table 5.21. Lower Core Plate Geometric Data

Component	*Number*	*Diameter (cm)*	*Square Pitch (cm)*
Lower core plate	1	20.3	
Heater Rods	56	1.59	1.86
Thermocouple rod	1	1.59	
Heater rod flow holes	57	1.72	
Auxiliary flow holes	76	0.635	1.86

Figure 5.12 illustrates the arrangement of the lower core plate in an *x-y* plane view.

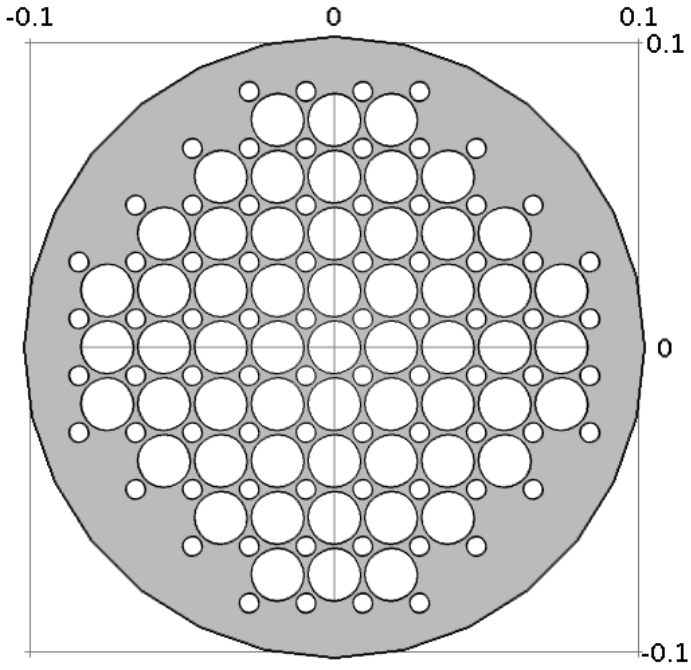

Figure 5.12. Lower Core Plate (*x*-*y* Plane View)

To ensure that each heater rod receives roughly equal axial coolant flow, the core shroud is designed to partially block the primary coolant flow through the outermost auxiliary flow holes. The amount of blockage is dependent on the number and location of heater rods adjacent to each auxiliary flow hole. The total flow area of each auxiliary flow hole is divided into four equal sized quadrants, and flow is permitted through the quadrant only if there is a core rod flow hole adjacent to that quadrant. Figure 5.13 illustrates the design of the core shroud from the –*z* axis perspective. The test facility contains core grid wires at the axial mid-plane of the core shroud to maintain the radial alignment of the heater rods. The COMSOL model does not account for these wires due to their size and negligible contribution to fluid flow or heat transfer,. Note the lower core plate and the varying blockage of the perimeter auxiliary flow holes.

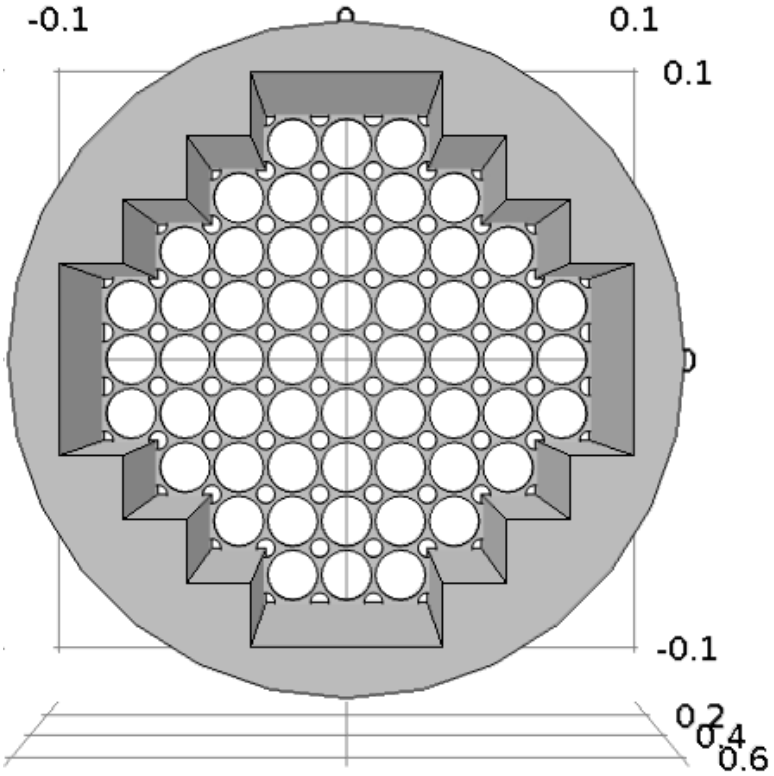

Figure 5.13. Core Shroud (-z Axis View)

After passing vertically across the heater rods, the flow exits the core vertically into the hot leg riser. Figure 5.14 illustrates the core as it sits inside the RPV. Note the presence of the unheated rods protruding below the lower core plate.

After leaving the core, the flow enters the chimney of the hot leg riser. The hot leg riser, extending above the core shroud from the chimney to the upper plenum, creates a riser/downcomer configuration to enable natural circulation. The lower region (chimney) of the hot leg riser is constructed from 8” Schedule 40 SS304 pipe with an OD of 20.32 cm, an ID of 19.71 cm, and a wall thickness of 0.305 cm. The upper region of the hot leg riser is constructed from 4”

Schedule 40 SS304 pipe with an OD of 11.43 cm, an ID of 10.23 cm, and a wall thickness of 0.602 cm.

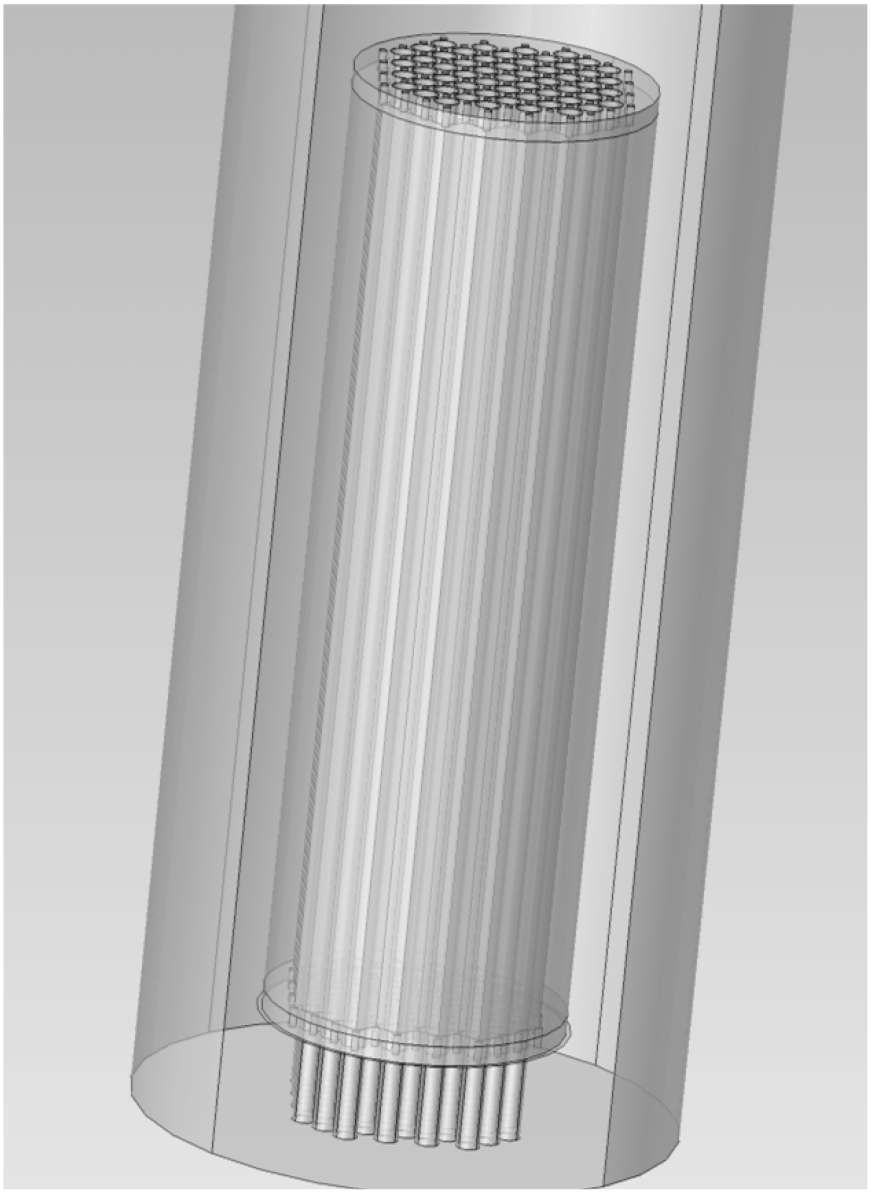

Figure 5.14. Full Core Geometry with Heater Rods

The transition from the lower to upper hot leg riser regions is accomplished with a 0.305 cm thickness SS304 cone. The cone has a half angle of 20.61 and spans an elevation change of 24.45 cm. The upper hot leg riser

exits into the upper plenum region at the bottom of the PZR section below the upper baffle plate. Figure 5.15 illustrates the hot leg riser design.

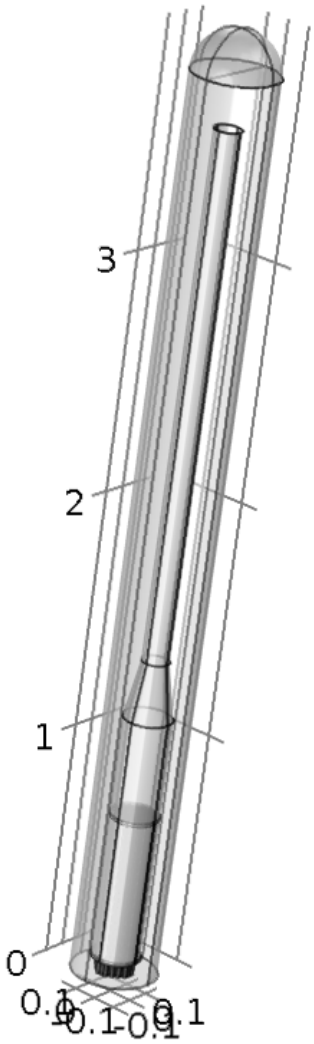

Figure 5.15. Hot Leg Riser (shown in RPV with Core Shroud)

After leaving the top of the hot leg riser, the flow enters the upper plenum. The upper plenum directs the flow radially outward and then down into the steam generator coil bundle of the steam generator section. The upper plenum is separated from the heated upper PZR section by a 0.95 cm thick baffle plate, at 308.6 cm above reference. The baffle plate has eight 2.54 cm diameter holes,

radially located at 12.7 cm and spaced uniformly around the baffle plate periphery which allows free communication of the PZR pressure to the remainder of the RPV during normal operation and for volume surges into and/or out of the PZR due to transients. Based on the justification provided in Section 5.4.1, the baffle plate is modeled with no holes and the PZR is eliminated for test case one and the sensitivity analysis. A constant pressure is maintained inside the RPV by establishing a constant set-point based on the operating pressure of the test facility. The PZR will be explored further in Section 5.5.2.

The SG of the test facility is a once through heat exchanger and is located within the RPV in the annular space between the hot leg riser and the inside surface of the RPV. As seen in Figure 5.16, the tube bundle consists of three concentric coils of stainless steel tubes.

Figure 5.16. Concentric Steam Generator Coils (Galvin)

The number of nodes created when generating a FEM mesh can rise exponentially in the presence of complex 3D geometry or large structures that cannot be simplified into 2D models based on symmetry. Therefore, the complexity, and directly proportional CPU run time, of the problem's geometry

must be minimized when formulating the best approach at modeling the physical structure. The SG presented here, in its originally designed form, creates an overly cumbersome number of nodes when introduced into the entire geometry of the MASLWR test facility. When modeled in its original form, the 14 tubes of the SG generate over 1,225,000 nodes, with an average mesh quality of 0.4886. Although the high mesh quality is desirable, this is roughly one quarter the number of nodes in comparison to the remainder of the MASLWR test facility's geometry. The addition of this number of nodes will exponentially increase the CPU time for a solution.

In order to reduce the number of nodes, and therefore reduce the computational effort, the SG's three banks of concentric helical tubes have been consolidated into one simplified helical SG. Figure 5.17 shows the arrangement of the helix in relation to the hot leg riser (shown values are in meters). Table 5.22 lists the geometric data for the simplified SG:

Table 5.22. Simplified Steam Generator Geometric Data

Property (units)	*Value*
Number of turns	30
Major radius (m)	0.1016
Minor radius (m)	0.0160
Axial pitch (m)	0.0352

A novel SG meshing technique and computational results from existing data is developed in Section 5.5.1.3

The flow continues downward through the steam generator section and into the cold leg downcomer region. The cold leg downcomer region is an annular region bounded by the RPV wall ID on the outside and the hot leg riser

OD on the inside, and the flow area reduces at the hot leg riser cone and core shroud. The flow exits the cold leg downcomer region into the lower plenum to complete the primary flow circuit as is illustrated in Figure 5.15.

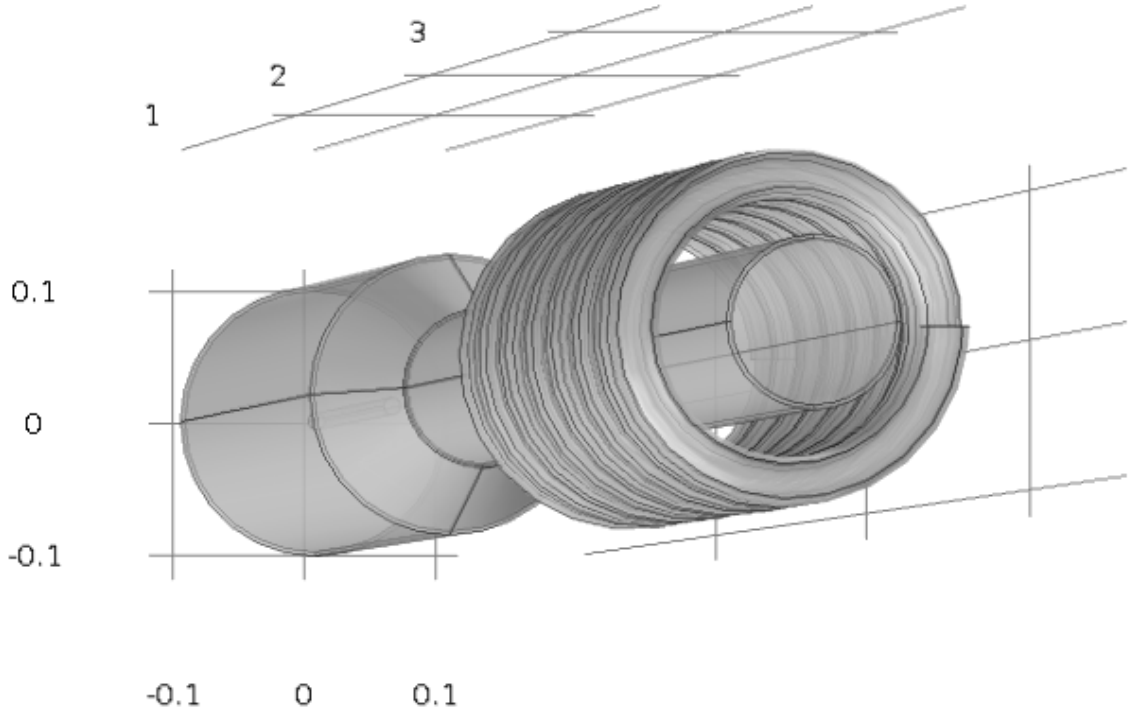

Figure 5.17. Simplified Steam Generator Configuration

5.5.1.3 MESH TECHNIQUES

For 3-D geometries, COMSOL's mesh generator discretizes the domains into tetrahedral, hexahedral, prism or pyramid mesh elements. The boundaries in the geometry are discretized into triangular or quadrilateral boundary elements, while the geometry edges are discretized into edge elements. The default COMSOL setting is to use a mesh that is controlled by the physics. The mesh is then adapted to the current multi-physics settings in the model. For fluid flow a somewhat finer set of defaults is used in comparison to those elements that experience conductive heat transfer only. For the two test cases and the

sensitivity analysis, the COMSOL physics-controlled mesh settings were utilized. Table 5.23 lists the default COMSOL 3-D physics-controlled settings for both general physics (heat transfer) and fluid dynamics:

Table 5.23. COMSOL Default 3-D Physics-Controlled Mesh Settings

Parameters (units)	*Fluid Dynamics*	*General Physics*
Maximum element size (m)	0.141	0.2
Minimum element size (m)	0.0624	0.36
Maximum element growth rate	1.2	1.5
Resolution of curvature	0.7	0.6
Resolution of narrow regions	0.6	0.5

The COMSOL Version 4.2a manual defines the maximum element growth as the degree to which the element size can grow from a region with small elements to a region with large elements. The value must be greater than or equal to one. A maximum element growth rate of 1.25 means the element size can grow by at most 25% from one element to another. The resolution of curvature is defined as the size of boundary elements compared to the curvature of the geometric boundary. The curvature radius multiplied by the resolution of curvature, which must be a positive scalar, gives the maximum allowed element size along the boundary. Higher values yield a more coarse mesh along curved boundaries. The resolution of narrow regions is defined as the number of layers of elements that are created in narrow regions. The value must be a non-negative scalar.

The default fluid dynamics physics-controlled mesh settings were applied to the working fluid inside the RPV resulting in the generation of 55,543 tetrahedral mesh elements. The general physics mesh was applied to all other materials in the model, including the RPV, the core and the chimney (SG

meshing is discussed subsequently). Figures 5.18 and 5.19 illustrate the physics-controlled meshing of the core.

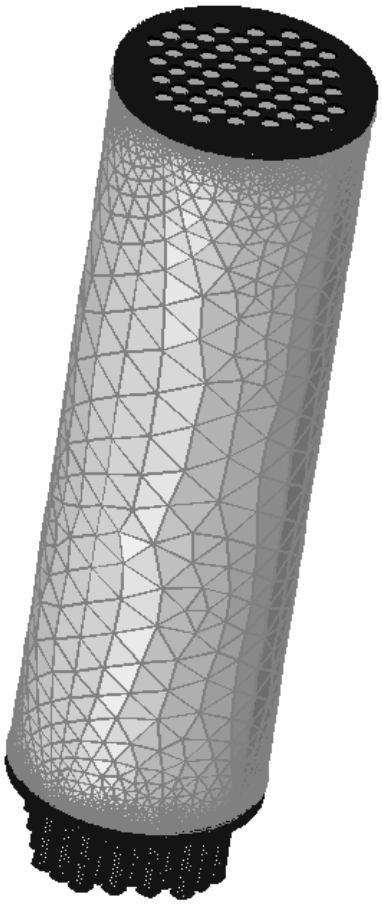

Figure 5.18. Core Mesh

As stated earlier, when modeled in its original form, the 14 tubes of the SG generate over 1.23 x 10^6 nodes, with an average mesh quality of 0.4886. This mesh technique relies on the previously detailed physics-controlled mesh. Continuing to apply the physics-controlled meshing on the simplified helix does decrease the number of nodes substantially, but still poses a computational penalty. When utilizing the default physics settings for fluid dynamics, the number of nodes is decreased to 4.0 x 10^5, but the mesh minimum quality drops

to less than 0.1. This is outside the acceptable range of mesh quality for solution convergence. Therefore, a user-controlled meshing technique is explored to further decrease the number of nodes without sacrificing quality. This is accomplished through a technique referred to as “slice nodalization”.

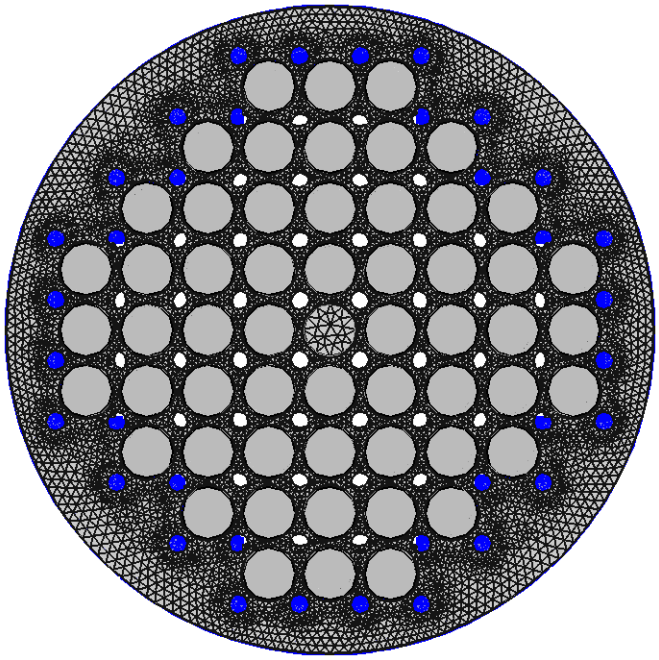

Figure 5.19. Core Mesh (*x-y* Plane View)

This technique involves creating a triangular mesh at one end of the helix while conforming to the mesh quality standards previously discussed. Next, a slice technique is utilized to replicate the triangular mesh at a fixed interval length, the “slice length” along the entire length of the helix. The fixed interval is modified to control the number of nodes while maintaining the desired mesh quality. Lastly, each boundary layer “slice” is converted from a rectangle into two triangles by dissection. This ensures the boundary layer between the helix and the external working fluid is composed of triangular elements, which is a

requirement in FEM analysis. Table 5.24 lists the fixed interval lengths, "slice lengths," along with the total number of nodes in the entire helix and mesh quality:

Table 5.24. Simplified Steam Generator Mesh Data

Parameters (units)				
Number of end triangles	86	64	40	40
"Slice Length" (m)	0.0050	0.0075	0.010	0.0125
Total nodes	329810	204270	76720	56840
Mesh quality	0.4266	0.3850	0.3124	0.1985

As can be seen in Table 5.24, there is a maximum effective "slice length" of approximately 0.01 meters that meets the criteria for minimal mesh quality of 0.2. This "slice length" was applied to the SG and used as the maximum length in creating a boundary mesh with the adjacent primary coolant when included in the COMSOL model. Figure 5.20 illustrates a detailed view of one end of the helical SG and its associated triangular end pieces and "sliced" dissected boundary elements that run along the length of the helix.

The methodology described herein is applied to a basic helical coil heat exchanger in a series of COMSOL comparison examples to check for solution accuracy. Figure 5.21 shows the unmeshed layout of the heat exchanger (shown values are in meters).

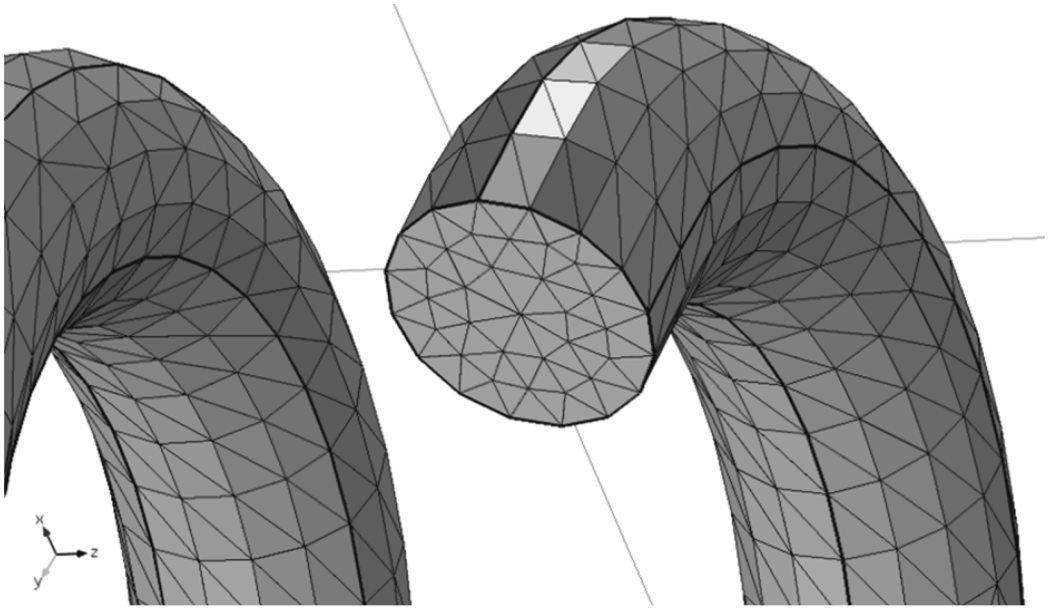

Figure 5.20. Detailed Mesh of Simplified Steam Generator

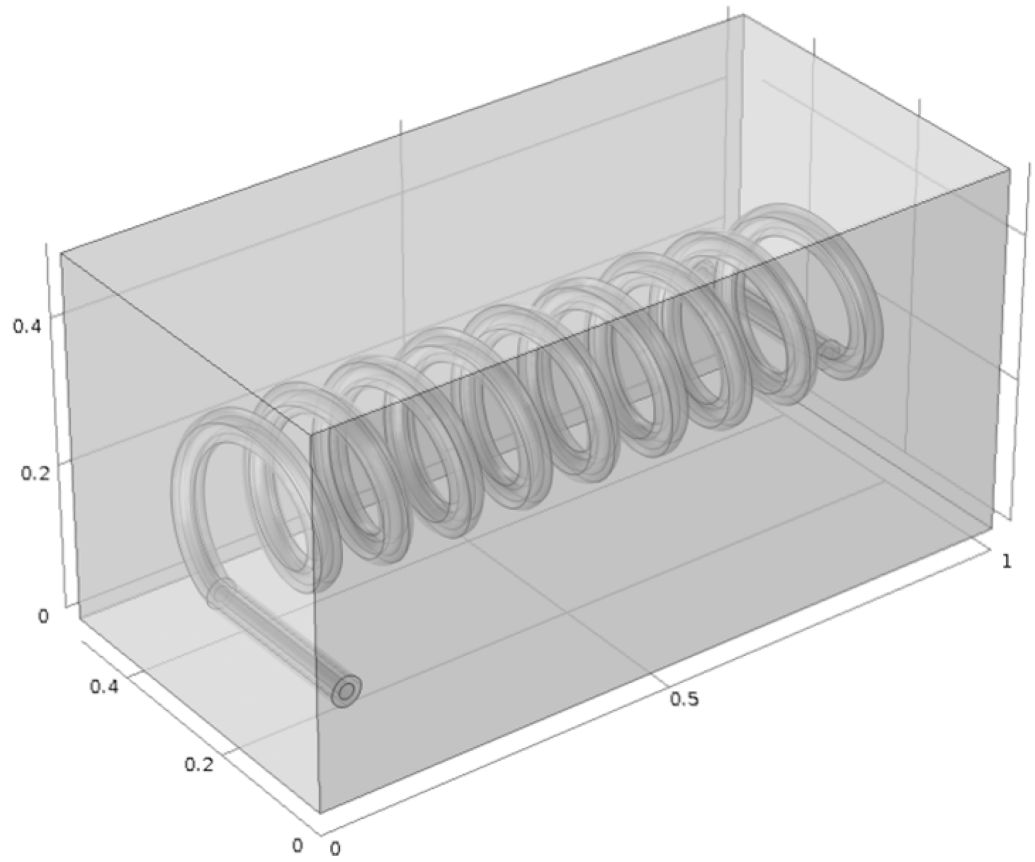

Figure 5.21. Unmeshed Helical Coil Heat Exchanger

In two of the examples, the helix is treated in the traditional sense with a tube side working fluid. The other two examples involve the use of a solid helix with comparable heat transfer properties that eliminates the tube side working fluid. The four examples are:

1. Helix with a tube side working fluid (traditional meshing)
2. Helix with a tube side working fluid ("slice" meshing)
3. Solid helix with comparable heat transfer properties (traditional meshing)
4. Solid helix with comparable heat transfer properties ("slice" meshing)

In the traditional meshing examples, the COMSOL default for physics-controlled meshing is utilized. The "slice" meshing technique described earlier is utilized in the other two examples.

Table 5.25 lists the total number of nodes and mesh quality for each example. The solid helix—"slice" test example contains the smallest number of nodes, and therefore the least CPU burden without sacrificing mesh quality. Obviously, the removal of the tube side working fluid eliminates the boundary layer between the working fluid and the inside of the thin walled helical tube, thereby vastly reducing the number of nodes in both the solid helix test examples.

Table 5.25. Helical Coil Examples Mesh Data

Example	*Number of Nodes*	*Mesh Quality*	*Time (sec)*
Tube Side Fluid—Traditional	1.0496×10^6	0.5681	1.1727×10^5
Tube Side Fluid—"Slice"	611974	0.3159	68377
Solid Helix—Traditional	557542	0.6871	62295
Solid Helix—"Slice"	324588	0.2984	26267

Each COMSOL example involved a steady state analysis of the heat exchanger with a shell side temperature and mass velocity of T_{shell} = 300.0 K and

v_{shell} = 0.2 m/s. The tube side initial temperature and mass flow rates are T_{tube} = 200.0K and v_{tube} = 0.1 m/s. The results of the example cases produced comparable results across a wide range of output data, including tube side exit temperatures and shell side temperatures at various locations along the axial length of the helix.

Figure 5.22 illustrates the tube side exit temperatures for both the tube side fluid—traditional example and the tube side fluid—"slice" example. The comparable results support the use of the "slice" technique in full scale geometry FEM analyses where the secondary fluid is contained in the tube. In these cases the CPU time is reduced by 40%.

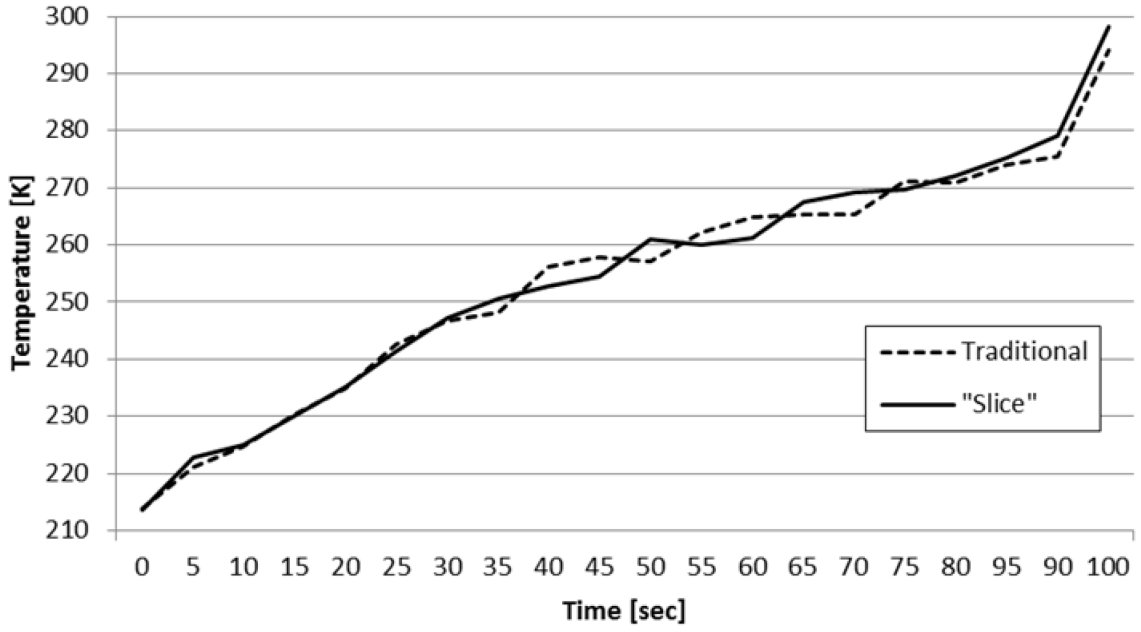

Figure 5.22. Tube Side Exit Temperatures

Figure 5.23 illustrates the shell side temperatures at the geometric midpoint of the shell along the axial length of the helix for the solid helix—

traditional case and the solid helix—"slice" case. These comparable temperatures support the use of the simplified geometry in replicating the heat transfer properties of the SG, and also result in a 58% reduction of CPU time.

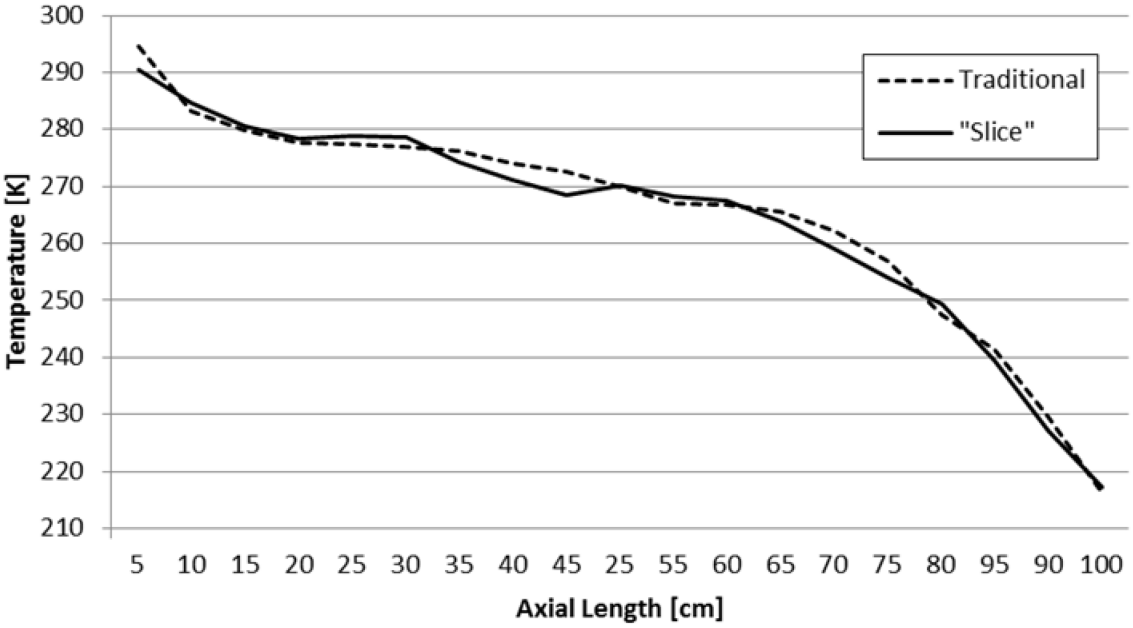

Figure 5.23 Shell Side Axial Temperatures

The methodology presented here is one example of the simplification techniques, including the use of geometric symmetry, used to reduce the computational effort required of FEM. As demonstrated, the simplified helical mesh "slice" technique accounts for a savings of over 4.3 x 10^5 nodes in the tube side working fluid test cases and 2.3 x 10^5 nodes in the solid helix cases. Consequently, the CPU run time is reduced by an average of 49% in both sets of test cases.

Additionally, as can be deduced from the figures presented, the SG is treated as a solid helix without a tube side secondary liquid and vapor mixture. The heat transfer properties of the SG were modeled to approximate the

experimental data. These properties can be modified based on the relationship between the heat flux across the SG tubes and a corresponding FW flow rate.

5.5.1.4 Multi-Physics Including Initial and Boundary Conditions

The multi-physics settings in COMSOL require the user to input various initial and boundary conditions based on the types of physics involved, the materials present and the complexity of the model's geometry. The non-isothermal interface then solves the set of equations previously developed in Chapter 3. These equations are summarized below.

$$\nabla \cdot \vec{v} = 0 \tag{5.6}$$

$$\rho_0 \left(\frac{\partial \vec{v}}{\partial t} + \vec{v} \cdot \nabla \vec{v}\right) = -\nabla p + \mu \nabla \cdot [(\nabla \vec{v}) + (\nabla \vec{v})^T] + \rho_0 \vec{f} + \rho_0 \vec{g} \beta (T - T_0) \tag{5.7}$$

$$\rho_0 C_v \left(\frac{\partial T}{\partial t} + \vec{v} \cdot \nabla T\right) = \nabla \cdot (k \nabla T) + \bar{\bar{\tau}} : \bar{\bar{s}} + q''' \tag{5.8}$$

Recalling Eqns. 5.6 – 5.8 are valid for a fluid region. In the presence of a solid region, annotated with an *s*, the fluid velocity is zero and Eqns. 5.6 and 5.7 are not relevant. The energy equation for the solid region is given by:

$$\rho_s C_s \frac{\partial T}{\partial t} = \nabla \cdot (k_s \nabla T) + q_s''' \tag{5.9}$$

Additionally, as was developed in Chapter 3, Eqn. 5.7 contains the buoyancy force arising from the temperature corrected density. This application of the Boussinesq approximation is valid in both test cases and the sensitivity analysis. Lastly, Eqn. 5.9 assumes the solid region is stationary with respect to the coordinate frame, such that the nonlinear part of Eqn. 5.8 need not be considered.

The initial and boundary conditions for test case one replicate those outlined in Section 5.3.1 and are applied to the COMSOL model via the “wizard” function previously discussed. The fluid properties feature of the “wizard”, in providing inputs for Eqn. 5.7 above, provides an interface for defining the material properties of the fluid. Unless noted here, the default fluid property values from COMSOL are utilized based on the built-in material properties library. The initial values feature of the “wizard” adds initial values for the velocity field, temperature and the pressure that serve as the initial guess for the solver. The velocity field, temperature and the pressure for test case one are outlined in Section 5.3.1.

Test case one varies the thermal output of the heater rods across a set of pre-defined power settings. This is accomplished by establishing a heat source. The heat source feature describes heat generation within a specified domain, in this case, the 56 heater rods. The heat source can be specified in terms of a heat per unit volume in the domain, as a linear heat source, or as a total heat source (power). The later choice is used in test case one by defining the total power setting for each level and distributing it evenly across the 56 heater rods.

Boundary conditions for the non-isothermal flow interface include wall conditions and a pressure point constraint. A no-slip boundary condition, the default COMSOL setting for all stationary solid surfaces, is established at the interface of all fluid/solid surfaces. The pressure point constraint feature adds a pressure constraint at a point in lieu of a pressure level boundary condition. If it is not possible to specify the pressure level using a boundary condition, as is the

case in this COMSOL model, the pressure must be set in some other way. In test case one this is accomplished by specifying a fixed pressure at the top of the upper plenum and baffle plate interface.

Of special note is the lack of the thermal insulation in the COMSOL models. The intent of the thermal insulation at the test facility is to make the heat flux normal to the boundary negligible. The inclusion of the thermal insulation in the TRACE cases did little to increase the CPU time required for each computational run. COMSOL, however, requires the thermal insulation to be meshed and therefore increase the CPU time exponentially based on an increased number of nodes. Therefore, a zero heat flux boundary condition was set on all outside surfaces of the RPV to decrease computational time.

5.5.1.5 SOLVER SETTINGS

Test case one features eight varying power levels spread out over a specified time period. As previously discussed, the CPU time required for a time-dependent study in COMSOL is much more cumbersome than a steady-state solution. Therefore, eight steady-state computation runs were performed for each power level. These steady-state runs each features a set of initial and boundary conditions specific to that power level, including the changing of the mass flow rates of the secondary system by varying the heat transfer properties of the simplified SG model.

The steady-state computational runs were accomplished utilizing the default solve settings for the non-isothermal flow interface. The default settings establish the initial values of the variables solved based on the initial conditions.

The stationary solver utilizes an iterative linear algebraic method called the generalized minimum residual (GMRES) solver.

The COMSOL Version 4.2a manual states that this solver is an iterative method for general linear systems. For fast convergence it is important to use an appropriate pre-conditioner, therefore, the iterative node specifies the number of iterations the solver performs until it restarts (the default is 50). A larger restart value increases the robustness of the interactive procedure, but it also increases memory use and computational time. For large problems, the computational cost is often very large to produce a pre-conditioner of such a high quality that the termination criteria are fulfilled for a small number of iterations and for a small restart value. For those problems it is often advantageous to set up a pre-conditioner with a somewhat lesser quality and instead increase the restart value or iterate more steps. Doing so typically increases the condition number for the preconditioned system, so an increase in the error-estimate factor might be needed as well. If the solver does not converge, it terminates when it reaches the default value of 10,0000 in the maximum number of iterations field.

When using the iterative solver, COMSOL estimates the error of the solution while solving. Once the error estimate is small enough, as determined by the convergence criterion, the computational run terminates and returns a solution.

5.5.2 TEST CASE TWO

As outlined in Section 5.3.2, test case two replicates the thermo-hydraulic coupling between the primary system and the high-pressure containment (HPC)

system. The purpose of this test, a design basis accident for the MASLWR concept design, is to determine the behavior of the RPV and containment pressures and core inlet and outlet temperatures following an actuation of an ADS vent valve and subsequent blowdown.

More specifically, test case two simulates the loss of FW, activation of safety systems and the long term cooling of the OSU-MASLWR test facility to determine the progression of a loss of FW transient. The test begins by bringing the OSU-MASLWR test facility to steady state at 75% power (300 kW) with a primary pressure of 8.72 MPa(g) and the main feed pump running on the secondary side.

Once the initial conditions are reached the test is initiated by stopping the main feed pump thus cutting off flow to the SG. With the subsequent loss of the reactor heat sink the primary pressure will begin to rise. When the PZR pressure reaches 8.963 MPa(g) the OSU-MASLWR core heaters will be set to decay power and the one line of the ADS vent system opens on a pressure reading of 9.064 MPa(g). This causes the primary system under rising pressure to vent into the high-pressure containment. The ADS blowdown system operates in automatic mode to vent the primary system to the high-pressure containment while at the same time preventing the high pressure containment from exceeding its maximum operating pressure of 2.068 MPa(g). When the difference between RPV pressure and HPC pressure is less than 0.034 MPa, the remaining ADS vent valves and ADS sump values open and long-term cooling is started. Test case two continues until the PZR pressure drops below 0.517 MPa(g) or five

hours have elapsed since commencing the procedure.. This is accomplished in COMSOL by running two time-dependent studies. The first time-dependent study is initiated at the time the core heaters begin decay power and the pressure inside the RPV is set at 9.064 MPa(g) and continues for 120 seconds. The second time-dependent study is initiated at long-term cooling initiation (approximately 4114 seconds) and continues for five hours.

As previously mentioned, the COMSOL CFD module was used to model test case one. The CFD module's general capabilities include stationary and time-dependent flows in 2-D and 3-D spaces. Formulations of different types of flow are predefined in a number of user interfaces, referred to as fluid flow interfaces. The fluid flow interfaces use physical quantities, such as pressure and flow rate, and physical properties, such as viscosity and density, to define a fluid flow problem. These will be explained below as they pertain to test case two.

5.5.2.1 Model Set-Up and Material Properties

The multiphase flow branch included with the COMSOL CFD module has a number of interfaces to describe momentum transport for multiphase flow. One or more interfaces can be added from the "wizard"; either singularly or in combination with other interfaces for application such as mass transfer and energy (heat) transfer.

According to the COMSOL Version 4.2a manual, the two-phase flow, level set interface included with the CFD module license has a number of options to solve for situations where the interphase of the fluids is changing or moving. In

this interface, a contour line of the globally defined function, the level set function, represents the interface between two phases. With the level set interface, the fluid-fluid interface can move within any velocity field.

The level set method is a technique to represent moving interfaces or boundaries using a fixed mesh. It is useful for geometries where the computational domain can be divided into two domains separated by an interface, as in test case two. The interface is represented by a certain level set of a globally defined function, the level set function, ϕ. In COMSOL, ϕ is a smooth step function that equals zero in a domain and one in the other. Across the interface, there is a smooth transition from zero to one. The interface is defined by the 0.5 isocontour, or the level set, of ϕ.

The interface moves in relation to the velocity field, $\vec{v}$ through a numerical stabilization technique involving the mesh size. Eqn. 5.10 shows the balance between the correct motion of the interface and the numerical stability based on the mesh size.

$$\frac{\partial \phi}{\partial t} + \vec{v} \cdot \nabla \phi = \gamma \nabla \cdot \left(\varepsilon \nabla \phi - \phi(1-\phi) \frac{\nabla \phi}{|\nabla \phi|} \right) \tag{5.10}$$

where γ ≡ numerical stability parameter

ε ≡ thickness of the region where ϕ goes from zero to one

The parameter γ determines the amount of re-initialization or stabilization of the level set function. The COMSOL Version 4.2a manual suggests a suitable value for γ is the maximum magnitude of the velocity field. By default, ε is constant within each domain and equals the largest value of the mesh size within the domain.

Although not directly coupled in the interface, the multi-physics nature of COMSOL allows for the inclusion of heat transfer in both fluids and solids. This coupling is necessary for the inclusion of the decay heat generated by the heater rods, the heat transfer in the fluid as it traverses the natural circulation loop and the heat transfer plate interface between the HPC and the CPV.

Materials used in the conduct of test two include SA312 TP304 Schedule 140 stainless steel, air, water and steam; all of which are included in a built-in selection of materials within COMSOL.

5.5.2.2 GEOMETRY

The RPV geometry used in test case two mirrors that of test case one. As outlined in Section 5.5.1.2, the RPV, core and HL riser make up the primary system. At the start of test case two, the core is set to a decay power that follows a time dependent set of values as listed in Table 5.8. The core continues to decay in power from an initial core power level of 300 kW to a minimum value of 3 kW in a five hour time period.

The 2-D geometry used in test case two provided several areas for simplification. A “slice” along the $y = 0$ plane of the entire facility was modeled in COMSOL. Figure 5.24 illustrates the 2-D RPV model for test case two.

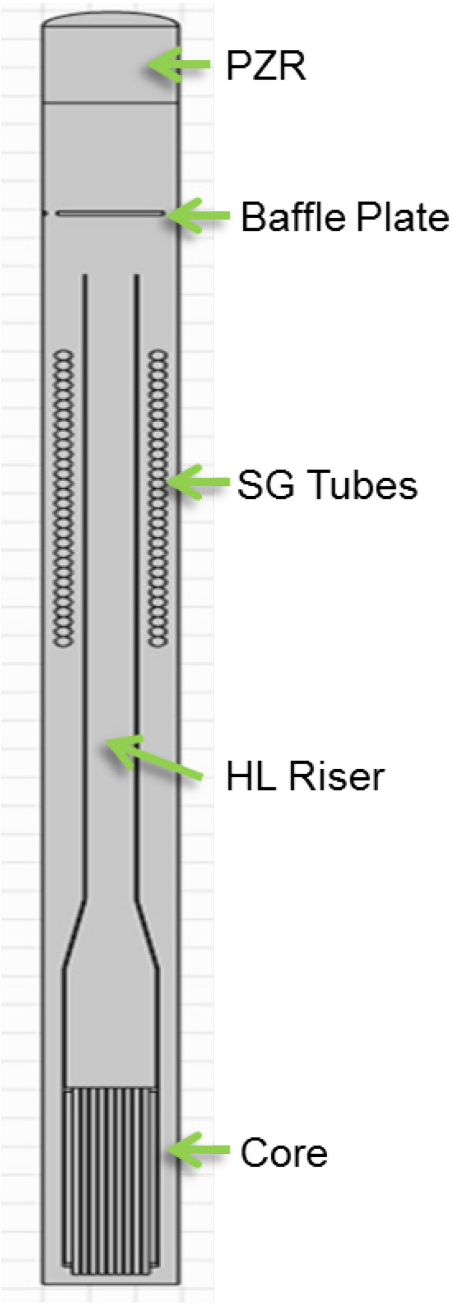

Figure 5.24. Test Case Two 2-D Reactor Pressure Vessel

The 2-D RPV illustrated in Figure 5.24 has several features worth noting.

The upper plenum is separated from the heated upper PZR section by a 0.95 cm thick baffle plate, at 308.6 cm above reference. The baffle plate has eight 2.54 cm diameter holes, radially located at 12.7 cm and spaced uniformly

around the baffle plate periphery which allows free communication of the PZR pressure to the remainder of the RPV during normal operation and for volume surges into and/or out of the PZR due to transients. During the geometry explanation of test case one, the upper baffle plate was modeled with no holes, as the RPV pressure remained constant. The baffle plate is modeled in test case two, split along the $y = 0$ plane with two of the 2.54 cm holes available for volume surges into the PZR.

The SG tubes are modeled as two vertical sets of 30 equally spaced circles on both sides of the hot leg riser. The 30 SG pipes maintain the same 0.0160 m radius and a radial spacing of 0.1016 m from the center of the hot leg riser. As previously explained, the SG in test case two loses the ability to dump the RPV heat load via a loss of main FW transient. Based on the start time of test case two, the SG tubes serve only as a physical impediment to the flow in the annulus between the HL riser and the ID of the RPV.

Additionally, the core is modified along the same $y = 0$ plane and features nine 2-D flow holes in both the upper and lower core plates and eight heater rods equally spaced horizontally across the core. The center rod is a thermocouple rod and serves only as a physical impediment to the flow at the axial center of the core. The eight heater rods are modeled as heat sources, and based on the core decay heat mode encountered in test case two, have a varying linear heat generation rate. The linear heat generation rate is explained in the initial and boundary conditions section below.

The ADS vent lines connect the PZR steam space to the HPC. They are horizontally oriented at 374.5 cm above reference and they are geometrically similar from the RPV to the HPC. The ADS vent lines are constructed with SS304 and all external surfaces are covered with 5.1 cm of Thermo-12 hydrous calcium silicate insulation. The ADS vent connection to the RPV is via a fillet welded 10.0 cm long, 1.91 cm nominal diameter schedule XXS pipe. The single ADS vent line leaving the RPV tees into two 1.27 cm diameter, 0.1651 cm wall thickness lines which lead to 1.27 cm fast-acting pneumatic motor operated globe valves PCS-106A and PCS-106B.

Downstream from each isolation valve is a transition piece with an internal 0.635 cm square-edge orifice. The transition piece serves two purposes: it transitions the line back from the 1.27 cm pipe to 1.91 cm diameter, 0.889 cm wall thickness pipe which is the pipe size to the HPC, and it presents the proper scaled flow area for the ADS vent line valve. This transition piece is repeated immediately following the isolation valve on the ADS blowdown and sump return lines. The two ADS vent lines enter the HPC via a fillet welded stub well above the waterline, penetrate 22.0 cm, and terminate in a sparger. Table 5.26 lists the ADS vent line geometric data:

Table 5.26. Automatic Depressurization System Vent Line Geometric Data

Component From	*Component To*	*Length (cm)*
RPV	tee	10.0
tee	PCS-106A	8.0
tee	PCS-106B	8.0
PCS-106A	HPC exterior	180.0
PCS-106B	HPC exterior	180.0
HPC Interior	Sparger	22.0

The automatic depressurization system (ADS) blowdown lines connect the RPV cold leg to the high pressure containment (HPC). They are horizontally oriented at 66.36 cm above reference and they are geometrically similar from the RPV to the HPC. The ADS blowdown lines are constructed with SS304 and all external surfaces are covered with 5.1 cm of Thermo-12 hydrous calcium silicate insulation. The ADS blowdown connection to the RPV is via a fillet welded 10.0 cm long, 1.91 cm nominal diameter schedule XXS pipe. The single ADS blowdown line leaving the RPV tees into two 1.27 cm diameter, 0.1651 cm wall thickness lines which lead to 1.27 cm fast-acting pneumatic motor operated globe valves PCS-107A and PCS-107B. The two ADS blowdown lines enter the HPC via a fillet welded stub, penetrate 22.0 cm, then turn downward for 72.6 cm before terminating below the HPC waterline at a sparger, similar to the one described above. Table 5.27 lists the ADS blowdown line geometric data:

Table 5.27. ADS Blowdown Line Geometric Data

Component From	*Component To*	*Length (cm)*
RPV	tee	10.0
tee	PCS-107A	8.0
tee	PCS-107B	8.0
PCS-107A	HPC exterior	203.8
PCS-107B	HPC exterior	203.8
HPC interior	90° elbow down	22.0
90° elbow down	Sparger	73.4

The ADS sump return (RPV re-flood) lines connect the RPV lower cold leg to the HPC. They are horizontally oriented at 5.40 cm above reference and they are geometrically similar from the RPV to the HPC. The ADS sump

return lines are constructed with SS304 and all external surfaces are covered with 5.1 cm of Thermo-12 hydrous calcium silicate insulation. Aside from their geometric layout, the ADS vent lines are otherwise similar to the ADS blowdown and vent lines.

The ADS sump return connection to the RPV is via a fillet welded 10.0 cm long, 1.91 cm nominal diameter schedule XXS pipe. The single ADS sump return line leaving the RPV tees into two 1.27 cm diameter, 0.1651 cm wall thickness lines which lead to 1.27 cm fast-acting pneumatic motor operated globe valves PCS-108A and PCS-108B. The two ADS sump return lines enter the HPC via a fillet welded stub, penetrate 22.0 cm, then turn downward for 10.0 cm before terminating well below the HPC waterline. There is no sparger on the end of the ADS. . Table 5.28 lists the ADS sump return line geometric data:

Table 5.28. ADS Sump Return Line Geometric Data

Component From	*Component To*	*Length (cm)*
RPV	tee	10.0
tee	PCS-108A	8.0
tee	PCS-108B	8.0
PCS-108A	HPC exterior	203.8
PCS-108B	HPC exterior	203.8
HPC interior	90° elbow down	22.0
90° elbow down	Sparger	21.0

The high pressure containment (HPC) vessel is a 5.75 m tall vessel consisting of three sections: a lower cylindrical section, an upper cylindrical section, and an eccentric cone section that joins the two. The lower cylindrical section is 27.0 cm outside diameter (OD), 0.318 cm wall thickness, and 3.87 m long. The lower end is closed with a 0.318 cm thickness plate. The upper

cylindrical section is 50.8 cm OD, 0.476 cm wall thickness, and 1.21 m long. The upper end is closed with a 16.0 cm high, 0.476 cm wall thickness, hemispherical head. The 0.476 cm wall thickness eccentric cone section is smoothly flared from the 27.0 cm OD lower section to the 50.8 cm upper section OD over an elevation of 20.0 cm. A 3.81 cm thick, 16.8 cm wide, heat transfer plate runs the entire 5.59 m vertical length (less hemispherical upper head) of the HPC and physically joins the HPC to the CPV. The entire HPC (less heat transfer plate) is covered by 10.2 cm of Thermo-12 hydrous calcium silicate insulation.

The cooling pool vessel (CPV) is a 7.37 m tall right cylindrical tank made from 76.2 cm OD, 0.635 cm wall thickness pipe. The CPV is covered by 5.08 cm of Thermo-12 hydrous calcium silicate insulation.

The heat transfer plate provides the heat conduction surface between the HPC and the CPV. It is the same height as the HPC without the hemispherical head (5.59 m), 16.8 cm wide and 3.81 cm thick. The heat transfer plate models the heat transfer area between the MASLWR conceptual design high pressure containment vessel and the cooling pool in which it sits. Table 5.29 lists the containment and cooling system geometric data.

Table 5.29. Containment and Cooling System Geometric Data

Component	*Length (m)*	*Diameter (cm)*
HPC Vessel	5.75	-
HPC lower cylinder	3.87	0.27
HPC eccentric cone (lower)	0.51	0.27
HPC eccentric cone (upper)	0.51	0.51
HPC upper cylinder	1.21	0.51
HPC head hemisphere	0.17	0.51
CPV	7.37	0.76
Heat transfer plate	5.59	3.81 cm thick, 16.8 cm wide

Figure 5.25 illustrates the to-scale 2-D COMSOL model for test case two.

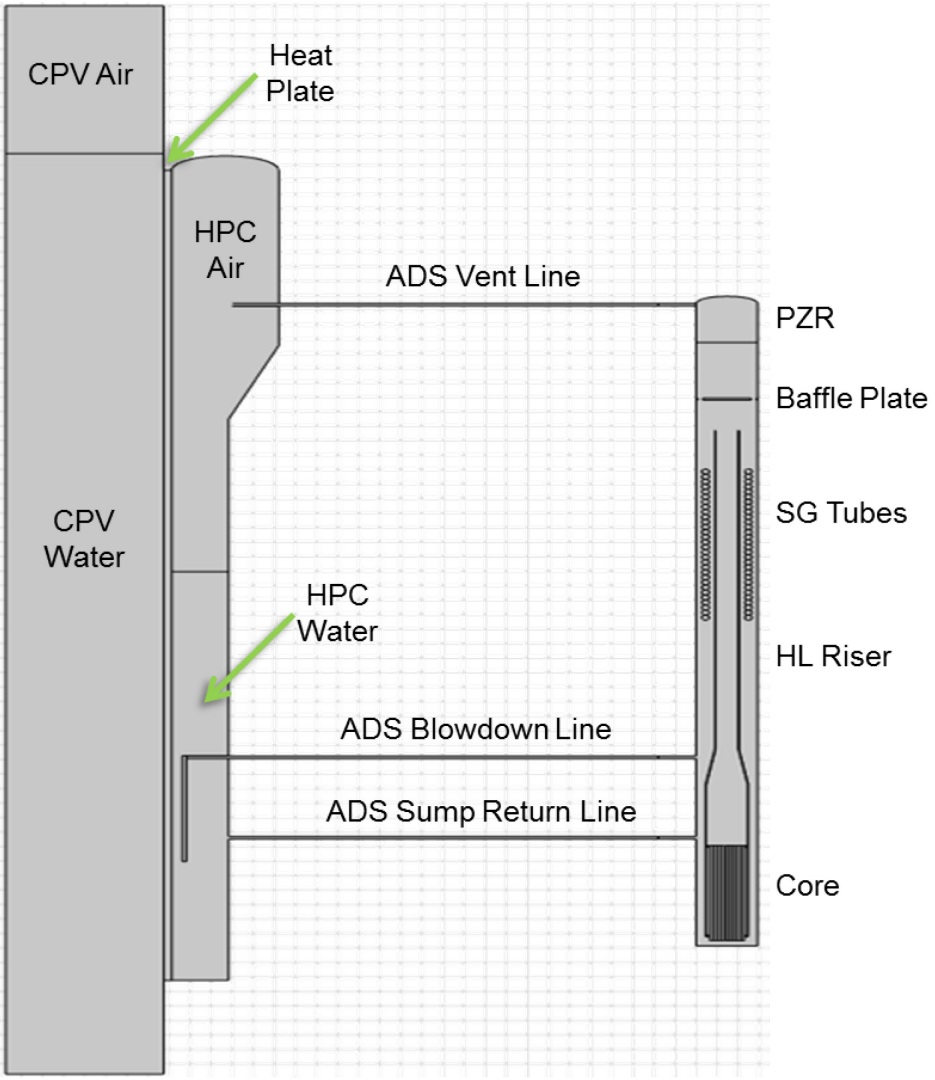

Figure 5.25 Test Case Two Full 2-D COMSOL Model

5.5.2.3 MESH TECHNIQUES

For 2-D geometries, COMSOL's mesh generator discretizes the domains into triangular or quadrilateral mesh elements. If the boundary is curved, these elements represent only an approximation of the original geometry. The boundaries defined in the geometry are discretized (approximately) into mesh edges, which must conform with the mesh elements of the adjacent domains.

As before, the default COMSOL setting is to use a mesh that is controlled by the physics. The mesh is then adapted to the current multi-physics settings in the model. For the two test case two, the COMSOL physics-controlled mesh settings were utilized. Table 5.23 lists the default 2-D COMSOL physics-controlled settings for both general physics (heat transfer) and fluid dynamics:

Table 5.30. COMSOL Default 2-D Physics-Controlled Mesh Settings

Parameters (units)	*Fluid Dynamics*	*General Physics*
Maximum element size (m)	0.239	0.747
Minimum element size (m)	0.107	0.015
Maximum element growth rate	1.2	1.5
Resolution of curvature	0.4	0.4
Resolution of narrow regions	1.0	1.0

The default 2-D fluid dynamics physics-controlled mesh settings were applied to the working fluids inside the RPV, the ADV lines, the HPC and the CPV. The general physics mesh was applied to all other materials in the model, including the RPV, the core, HL riser, SG and the heat transfer plate. Figures 5.26 thru 5.28 illustrate the physics-controlled meshing of the core.

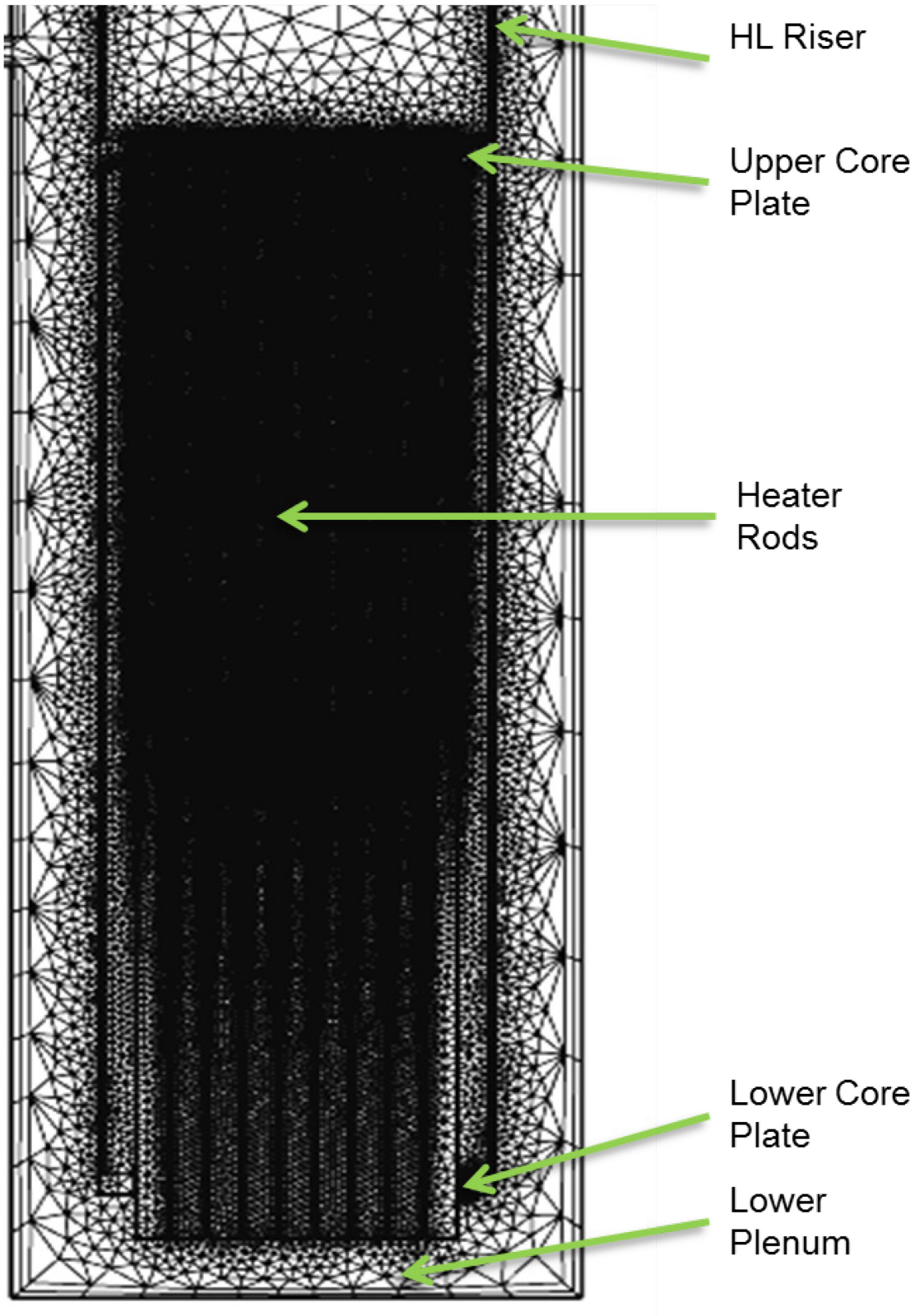

Figure 5.26. Test Case Two Core Mesh

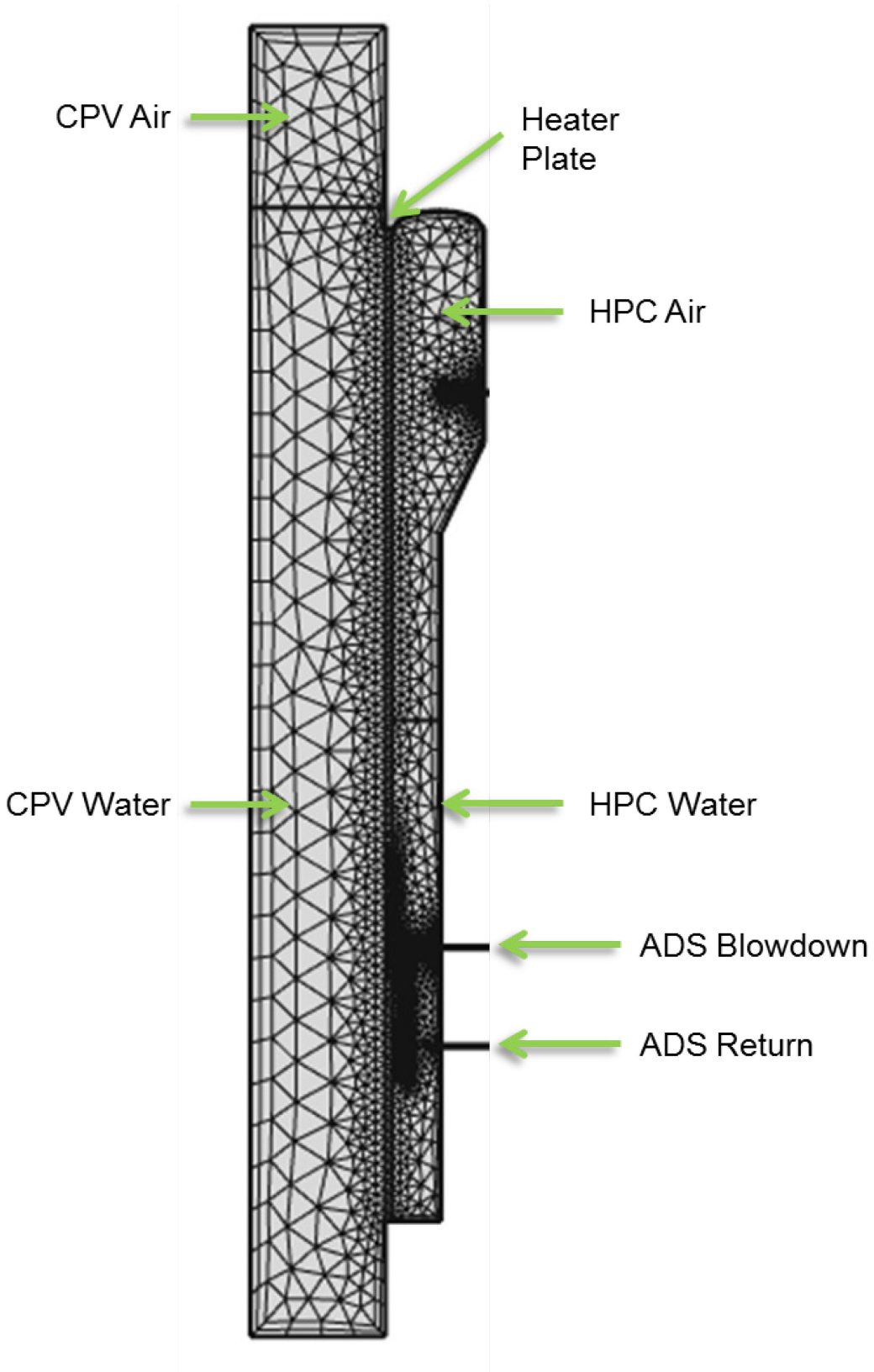

Figure 5.27. Test Case Two HPC, Heater Plate and CPV

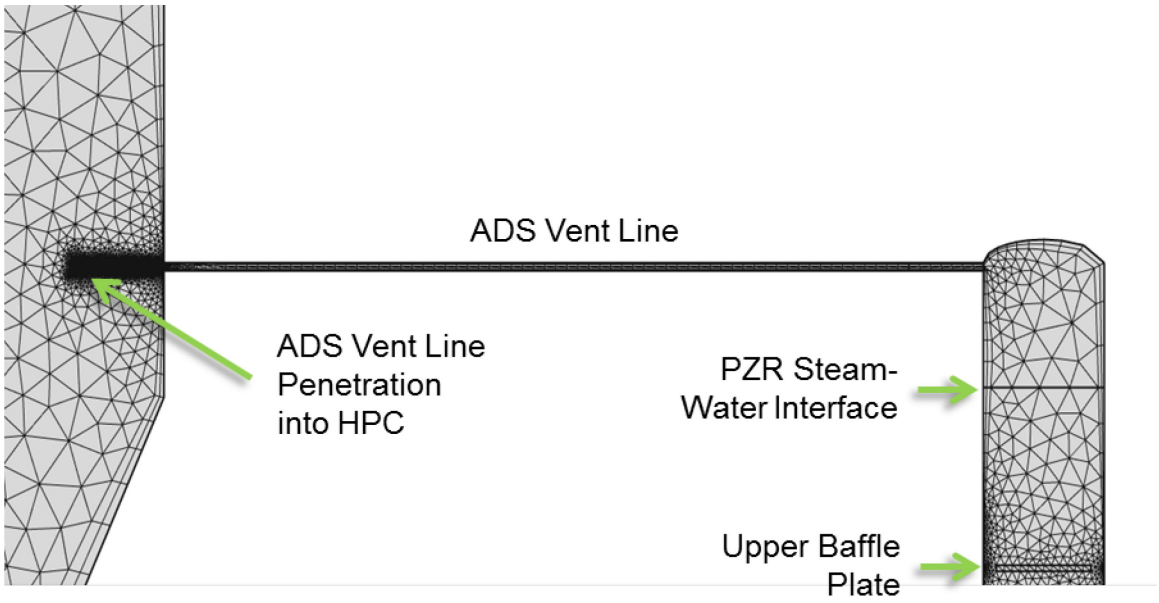

Figure 5.28. Test Case Two ADS Vent Line Mesh

The figures shown are an indication of the starting mesh for test case two. Due to the vertical movement of the steam/water and air/water interface in the RPV and HPC, an adaptive mesh is generated once the time-dependent problem is initiated. The mesh will be updated in order to keep the mesh refined in the interface regions.

5.5.2.4 Multi-Physics Including Initial and Boundary Conditions

The multi-physics settings in COMSOL require the user to input various initial and boundary conditions based on the types of physics involved, the materials present and the complexity of the model's geometry. The two-phase flow, level set interface then solves the default set of equations. These equations are summarized below.

$$\nabla \cdot \vec{v} = 0 \tag{5.11}$$

$$\rho\left(\frac{\partial \vec{v}}{\partial t} + \vec{v} \cdot \nabla \vec{v}\right) = -\nabla p + \mu \nabla \cdot [(\nabla \vec{v}) + (\nabla \vec{v})^T] + \rho \vec{f} + \rho \vec{g} \beta (T - T_0) + \vec{F}_{st} \tag{5.12}$$

where ρ and μ are functions of the level set function according to:

$$\rho = \rho_1 + (\rho_2 - \rho_1)\phi \tag{5.13}$$

$$\mu = \mu_1 + (\mu_2 - \mu_1)\phi \tag{5.14}$$

ρ_1 and ρ_2 ≡ constant densities of fluid 1 and fluid 2

μ_1 and μ_2 ≡ dynamic viscosities of fluid 1 and fluid 2

where $\vec{F}_{st}$ ≡ surface tension force

The initial values for the velocity field and the pressure are required as initial conditions in the level set interface. These values were taken from the experimental data at the beginning of test case two and summarized in Tables 5.6 and 5.7. As explained earlier, test case two is modified to begin at the moment the ADS vent valve actuates. This is done to eliminate the need for a valve actuation. The valve actuation in COMSOL Version 4.2a must be accomplished through a varying viscosity setting and introduces undue computational effort. For this reason, test case two begins immediately after its opening. The Boussinesq approximation is also included as part of the volume force to account for the effects of the decay heating continuing in the core.

Test case two was broken into two geometric phases for ease of providing the boundary conditions. Two separate COMSOL computational run sets were conducted to accomplish this. The first computational run focused on the PZR steam and downstream air interface at the ADS vent line location. The boundary conditions for this phase included the use of the wetted wall boundary condition that allows for the movement of the interface along the wall, or in this case, inside the pipe. Phase one did not account for any heat transfer in the RPV shell. The

only heat transfer accounted for was within the mixing of the steam from the PZR and the cooler air within the HPC vessel and piping.

The second computational run focused specifically on the RPV and the onset of decay heating. The boundary conditions for this phase again included the establishment of the wetted wall to allow for the movement of the PRZ steam and primary coolant level above the upper baffle plate. The actuation of the ADS sump line was also accounted for in this phase as it contributes to the long term cooling of the core in decay power mode. These boundary conditions were taken from the experimental data at the moment the ADS sump line opened. The inlet condition for this phase was the inflow of coolant from the sump return line into the RPV. The outlet condition was the return of fluid to the HPC through the ADS blowdown line.

The second phase also included the heat transfer interface in evaluating the temperatures inside the HL riser and the area above and below the SG in the CL downcomer. These three areas are of main concern as they contribute directly to the establishment of a natural circulation loop as part of the decay heating process.

In both phases, an initial interface was established to define the initial position as a boundary condition on the interior boundaries. During the initialization step, discussed in the next section, this boundary condition sets the level set function to 0.5. For phase one, this initial interface is the steam-air interface at the ADS vent line location. For phase two, this initial interface is the

steam-water interface between the steam in the PZR and the primary coolant inside the RPV.

5.5.2.5 SOLVER SETTINGS

In order to initialize the level set function so that it varies smoothly between zero and one, COMSOL creates two study steps, a phase initialization step and a problem specific time dependent step. The phase initialization step solves for the distance to the initial interface, D_{wi}. The time dependent study then uses the initial condition for the level set function according to Eqns. 5.15 and 5.16.

$$\phi = \frac{1}{1+e^{-D_{wi}/\varepsilon}} \tag{5.15}$$

in domains initially outside the interface and

$$\phi = \frac{1}{1+e^{-D_{wi}/\varepsilon}} \tag{5.16}$$

in domains initially inside the interface.

Two time dependent studies were completed based on running the two computational phases discussed above.

5.5.3 SENSITIVITY ANALYSIS

As outlined in Section 5.3.3, a sensitivity analysis was conducted to determine those parameters that have the most impact on the CFD code results. The sensitivity analysis was completed on the geometry, initial and boundary conditions of test case one, at a maximum power level of 320kW, to gain a better understanding of the natural circulation flows in the reactor coolant system and the parameters that can impact them during steady-state operations at various power levels.

An altered set of test case one computer runs was completed with the initial and boundary conditions found in Tables 5.3 and 5.5. Table 5.31 lists those parameters that were altered and the range of values that were evaluated. A more detailed discussion of the sensitivity analysis is explored in the COMSOL model development contained in Section 5.5.3. The results of the sensitivity analysis are presented in later chapters.

5.5.3.1 Model Set-Up and Material Properties

The same model set-up and material properties utilized in the computational runs of test case one were applied for the sensitivity analysis. Exceptions to the maximum power level test case are listed in Table 5.30 above.

5.5.3.2 Geometry

No changes were made to the geometry utilizes in the computational runs of test case one.

Table 5.31. Sensitivity Analysis Parameters

Value	*Variation from Reference Calculation*	*Range*
REF	Reference calculation	
SEN1	Decrease FW mass flow rate	0.1 – 0.01 kg/s in 0.01 kg/s increments for maximum power level
SEN2	Increase FW mass flow rate	0.1 – 0.3 kg/s in 0.05 kg/s increments for maximum power level
SEN3	Decrease the thermal conductivity of the hot leg riser around the SG	44.5 – 14.5 W/(m·K) in 10 W/(m·K) increments for maximum power level
SEN4	Increase the thermal conductivity of the hot leg riser around the SG	44.5 – 74.5 W/(m·K) in 10 W/(m·K) increments for maximum power level

5.5.3.3 Mesh Techniques

The default mesh sizes for the sensitivity analysis were increased to those listed in Table 5.30 for both the fluid dynamic and heat transfer analysis.

5.5.3.4 Multi-Physics Including Initial and Boundary Conditions

No changes were made to the multi-physics interface or the initial and boundary conditions utilized in the computational runs of test case one.

5.5.3.5 Solver Settings

No changes were made to the solver settings utilized in the computational runs from test case one.

CHAPTER 6

COMPUTATIONAL RESULTS AND ANALYSIS

The results of the thermal hydraulic code TRACE and the COMSOL CFD analysis are benchmarked against the experimental test results of a 1:3 length, 1:254 volume, full pressure and full temperature scale SMR during steady-state power operations and during a depressurization transient (known as test case one and test case two). This comparative evaluation of the experimental data, the thermal hydraulic code results and the CFD code results provides an opportunity to validate the best-estimate thermal hydraulic code's treatment of a natural circulation loop and provide insights into expanded use of the CFD code in future designs and operations. Additionally, a sensitivity analysis was conducted to determine those physical phenomena most impactful on operations of the proposed reactor's natural circulation loop. The combination of the comparative evaluation and sensitivity analysis provides the resources for increased confidence in model developments for natural circulation loops and could provide for reliability improvements of the thermal hydraulic code.

6.1 TEST CASE ONE RESULTS AND ANALYSIS

Test case one characterizes the steady-state natural circulation in the primary side during various core power inputs. As outlined in the original facility test plan, this was accomplished by configuring the OSU-MASLWR test facility in a natural circulation state and varying the power inputs of the core heaters.

Power inputs of the core heaters were increased step by step from 10 percent of full power to 80 percent of full power, with a 10 percent increment at each step. For each power input, the primary side flow rate, hot leg and cold leg temperatures were monitored to determine whether the flow stabilization was achieved. The primary side and steam generator pressures were maintained at 8.72 MPa gage and 1.44 MPa gauge, respectively, for all power inputs.

The OSU-MASLWR test facility experimental data utilized in this analysis was made available to the participants of an International Atomic Energy Agency (IAEA) International Collaborative Standard Problem (ICSP) on integral water cooled reactor designs. This ICSP is in its fourth year of collaboration and had previously made the initial and boundary conditions available as part of a blind calculation conducted by many international agencies. Eventually, the experimental data was made publically available for use in conducting a series of open calculations involving the procedures outlined in the two test cases.

In the course of initially analyzing the experimental data of the test facility it became evident there was a departure from the test procedures in regards to the FW mass flow rate of test case one. According to the test procedures, the FW mass flow rate was to vary according to time, as is listed in Table 6.1. This did not occur as part of the test protocol in collecting the experimental data. Figure 6.1 illustrates these planned test procedure values compared to the actual rates used in the conduct of test case one. The TRACE computational runs were subsequently modified to account for the experimental FW flow rates shown in Figure 6.1 as opposed to the published protocol test conditions.

Table 6.1. Test Case One Feedwater Mass Flow Rates

Time (s)	*FCM-511 (kg/s)*	*FCM-521 (kg/s)*	*FCM-531 (kg/s)*	*FMM-501 (total) (kg/s)*
190	0.0034	0.0032	0.0036	0.0102
1060	0.0134	0.0157	0.0144	0.0435
1830	0.0128	0.0148	0.0131	0.0407
2367	0.0182	0.0195	0.0177	0.0554
4195	0.0240	0.0268	0.0224	0.0732
4687	0.0291	0.0327	0.0271	0.0889
5286	0.0332	0.0375	0.0310	0.1017

As can be seen in Figure 6.1, the experimental FW mass flow rate maintains a constant increase, following the trend of the protocol values, until the 2800 second time frame. At this point, the testers greatly increased the mass flow rate on the secondary side to lower the superheat values being produced in the tube side of the helical steam generator. This increase in FW mass flow rate increased the rate of heat transfer across the shell side of the SG. The effects of this increase will be explored further in this section.

Although the COMSOL model for test case one utilizes a simplified helical SG, the initial methodology relied on a varying heat transfer coefficient. The simplified SG heat transfer coefficient, and subsequent heat transfer capability was initially modeled as a function of the FW mass flow rate. After discovery of the departure from the test procedure, the SG was modeled with a constant linear heat transfer rate at each power level. These values were calculated from the experimental temperature data of the SG. An average heat transfer across the SG was calculated at each power level and then the length of the simplified helical SG was used to calculate an appropriate linear heat transfer rate.

The core power ranges in test case one from an initial value of 40 kW to a maximum of 320 kW. This power ramping is accomplished by raising the heater rod output within the test facility. Table 6.2 lists the core power levels as a function of time. Figure 6.2 illustrates the experimental values compared to those modeled in TRACE and COMSOL. Note that all COMSOL data in test case one is constant for each power level. This is due to the conduct of a steady-state solution as opposed to a time dependent study in order to save computational time.

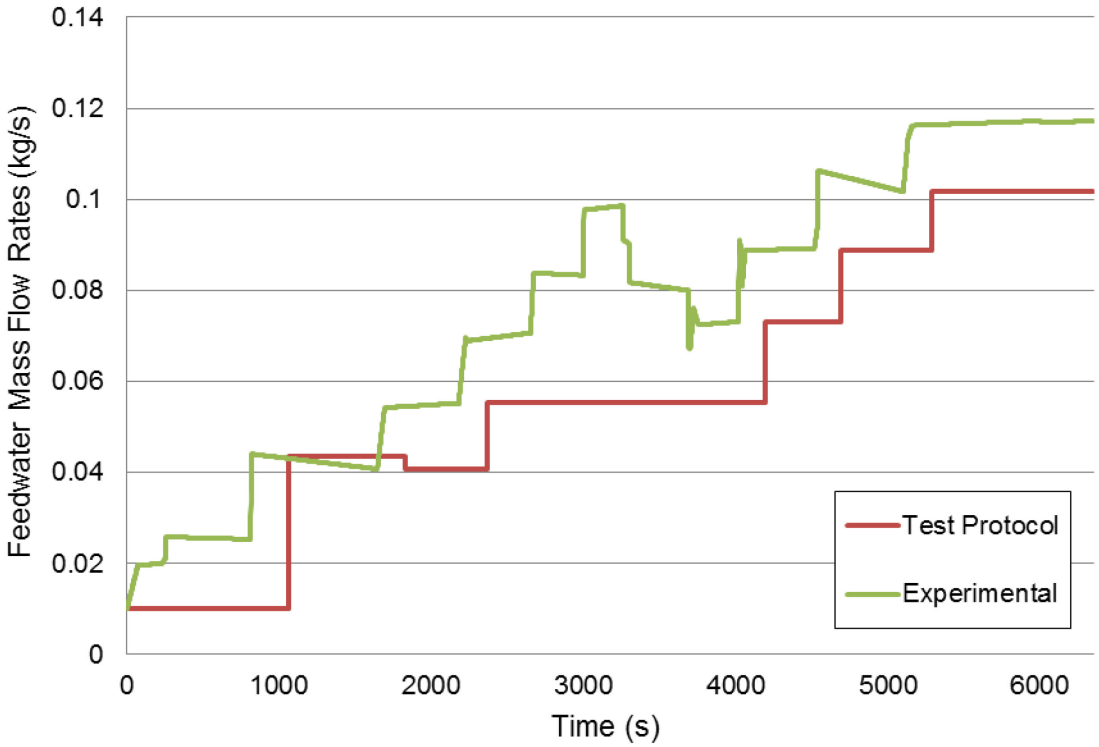

Figure 6.1. Feedwater Mass Flow Rates (Protocol versus Experimental)

Table 6.2. Core Power as a Function of Time

Event	*Test Time (sec)*
Begin data collection at 40 kW	0
Initiate core power increase to 80 kW	180
Initiate core power increase to 120 kW	1060
Initiate core power increase to 160 kW	1830
Initiate core power increase to 200 kW	2367
Initiate core power increase to 240 kW	4195
Initiate core power increase to 280 kW	4687
Initiate core power increase to 320 kW	5286
End of test	6347

The next series of results focuses on the primary coolant temperature at various points inside the HL riser and the CL downcomer and the mass flow rate inside the HL riser at a point below the SG coil. The primary coolant water temperature inside the HL riser below the SG coil is shown in Figure 6.3.

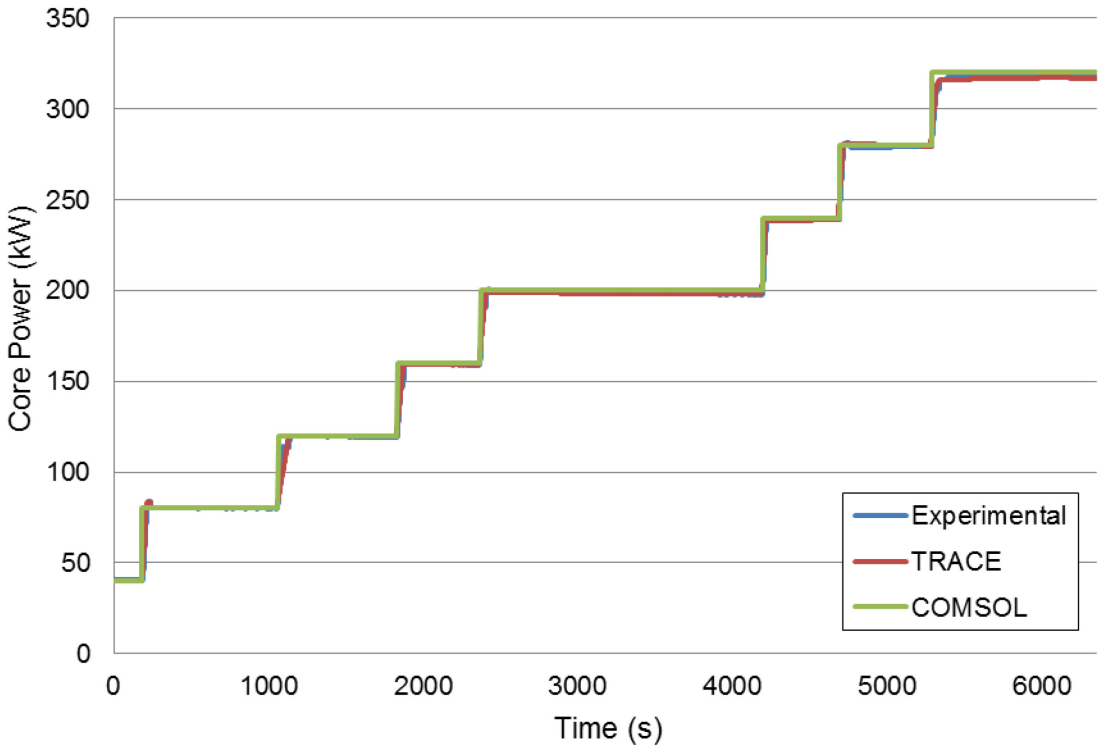

Figure 6.2. Test Case One Core Power Levels

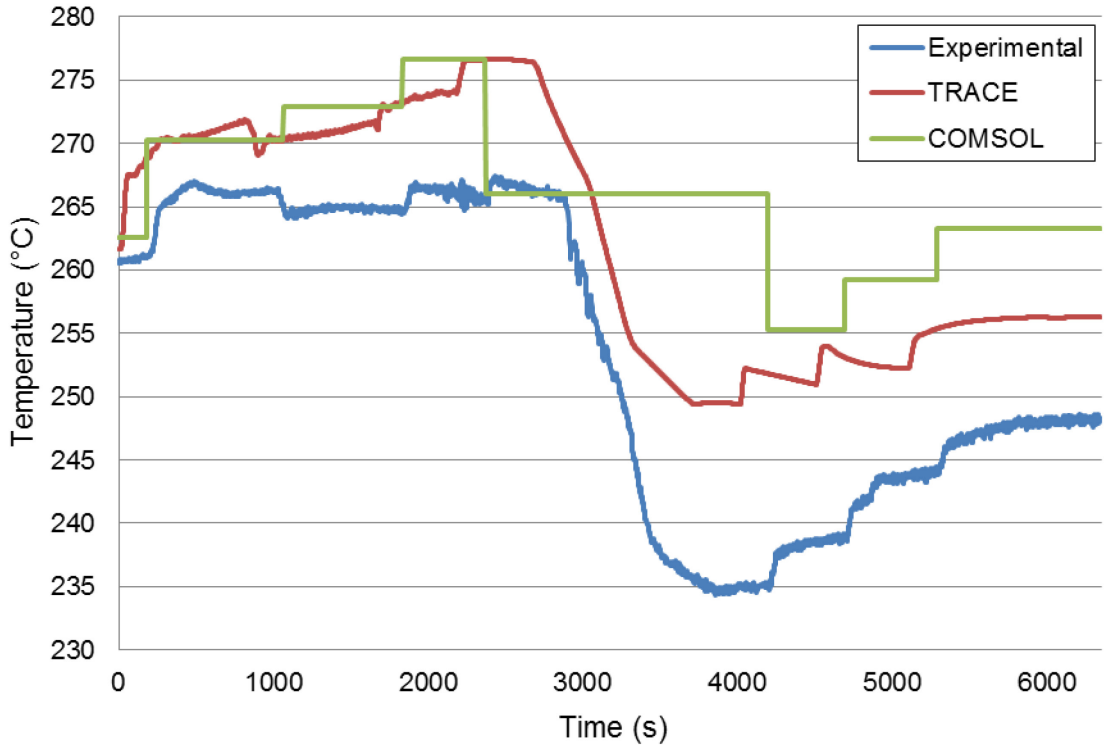

Figure 6.3. Primary Coolant Temperature Inside HL Riser (below SG)

Figure 6.3 clearly illustrates the impact of the increased FW mass flow rate initiated at approximately 2800 seconds. This increase in FW mass flow rate leads to a steep decrease in the primary coolant temperature leaving the top of the core and flowing into the chimney portion of the HL riser. The TRACE results overestimate the temperature of the coolant in relation to the experimental data, but follow the general trend of the test facility data. The COMSOL averages at each power level agree with the TRACE data up to the point of the FW rate increase. From 2800 seconds until the completion of the test, the COMSOL data averages a 18°C higher temperature in relation to the experimental data and a 10°C higher temperature in relation to the TRACE calculations.

The next instrumentation point is the temperature of the primary coolant at the top of the HL riser before it enters the upper plenum. This data is shown in Figure 6.4.

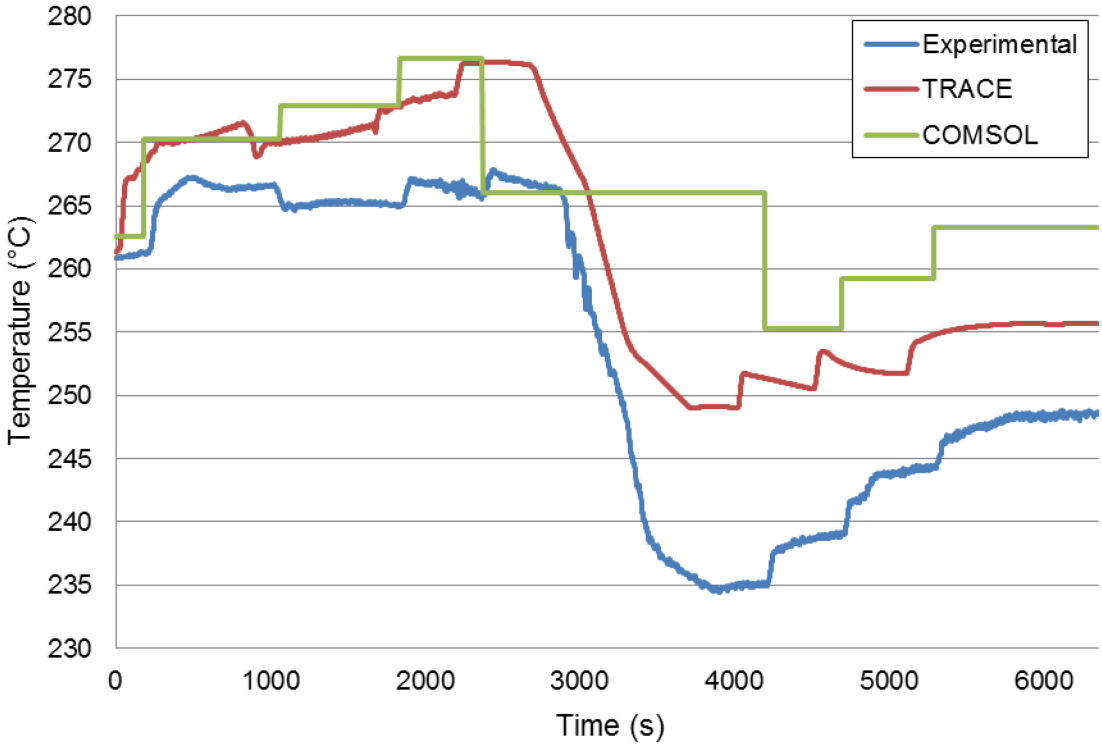

Figure 6.4. Primary Coolant Temperature at HL Riser Top

As is expected, the primary coolant temperature does not deviate much in temperature as it travels the vertical length of the HL riser. Although some heat transfer effects might be expected in the HL riser region surrounded by the SG, the experimental data and computational results show little deviation. The same trends are again observed in relation to the TRACE and COMSOL data. The COMSOL steady-state values continue to average 18°C and 10°C above the temperatures observed experimentally and in the TRACE results, respectively.

After leaving the top of the HL riser and mixing in the upper plenum, the primary coolant begins to flow downward in the annulus between the ID of the RPV and the OD of the HL riser. A very short distance later the primary fluid comes in contact with the helical SG. As the fluid flows over the tubes of the SG, it transfers heat into the secondary system. Primary coolant temperatures should be noticeable lower in the region of the CL downcomer just below the SG. This data is shown in Figure 6.5.

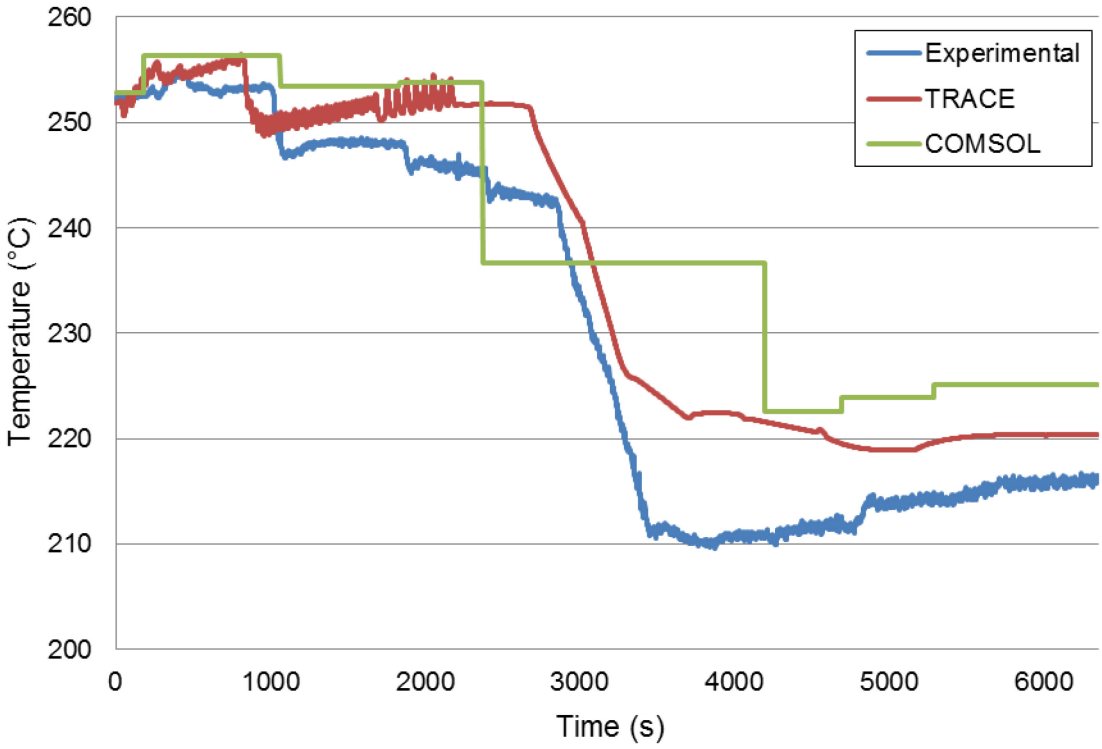

Figure 6.5. Primary Coolant Temperature in the CL Downcomer (below SG)

The primary coolant average temperature at each power level is roughly 10°C cooler in comparison to the coolant before it enters the SG region. This is due to the heat transfer occurring around the SG as the primary coolant's energy is utilized in making steam on the secondary side. The TRACE results are more closely aligned with the experimental data and the COMSOL results are much

less divergent. The COMSOL results are now, on average, only 11°C and 5°C above the temperatures observed experimentally and in the TRACE results, respectively. Although this might be an indication of better modeling, the contrary is likely true. The SG modeling and subsequent transfer of heat in both the TRACE and COMSOL models suggest the models are over estimating the heat transfer results in comparison to the experimental data.

After traveling in the annulus between the CL downcomer and the HL riser, the primary coolant enters the lower plenum and begins to flow through the lower core plate. The coolant, theoretically at this point, should be at its lowest temperature of the natural circulation loop. From this point the coolant travels radially inward and enters the heater rod region of the core. Figure 6.6 shows the coolant temperature in the lower plenum.

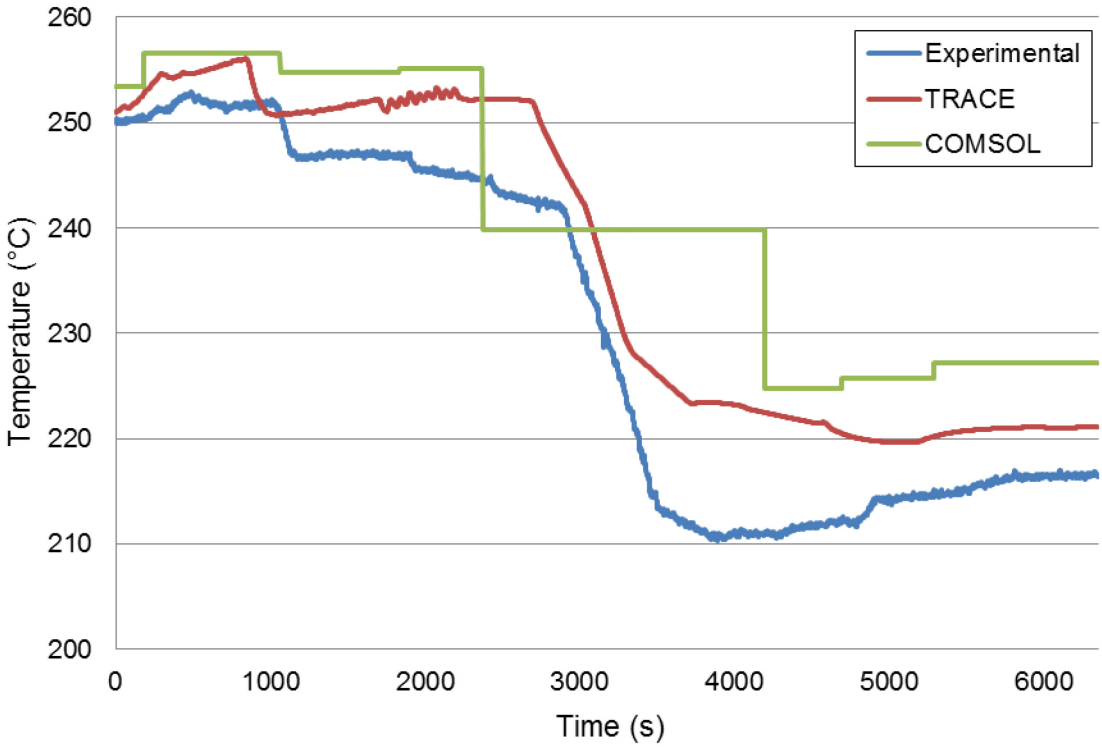

Figure 6.6. Primary Coolant Core Inlet Temperatures

By analyzing the experimental data and the TRACE and COMSOL results, related to the flow temperature after the SG coils primary side section and the core inlet temperature, it is evident that the direct heat exchange, through the internal shell, between the fluid ascending the hot leg and the fluid descending the cold leg, is a crucial parameter for the evaluation of the core inlet temperature and, therefore, the core outlet temperature. In fact, the experimental data show that, along the downcomer region, the fluid increases its temperature between the end of the SG primary side section and the core inlet at higher power levels. Figure 6.7 shows this data along with the TRACE and COMSOL results.

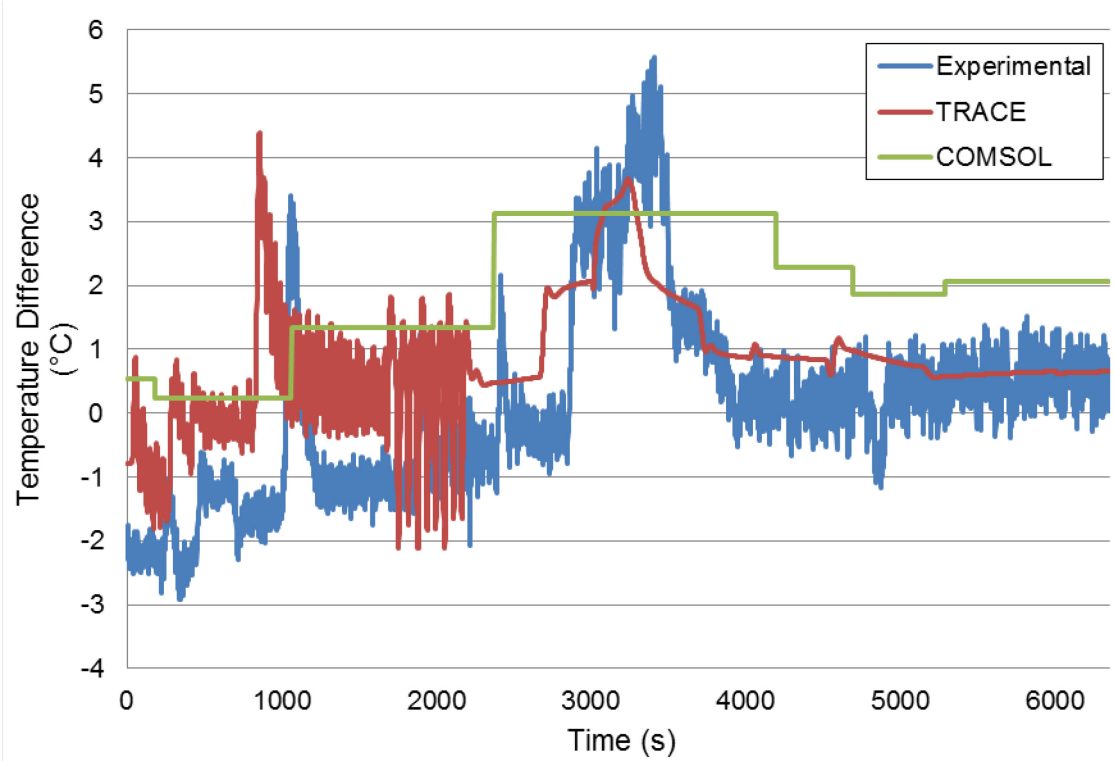

Figure 6.7. Differences in CL Downcomer Temperatures

The temperature differences graphed on the ordinate show the difference between the core inlet flow, T_{inlet}, and the coolant at a point just below the SG in

the CL downcomer, $T_{CL-belowSG}$. Negative differences represent cooling as the flow progresses and positive differences represent heating.

Figure 6.7 illustrates several key areas worth noting. The experimental temperature differences at lower powers, 40 kW to 160 kW, show a cooling (negative differences) of the primary coolant as it flows along the CL downcomer; however, the cooling is decreasing at a rate proportional to the power increase. This suggests the heating across the HL riser is having a small effect on the coolant at low powers. In contrast is the effect at power levels above 200kW. The effect of heating across the HL riser becomes more pronounced, notwithstanding the effects of the increased FW flow rate from 2800 to 3400 seconds. After this point the experimental data shows the primary coolant actually increases in temperature by an average of 0.75°C. While this may seem insignificant, any deviation in the heat transfer properties of the SG or the HL riser could lead to the primary coolant rising above the saturation temperature while in the core, leading to in-core boiling. A more detailed analysis of this trend is explored in the sensitivity analysis in Section 6.3.

The TRACE and COMSOL results presented n Figure 6.7 suggest the direct heat exchange is more pronounced. The TRACE results show an initial cooling of the coolant, but quickly move into a heating scenario with an average increase in temperature of 1.15°C at power levels between 120 kW and 320 kW. The COMSOL results never show a cooling of the coolant. The temperature difference follows the same trend as the experimental and TRACE results, but the average difference is more than double the experimental results at 1.67°C.

As the primary coolant enters the heater rod region of the core, it begins to increase in temperature leading to the completion of the natural circulation loop. This process brings the water temperature near the saturation point and the density differences establish the natural flow. Figure 6.8 shows the temperature of the primary coolant as it leaves the top of the core and enters the bottom of the HL riser.

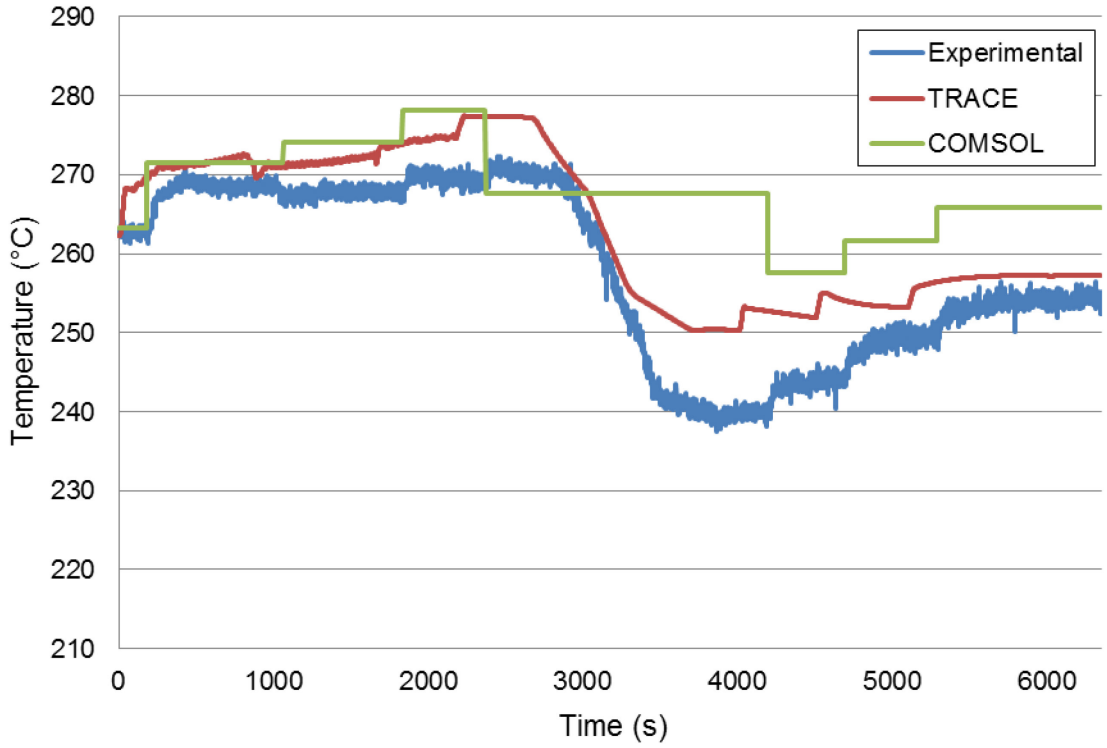

Figure 6.8. Primary Coolant Temperature Leaving the Core

The experimental data suggest a gradual increase in the coolant temperature as it leaves the core of the test facility. The FW mass flow rate transient at 2800 seconds has a definite impact on the temperatures leaving the core as the inlet temperatures have a corresponding decrease. Without the FW transient it is unlikely the core water temperatures would have increased enough to reach saturation. At 8.72 MPa the saturation temperature is 301.119°C. Even

at this highest power of 320 kW it is assumed this value would not be reached at the primary coolant leaves the core. The TRACE and COMSOL results follow a similar trend as before with the TRACE results more closely matching the experimental data. The COMSOL results continue to indicate an over-estimation of the temperature profile, but again, do not suggest the saturation point would be reached without the FW transient. As the primary coolant leaves the core the COMSOL results are, on average, only 10°C and 4°C above the temperatures observed experimentally and in the TRACE results, respectively.

The mass flow rate of the primary coolant was captured experimentally at a location just above the transition cone of the HL riser. The mass flow rates are vitally important as the only means of circulating the primary coolant is through the establishment of a natural circulation loop. Figure 6.9 shows the experimental data in comparison to the TRACE and COMSOL results.

The experimental mass flow rates show a gradual increase in primary coolant flow as the power is increased. This is expected as the average temperature difference across the core increases, as shown in Figure 6.10. The TRACE and COMSOL results more closely match the experimental data with the noticeable difference in the COMSOL results after the FW transient. After 2800 seconds, the COMSOL results underestimate the experimental data, but to a much lesser degree. The COMSOL results underestimate the experimental data by 8.8% and the TRACE results by 6.5%.

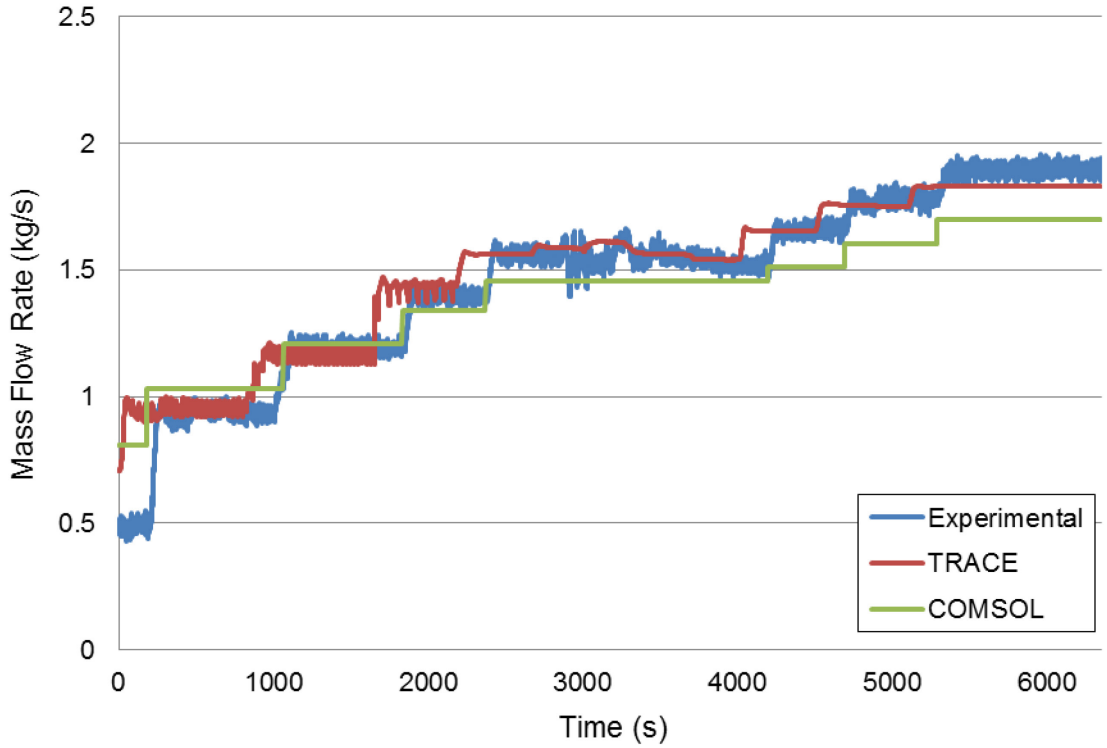

Figure 6.9. Primary Coolant Mass Flow Rate (Test Case One)

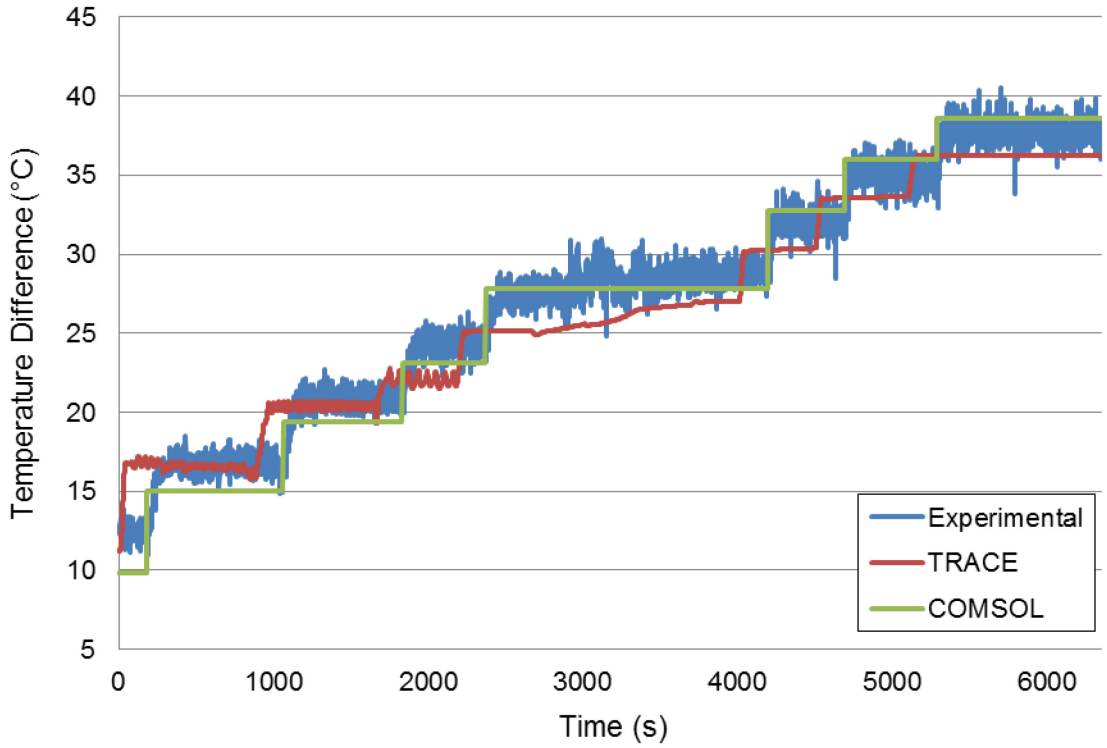

Figure 6.10. Temperature Difference Across the Core (Test Case One)

The increase in the temperature difference across the core varies very little in comparison of the experimental data with the TRACE and COMSOL results. This trend supports the gradual increase in mass flow rates as higher temperature differences lead to greater density differences and buoyancy forces. The TRACE and COMSOL results also support the idea that the models very closely replicate the heat transfer in the core in comparison to the experimental data.

The results of test case one are summarized in Table 6.3. The percent error contained in the table represents the departure of each computational model at various temperature and mass flow readings in the primary coolant loop from the experimental values. These results support the idea that the T-H code accurately replicates the natural circulation of the OSU-MASLWR test facility. The results, however, do not support a reliance on the CFD model and its ability to produce accurate results. This idea will be explored further in the conclusions.

Table 6.3. Test Case One Summary

Measured Value (Location)	*Percent Error from Experimental*	
	TRACE	*COMSOL*
Coolant temperature (inside HL riser)	4.05	6.91
Coolant temperature (top of HL riser)	3.64	6.95
Coolant temperature (CL below SG)	2.30	4.65
Coolant temperature (core inlet)	2.31	5.66
Coolant temperature (core outlet)	0.78	4.32
Mass flow rate (inside HL riser)	6.52	8.80

6.2 Test Case Two Results and Analysis

As detailed earlier, the purpose of this test, a design basis accident for the MASLWR concept design, is to determine the behavior of the RPV and

containment pressures and core inlet and outlet temperatures following an actuation of an ADS vent valve and subsequent blowdown.

More specifically, test case two simulates the loss of FW, activation of safety systems and the long term cooling of the OSU-MASLWR test facility to determine the progression of a loss of FW transient. The test begins by bringing the OSU-MASLWR test facility to steady state at 75% power with a primary pressure of 8.72 MPa(g) and the main feed pump running on the secondary side.

For the TRACE model, once the initial conditions were reached the test was initiated by stopping the main feed pump thus cutting off flow to the SG. With the subsequent loss of the reactor heat sink the primary pressure began to rise. At a set-point corresponding to a PZR pressure of 8.963 MPa the core heaters were set to the decay power settings listed in Table 5.8. One line of the ADS vent system opened on a pressure reading of 9.064 MPa(g). This caused the primary system under rising pressure to vent into the high-pressure containment. When the difference between RPV pressure and HPC pressure was less than 0.034 MPa, the ADS sump value opened and long-term cooling was started. Test case two continued until five hours elapsed.

The COMSOL model was more involved and, as earlier detailed, had to be broken into two different phases. Table 6.4 lists the phase times for the COMSOL computational runs. Test case two was broken into two geometric phases for ease of providing the boundary conditions. Two separate COMSOL computational run sets were conducted to accomplish this. The first computational run focused on the PZR steam and downstream air interface at

the ADS vent line location. The boundary conditions for this phase included the use of the wetted wall boundary condition that allows for the movement of the interface along the wall, or in this case, inside the pipe. Phase one did not account for any heat transfer in the RPV shell. The only heat transfer accounted for was within the mixing of the steam from the PZR and the cooler air within the HPC vessel and piping.

Table 6.4. Test Case Two Phase Times

Phase	*Experimental Time (sec)*
Blowdown	0 – 120
Decay power	4114 – 10000

The second computational run focused specifically on the RPV and the onset of decay power. The boundary conditions for this phase again included the establishment of the wetted wall to allow for the movement of the PRZ steam and primary coolant level above the upper baffle plate. The actuation of the ADS sump line was also accounted for in this phase as it contributes to the long term cooling of the core in decay power mode.

The initiation of the blowdown phase occurs at a set pressure of 9.064 MPa. Figure 6.11 shows the behavior of the primary system pressure inside the PZR during the blowdown. Figure 6.12 shows the behavior of the HPC pressure during the same time period. As before, the experimental data is compared to the TRACE and COMSOL results. It should be noted that the COMSOL results for test case two are available in one second time increments as a time-dependent study was used for both the blowdown and decay power phases.

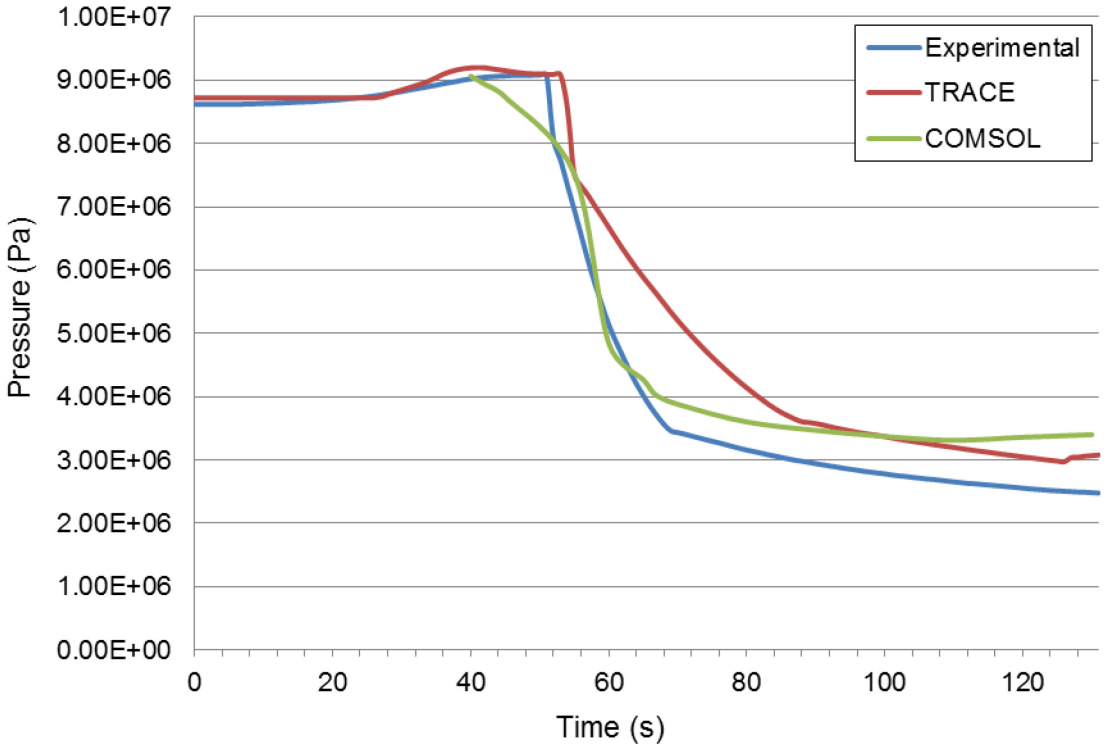

Figure 6.11. Reactor Pressure Vessel Pressure during Blowdown

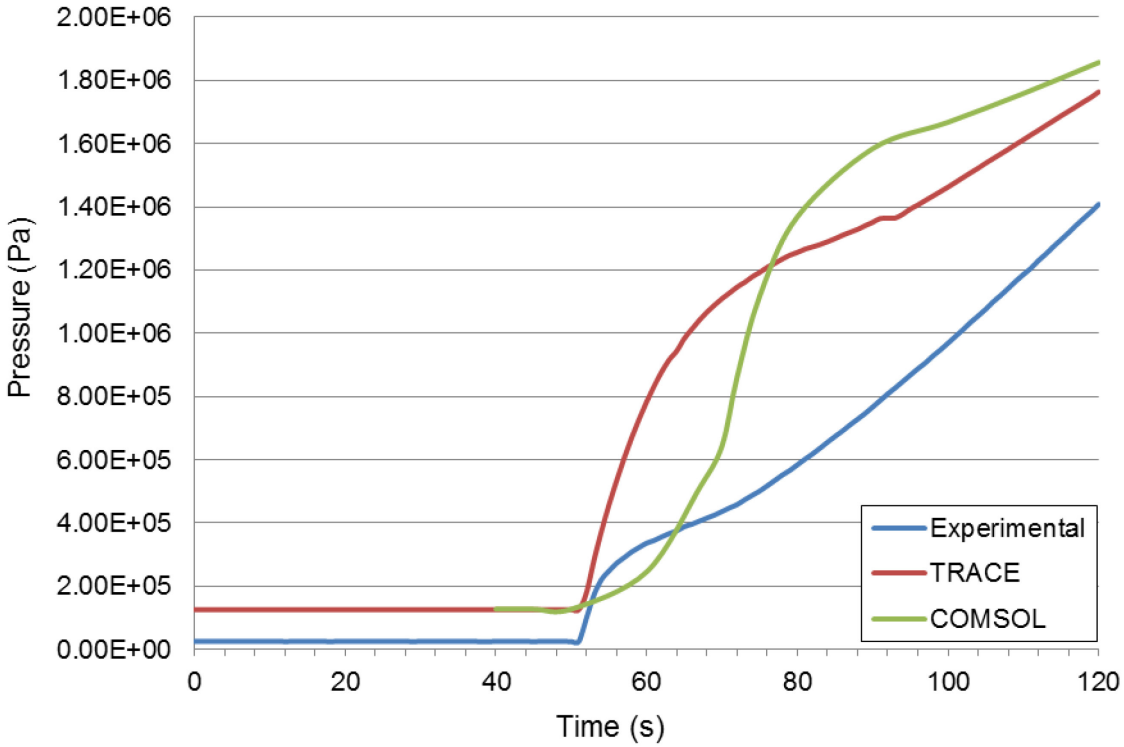

Figure 6.12. High Pressure Containment Pressure during Blowdown

The time period for the blowdown phase of 120 seconds was chosen due to the continuous opening and closing of the ADS vent line valve during the conduct of test case two. The valve operated on a cyclic opening and closing cycle between 120 and 4114 seconds; opening and closing 47 times . While the experimental data is available and the valve actuation is easily set in a TRACE model, the ability to open and close a valve in COMSOL proved outside the scope of the research and available module licenses. This is, however, not detrimental in establishing the initial blowdown for both the RPV and HPC. An analysis of the experimental data and TRACE and COMSOL results was still possible with the 120 seconds of available COMSOL results.

The initial blowdown of the RPV pressure was initiated at the set point for both the experimental test and the TRACE model. The COMSOL results reflect the previously discussed methodology of beginning the test at the opening of the valve. Therefore the COMSOL data begins 40 seconds later on Figures 6.11 and 6.12. The TRACE and COMSOL results for the RPV pressure are closely matched to the experimental data. The blowdown phase, beginning at the set point of 9.064 MPa is quickly followed by the increase in HPC pressure as seen in Figure 6.12.

While the RPV pressure results track closely to the experimental data, the HPV pressures from the TRACE and COMSOL results do not. Both the TRACE and COMSOL HPC pressures are increasing at a rate 35% faster than the experimental value. The result of this increase would be a faster time in reaching pressure equalization between the HPC and the CPV. The level of decay power

is linked to the eventual equalization of pressures and this phenomenon could lead to saturated liquid in the core. This idea will be explored in the decay cooling phase.

Although the COMSOL results were terminated at 120 seconds for the blowdown phase, the experimental data and TRACE results are available for the entire 4000 second event. Figure 6.13 shows both the RPV pressure and HPC pressure as a function of time.

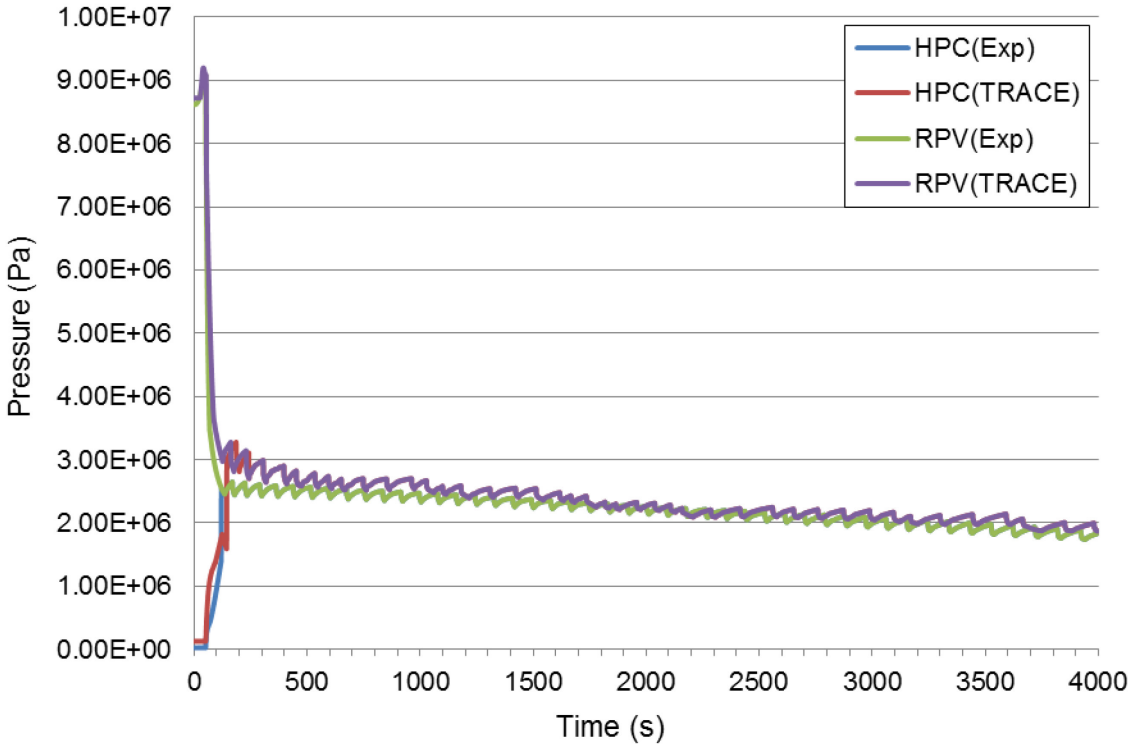

Figure 6.13. HPC and RPV Pressure Equalization

The experimental data and the TRACE results very closely match in regards to their behavior due to the opening and closing of the ADS vent line valve. The TRACE results do show a higher RPV pressure over a longer period of time suggesting the rate of equalization taking a longer period of time. This delay is likely attributed to a slower rate of heat transfer occurring the HPC. This

is verified in the TRACE results as the pressure equalization (within 0.034 MPa) doesn't occur until 4614 seconds, or a 14.5% difference from the experimental data.

The second phase of test case two focuses on the core inlet and outlet temperatures and the temperature difference across the core. The decay cooling phase is initiated at 4114 seconds and runs until 15822 seconds. Figure 6.14 shows the experimental data and TRACE and COMSOL results during the decay cooling phase.

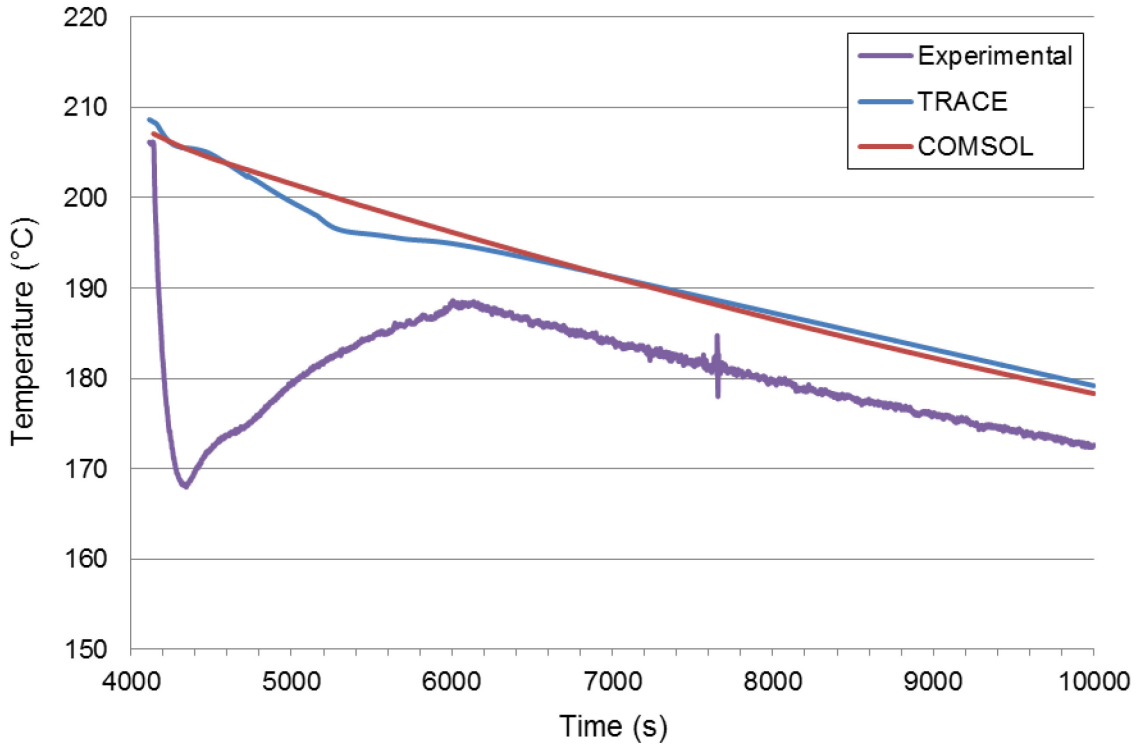

Figure 6.14. Core Inlet Temperatures (Decay Cooling Phase)

The experimental data shows a severe decrease in the core inlet temperature from the initiation of the second phase until 6000 seconds. The reason this occurs is due to the location of the thermocouples that measure the core inlet temperature. At the time of the ADS sump line opening (4114

seconds), the cool water from the HPC flows into the CL downcomer and into the lower plenum. The cooler HPC water mixes with the primary coolant and leads to the drastic lowering of the inlet conditions for a period of time. The TRACE results show a noticeable small decrease in the inlet temperatures, but the COMSOL results do not. The COMSOL model was verified and the inlet conditions for the ADS sump line mirrors those of the experimental data at the start of the second time-dependent phase. The lack of temperature drop is not attributed to the initial or boundary conditions and remains a point of interest in the continuance of this research.

After 6000 seconds, the TRACE and COMSOL results show a 8°C higher temperature, or 5.75% error, when compared to the experimental data, yet have agreement between their results. The introduction of the cooler HPC water, evident in the experimental data in the first 2000 seconds of the decay cooling phase, is responsible for this large difference, as the decay heaters are at 17.3% of their original operating power at this point. As time progresses, the cooler HPC water mixes with the primary coolant and the overall core inlet temperature rises, but not enough to account for the lack of this phenomenon in the TRACE and COMSOL results.

Figure 6.15 shows the temperature of the primary coolant as it leaves the top of the core and enters the bottom of the HL riser. Recall the heaters are in decay mode and the outlet temperatures are decreasing with time.

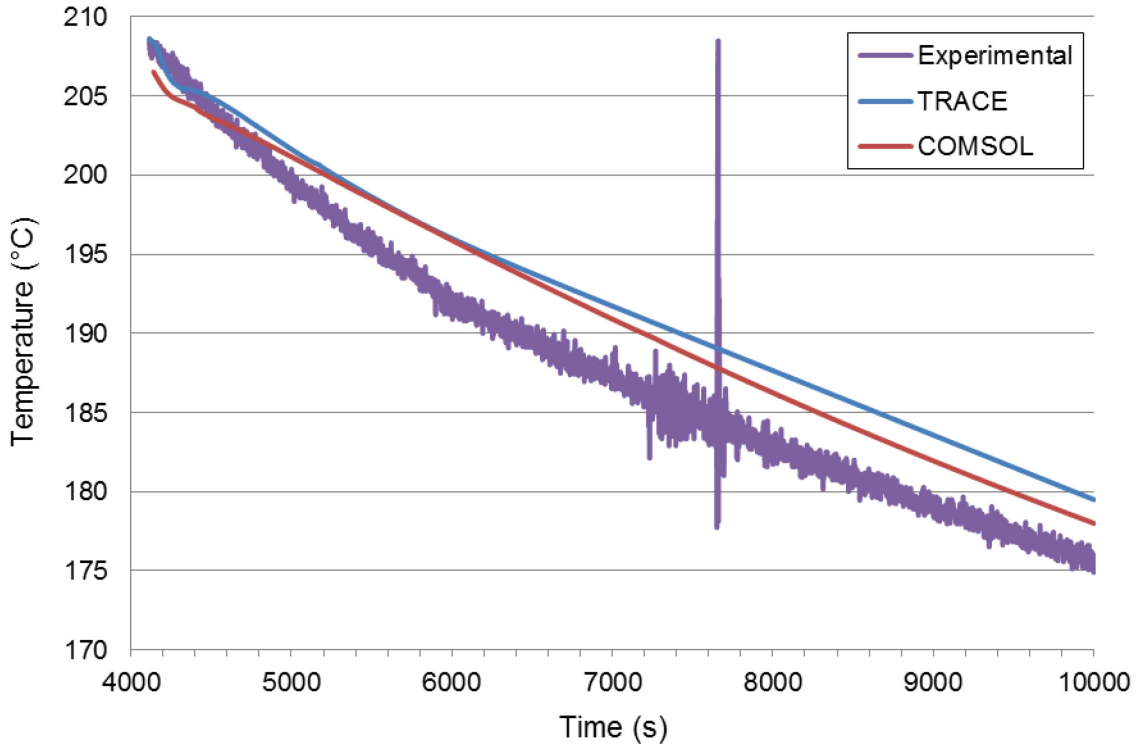

Figure 6.15. Core Outlet Temperatures (Decay Cooling Phase)

Several key items are evident in Figure 6.15. Most noticeably is the spike in the experimental data in the 7200 to 8000 second range. This temperature spike is likely an anomaly and will not be considered as part of the comparison between the TRACE and COMSOL results. Secondly, the core outlet temperatures have less than a 3% error in comparing the experimental data to the TRACE and COMSOL results. The experimental data is lower by comparison, but this agrees with the higher inlet temperatures in the TRACE and COMSOL results. Lastly, the experimental data inlet temperature decrease does not have a noticeable effect on the outlet temperatures. This is likely the result of complete mixing in the geometrically complex test facility core, including the upper and lower core plates, the core shroud and the small pitch-to-diameter ratio of the heater rods.

The average temperature difference across the core is shown in Figure 6.16. The large spike in the experimental data is again attributable to the inflow of the cooler HPC water into the lower plenum at the start of the decay cooling phase. The TRACE results also reflect a small increase, but again are negligible in comparison to the experimental results. The COMSOL results underestimate the experimental data by 5.75% and the TRACE results by less than one percent

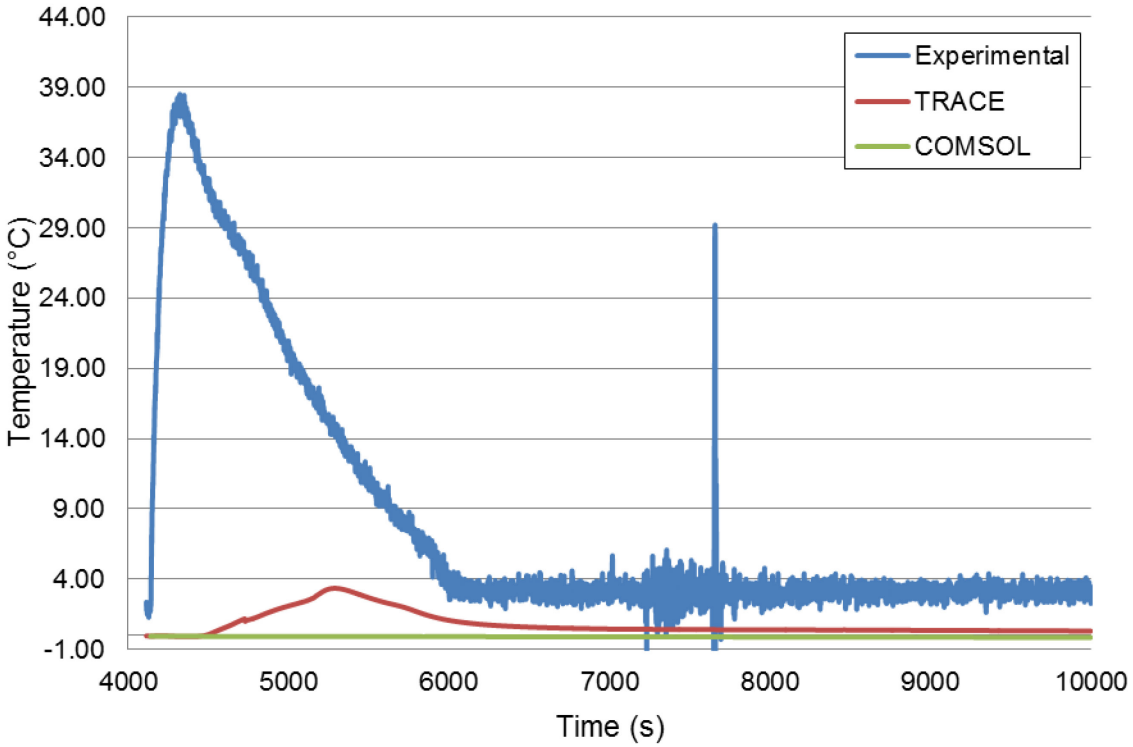

Figure 6.16. Temperature Difference Across the Core (Test Case Two)

The results from test case two vary widely in the application of the TRACE and COMSOL models and the development of the initial and boundary conditions to support the time-dependent studies. The TRACE results more closely match the experimental data in most all measured areas and are a good indication of the expected behavior of the test facility. The COMSOL results are more closely

aligned with the experimental data when compared to test case one, but the analysis is lacking in detail due to the rapid opening and closing of the ADS vent valve. The ability to model the vent valve in the time-dependent study would have proven valuable to a more detailed analysis.

6.3 Sensitivity Analysis Results

The sensitivity analysis was conducted to determine how the COMSOL model reacts to changes in the values of several key parameters. In this case, the experimental data available is compared to a set of reference COMSOL parameters from test case one. These are briefly reviewed below.

An altered set of test case one computer runs was completed with the initial and boundary conditions found in Tables 5.3 and 5.5. Table 6.5 lists those parameters that were altered and the range of values that were evaluated. A more detailed description of the sensitivity analysis was previously discussed in the COMSOL model development contained in Section 5.5.3.

The same model set-up and material properties utilized in the computational runs of test case one were applied for the sensitivity analysis. Exceptions to the maximum power level test case are listed in Table 5.30 and include changes to the mesh sizes for ease of computational effort. Additionally, no changes were made to the geometry utilized in the computational runs of test case one. The reference case is a full 3-D steady-state model featuring non-isothermal flow. The reference calculations were made at a power level of 320 kW and all subsequent sensitivity analyses were performed at that power level.

The first variation from the reference case was to “artificially” vary the FW mass flow rate. This was done in two batches: one that featured a decrease in the rate from 0.1 to 0.01 kg/s in 0.01 kg/s increments, and one that featured an increase in the rate from 0.1 to 0.3 kg/s in 0.05 kg/s increments. As explained previously, the “artificial” variation was accomplished by changing the heat transfer coefficient of the simplified helical SG to mirror the effect of changing the FW flow rates.

Table 6.5. Sensitivity Analysis Parameters

Value	*Variation from Reference Calculation*	*Range*
REF	Reference calculation	
SEN1	Decrease FW mass flow rate	0.1 – 0.01 kg/s in 0.01 kg/s increments for maximum power level
SEN2	Increase FW mass flow rate	0.1 – 0.3 kg/s in 0.05 kg/s increments for maximum power level
SEN3	Decrease the thermal conductivity of the hot leg riser below the SG	44.5 – 14.5 W/(m·K) in 10 W/(m·K) increments for maximum power level
SEN4	Increase the thermal conductivity of the hot leg riser below the SG	44.5 – 74.5 W/(m·K) in 10 W/(m·K) increments for maximum power level

Three experimental data points were used as assessment tools in the first two parameter variations: the primary coolant temperature in the CL downcomer below the SG, the core outlet temperature and the primary coolant mass flow rate. Table 6.6 lists the results of the decrease in FW mass flow rates (the top data set is the experimental value from the test facility data and is intended as a basis of initial comparison to the initial COMSOL reference result.

Table 6.6. Sensitivity Analysis—Feedwater Mass Flow Rate Decrease

FW Mass Flow Rate (kg/s)	*$T_{belowSG}$ (°C)*	*$T_{coreout}$ (°C)*	*Primary Mass Flow (kg/s)*
0.10 (exp)	216.5	252.2	1.8
0.10 (ref)	255.3	290.4	1.9
0.09	257.2	292.0	1.9
0.08	259.5	293.5	2.0
0.07	260.4	294.7	2.0
0.06	262.7	296.1	2.1
0.05	264.5	298.9	2.2
0.04	266.4	300.4	2.4
0.03	n/a	n/a	n/a
0.02	n/a	n/a	n/a
0.01	n/a	n/a	n/a

Table 6.7 lists the results of the increase in FW mass flow rates.

Table 6.7. Sensitivity Analysis—Feedwater Mass Flow Rate Increase

FW Mass Flow Rate (kg/s)	*$T_{belowSG}$ (°C)*	*$T_{coreout}$ (°C)*	*Primary Mass Flow (kg/s)*
0.01 (exp)	216.5	252.2	1.8
0.10 (ref)	255.3	290.4	1.9
0.15	251.7	287.4	1.8
0.20	247.6	284.2	1.8
0.25	243.4	280.5	1.7
0.30	238.8	274.8	1.7

The results in Table 6.6 support the physics of decreasing the amount of heat transferred to the secondary side. The decrease in secondary side heat transfer results in an increased temperature in the CL downcomer below the SG. As these temperatures increase from a lack of FW flow, the primary coolant continues to increase in temperature as it passes through the core. This is evident in the increased $T_{coreout}$ values. The mass flow rates also behave in accordance with the experimental data presented earlier. As the temperature difference across the core increases, the mass flow in the HL riser increases.

An unintentional result was observed in lowering the FW mass flow rate. The results of altering the FW mass flow rates in COMSOL show the minimum rate to be 0.04 kg/s in order to prevent the onset of nucleate boiling. The saturation temperature at a pressure of 8.72 MPa is 301.119°C. The non-isothermal interface in COMSOL does not allow a phase change and the solution to the FW mass flow rate of 0.03 kg/s did not converge. This suggests the saturation point was surpassed resulting in the stoppage of the computational run. Figure 6.17 shows the two temperature changes due to a decrease in the FW mass flow rate.

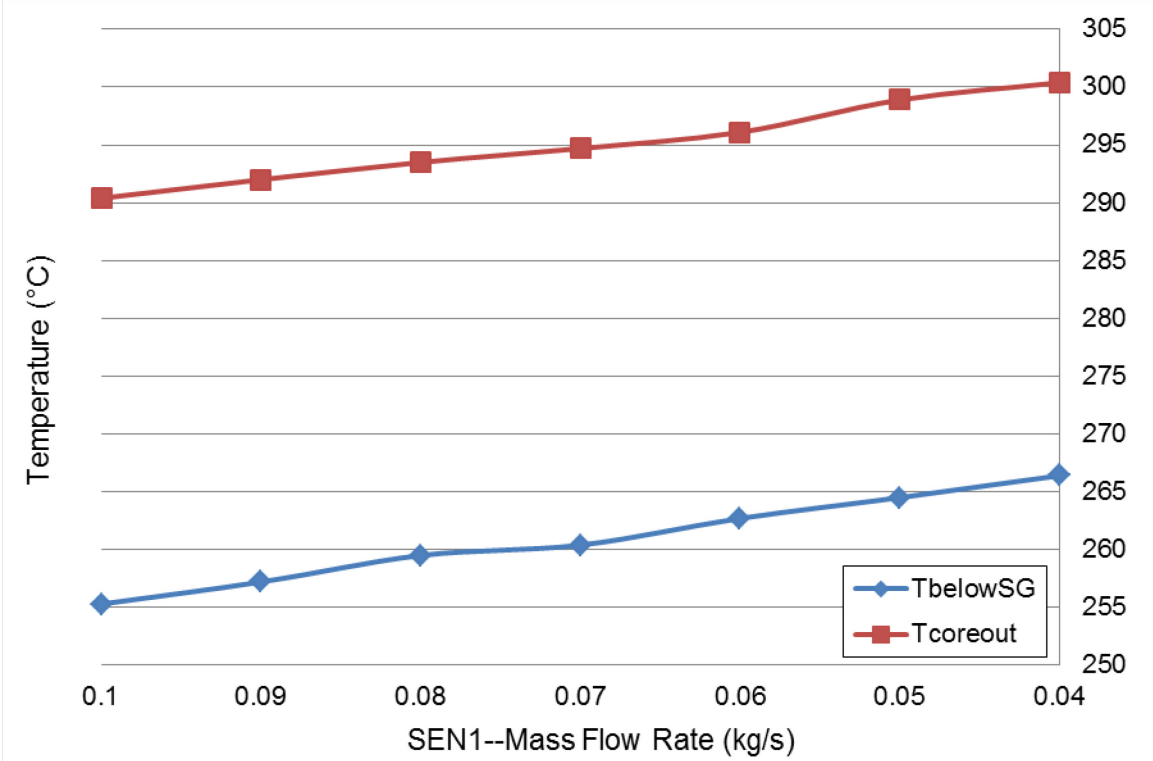

Figure 6.17. Sensitivity Analysis—Feedwater Mass Flow Rate Decrease

The results of increasing the FW mass flow rates, as listed in Table 6.7, show the opposite effect. This expected result shows the deviation from the experimental value rather quickly as the FW mass flow rate is increased in 0.5

kg/s increments. The initial increase yields a 3.6°C decrease in the $T_{belowSG}$ values and continues in a non-linear fashion to a low value of 238.8°C. The analysis also shows a decrease in the mass flow rate through the HL riser. Figure 6.18 shows the two temperature changes due to an increase in the FW mass flow rate.

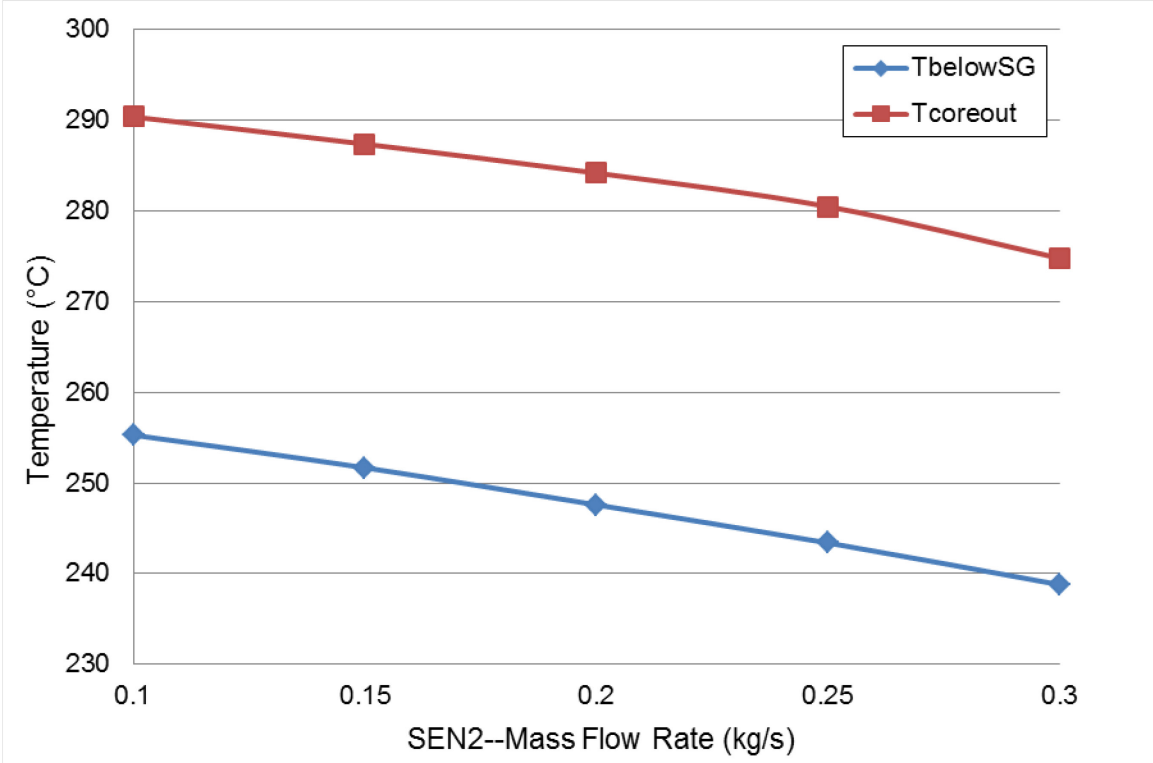

Figure 6.18. Sensitivity Analysis—Feedwater Mass Flow Rate Increase

The third and fourth set of parameter variations involved the changing of the thermal conductivity of the HL riser material located between the bottom of the SG and the upper core plate. As detailed previously, in analyzing the experimental data related to the flow temperature after the SG coils primary side section and the core inlet temperature, it is evident that the direct heat exchange, through the internal shell, between the fluid ascending the hot leg and the fluid descending the cold leg, is having an effect on the natural circulation behavior of

the design. The experimental data, shown in Figure 6.19 shows that along the downcomer region, the fluid increases its temperature between the end of the SG primary side section and the core inlet at 320 kW for 1000 seconds of operation.

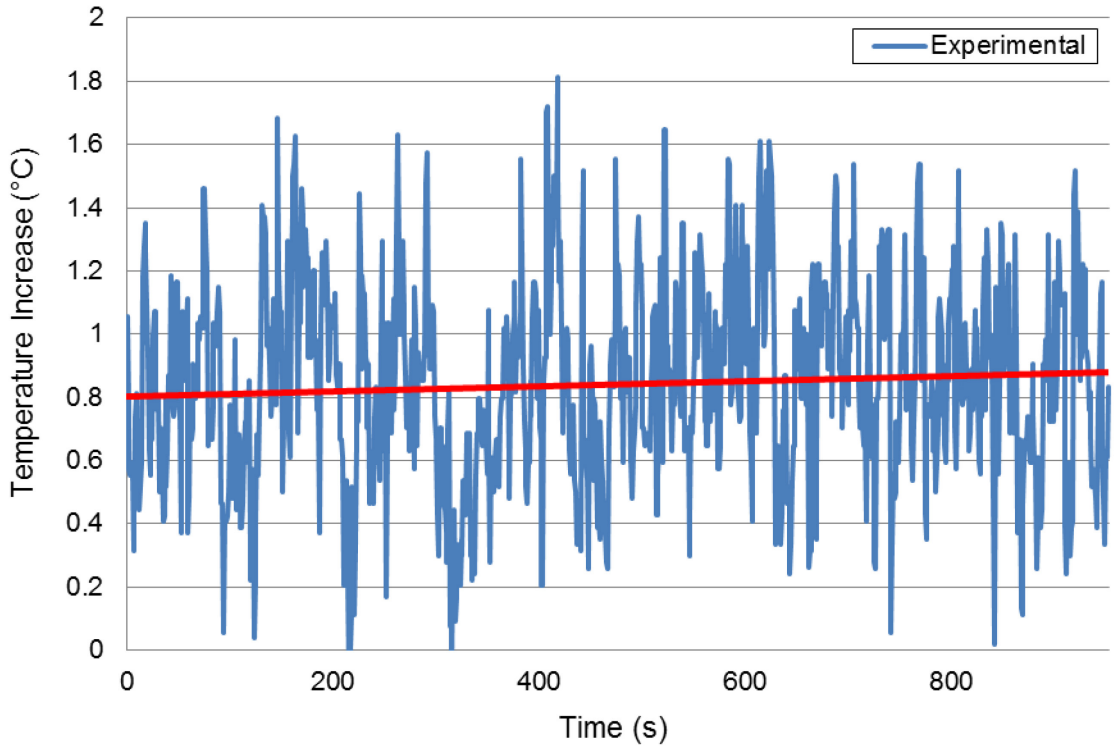

Figure 6.19. Primary Coolant Temperature Increases

The temperature differences graphed on the ordinate show the difference between the core inlet flow, T_{inlet}, and the coolant at a point just below the SG in the CL downcomer, $T_{CL-belowSG}$.

The effect of heating across the HL riser becomes more pronounced at higher reactor power levels. The trendline in Figure 6.19 shows an increasing slope. This effect, in regards to long-term operation of the reactor, would lead to continuously increasing core inlet temperatures if not addressed. While this may seem insignificant, with a less than 1°C increase over 1000 seconds, any deviation in the heat transfer properties of the SG or the HL riser could lead to

the primary coolant rising above the saturation temperature while in the core, leading to in-core boiling.

The sensitivity analysis was conducted by altering the thermal conductivity of the HL riser in the COMSOL model and then conducting a series of steady-state analysis. Table 6.8 lists the results of the decrease in the thermal conductivity of the HL riser (the top data set is the experimental value from the test facility data and is intended as a basis of initial comparison to the initial COMSOL reference result.

Table 6.8. Sensitivity Analysis—HL Riser Thermal Conductivity Decrease

Thermal Conductivity (W/m·K)	$T_{belowSG}$ *(°C)*	T_{corein} *(°C)*	*Primary Mass Flow (kg/s)*
44.5 (exp)	216.5	217.4	1.8
44.5 (ref)	255.3	256.2	1.9
34.5	254.5	254.6	1.9
24.5	254.2	253.5	1.9
14.5	253.7	252.9	1.9

Table 6.9 lists the results of the increase in the thermal conductivity of the HL riser.

Table 6.9. Sensitivity Analysis—HL Riser Thermal Conductivity Increase

Thermal Conductivity (W/m·K)	$T_{belowSG}$ *(°C)*	T_{corein} *(°C)*	*Primary Mass Flow (kg/s)*
44.5 (exp)	216.5	217.4	1.8
44.5 (ref)	255.3	256.2	1.9
54.5	257.2	258.4	1.8
64.5	259.7	261.4	1.8
74.5	262.3	265.5	1.7

The results in Table 6.8 support the idea of a decrease in the thermal conductivity of the HL riser. The decrease in the heat transfer properties leads to a gradual decrease in the T_{corein} values. The reference value shows a slight

increase in the primary coolant as it travels below the SG to the lower plenum. The decrease in the thermal conductivity eventually leads to a loss in primary coolant temperature in the same volume at a thermal conductivity of approximately 34.5 W/m·K. Of key interest here is the cross-over of the temperatures at 34.5 W/m·K. Due to the perfect thermal insulation of the RPV, the core inlet temperatures should never be lower than those below the SG as there is no loss of heat across the RPV walls. The loss of heat in decreasing thermal conductivities cannot be physically explained and this phenomenon requires further investigation. Figure 6.20 illustrates the decrease in the thermal conductivity on both temperatures.

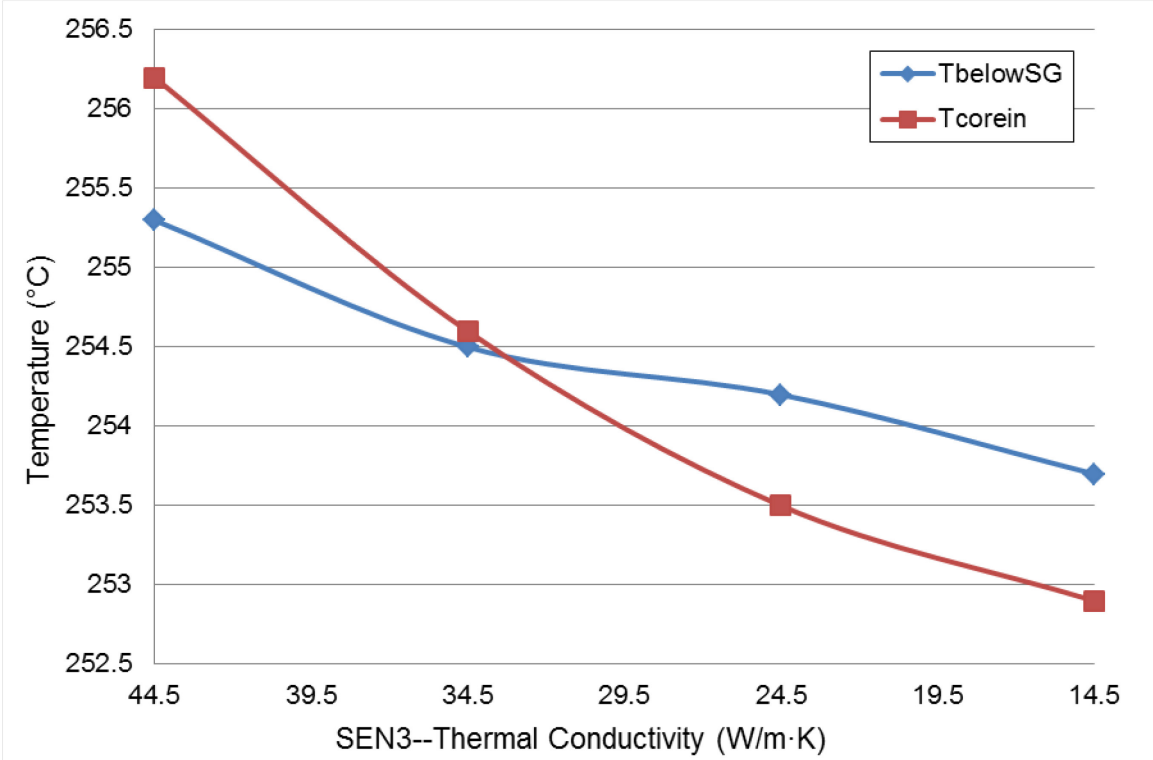

Figure 6.20. Sensitivity Analysis—HL Riser Thermal Conductivity Decrease

The results in Table 6.9 show the opposite effect as the thermal conductivity is increased in the same increments. The initial difference between

the CL downcomer temperature and the core inlet temperature is 0.9°C, which is consistent with the experimental data. As the thermal conductivity is increased, as shown in Figure 6.21, the temperature difference between the CL downcomer and the core inlet temperature increases to 3.2°C. Given an average experimental core temperature increase of 35.7°C, the $T_{coreout}$ value for a thermal conductivity of 74.5 W/m·K is 300.2°C. This is less than one degree from the T_{sat} value of 301.119°C. Any further increase in the thermal conductivity will lead to saturation conditions in the core.

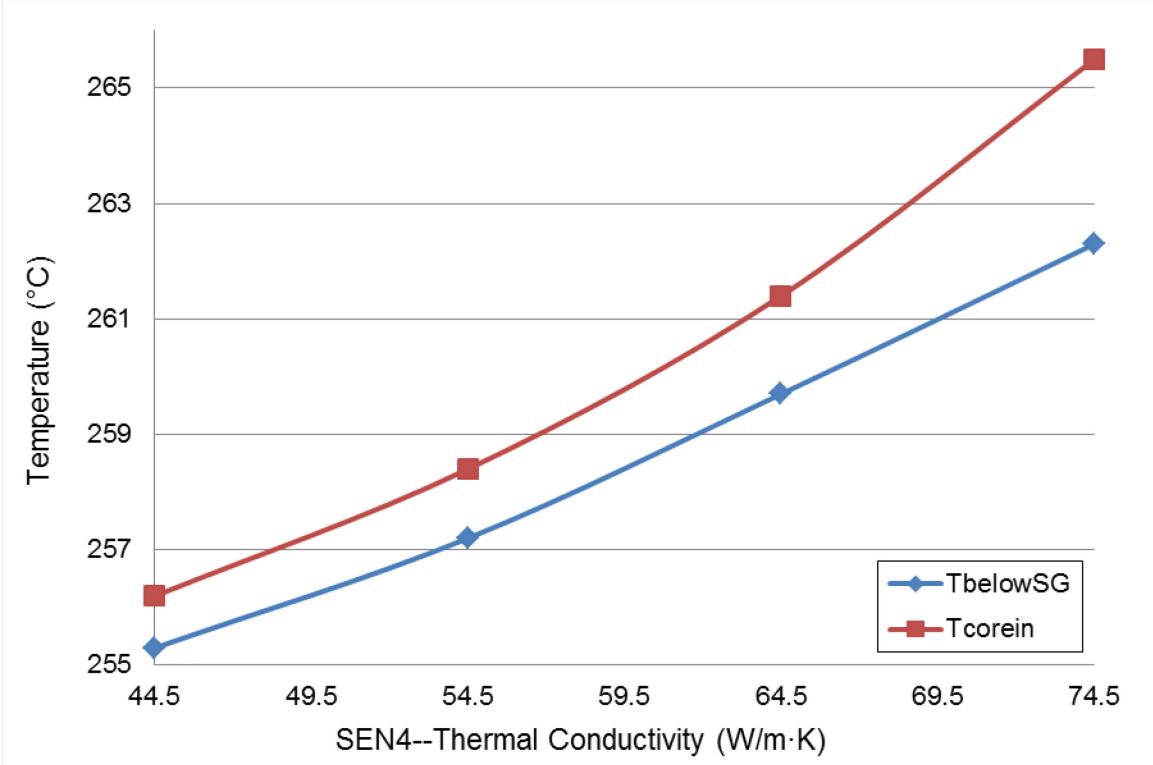

Figure 6.21. Sensitivity Analysis—HL Riser Thermal Conductivity Increase

CHAPTER 7

CONCLUSIONS AND FUTURE WORK

7.1 OVERALL CONCLUSIONS

This research focused on improving the use of the widely accepted T-H codes in the analysis of new and innovative nuclear reactor designs. Its intended purpose was to use a CFD code to model the primary natural circulation loop of a proposed SMR for comparison to experimental data and best-estimate T-H code results. The recent advances in CFD code modeling capabilities have made them attractive surrogates to the current conservative approach of coupled best-estimate thermal hydraulic codes and uncertainty evaluations.

The results of the CFD analysis were benchmarked against the experimental test results of the OSU-MASLWR during steady-state power operations and during a depressurization transient. The comparative evaluation of the experimental data, the thermal hydraulic code results and the CFD code results validate TRACE's treatment of a natural circulation loop. The insights into the expanded use of the CFD code in future designs and operations remain challenging as is discussed below.

The sensitivity analysis with COMSOL focused on two primary areas of design and explored their impact on those physical phenomena most impactful on operations of the natural circulation loop. Overall, the combination of the comparative evaluation and sensitivity analysis led to increased confidence in the

model's design and for the establishment of a natural circulation loop.

The characteristics of dynamic physical phenomena, uncertainty and low driving forces for passive systems justified the comparative evaluation of the best-estimate T-H code to the rapidly expanding role of CFD in new nuclear power plant design. The initial assumption of using CFD arose because the best-estimate T-H codes are based on a network of 1-D volumes and correlation databases that could lead to artificial confidence in the passive systems.

While obvious that the flow patterns in most, if not all, components in the core of a nuclear power plant, are strongly 3-D, the T-H code results were more consistent with the experimental data. The combination of natural circulation, complex geometric flow patterns and multi-phase mixing proved challenging for accurate CFD code predictions in both 3-D and time-dependent studies. Modeling complex flows through the use of existing best-estimate T-H codes was computationally more efficient and yielded less error in the benchmarking against experimental data. The confidence in these code's accurate predictions was increased as a result of this analysis of natural circulation in passive systems. Ultimately, the CFD code's ability to replicate the experimental data was not as accurate as the T-H code's results, with a wider margin of error in all evaluated areas.

7.2 Comparison of TRACE and COMSOL

The TRACE and COMSOL results presented here were aimed at the evaluation of the codes' capability in predicting natural circulation phenomena and heat exchange from primary to secondary side by helical SG in superheated

conditions and to evaluate the fidelity of various methods to model the SG in COMSOL.

The OSU-MASLWR was successfully modeled in both TRACE and COMSOL for test case one. The TRACE model featured all aspects of the test facility including the primary and secondary systems, the HPC and the CPV. The COMSOL model focused on the RPV vessel solely and included an simplified internal helical SG. The SG was modeled in a simplified fashion due to the geometric complexity of the test facility design and the resultant increase in CPU time based on the number of mesh nodes in the FEM analysis. The COMSOL model was a full to-scale 3-D model of the test facility otherwise.

The main difference between the benchmark analysis of the experimental data for test case one was the treatment of time. The TRACE model was run on a time-dependent basis with increases in the test facility's core power based on the test protocol. The COMSOL model was not run on a time-dependent study, and focused on a steady-state study due to the CPU computational penalty. The COMSOL computational effort was completed on a parallel computing network cluster. The cluster combines a mixture 264 CPU cores and 57 GPGPU accelerator boards to form a hybrid supercomputer with a theoretical peak performance of 59 teraflops. Even so, the computational effort of the steady-state COMSOL runs, which featured over 3.0×10^6 nodes took an average of 17 hours to complete. This is a 400% increase over the TRACE computational time.

TRACE's error in comparison to COMSOL for test case one was roughly 50% less in all areas expect the core outlet temperatures. As shown in Table

7.1, the error in the TRACE results for the core outlet temperatures was less than 1%. This is compared to a 4.32% error in COMSOL.

Table 7.1. Test Case One Summary

Measured Value (Location)	*Percent Error from Experimental*	
	TRACE	*COMSOL*
Coolant temperature (inside HL riser)	4.05	6.91
Coolant temperature (top of HL riser)	3.64	6.95
Coolant temperature (CL below SG)	2.30	4.65
Coolant temperature (core inlet)	2.31	5.66
Coolant temperature (core outlet)	0.78	4.32
Mass flow rate (inside HL riser)	6.52	8.80

Test case two featured the same TRACE model and a modified COMSOL model that was split into two time-dependent phases. The TRACE model was able to reproduce the phenomena of interest in test case two in comparison to the experimental data, again with little error. The COMSOL analysis was hampered by the CFD codes inability to handle the complexity of multiple moving phase interfaces over time. The initial and boundary conditions had to be broken into the two phases within the multi-phase, level set interface.

The COMSOL computational effort for test case two also increased. The average run time for the first phase was 26 hours and the second phase was over 30 hours. This level of computational effort was expected to yield greater fidelity in all phenomena of interest due to the 3-D FEM analysis. Although the COMSOL results were consistent with the experimental data, they proved to be less accurate than the TRACE results in all aspects of comparison to the experimental data.

7.3 Sensitivity Analysis Conclusions

The sensitivity analysis with COMSOL did offer several areas of consideration in continuing with the current MASLWR design. Both of these results indicate the sensitivity of the MASLWR's normal operating conditions when encountering transients involving the FW mass flow rate and in design and materials choices in the overall design.

In the first set of altered parameters, both the CL downcomer temperature and subsequent core outlet temperatures were susceptible to the FW mass flow rate. A decrease in the FW mass flow rate below 0.04 kg/s resulted in formation of sub-cooled liquid within the core. The increase in FW mass flow rate yielded results consistent with the experimental data and reference values.

Changing the thermal conductivity of the HL riser also yielded interesting results. A decrease in the thermal conductivity led to a primary coolant temperature decrease as it moved in the annulus between the bottom of the SG and the lower plenum. This phenomenon was only observed at very low power levels in the experimental data. Conversely, an increase in the thermal conductivity led to an increase in the core outlet temperatures and ultimately to formation of sub-cooled liquid in the core.

7.4 Recommendations For Future Work

The next logical step is to use the T-H code to provide input data to the CFD simulation in terms of (transient) inlet boundary conditions, and then run the CFD program in isolation. However, the problem remains of specifying the initial conditions (of velocities and field variables) for the CFD computation within the 3-

D domain. To complete the link, the procedure has to be extended by coupling the averaged exit boundary conditions from the CFD computation to the T-H code, and then the system analysis has to be continued. This provides a means of coupling the CFD module to an existing T-H code in order to perform a localized 3-D computation within the framework of an overall 1-D description of the geometry.

REFERENCES

Becker, Eric B., Graham F. Carey, and J. Tinsley Oden. *Finite Elements*. Englewood Cliffs, NJ: Prentice-Hall, 1981.

Bertolotto, Davide, Annalisa Manera, Simon Frey, Horst-Michael Prasser, and Rakesh Chawla. "Single-phase Mixing Studies by Means of a Directly Coupled CFD/system-code Tool." *Annals of Nuclear Energy* 36.3 (2009): 310-16.

Boyack, B. E.; Ward, L.W. Validation Test Matrix for the Consolidated TRAC (TRAC-M) Code. Los Alamos National Laboratory, LA-UR-00-778, February 2000.

Burgazzi, L. "Evaluation of Uncertainties Related to Passive Systems Performance." *Nuclear Engineering and Design* 230.1-3 (2004): 93-106.

Burnett, David S. *Finite Element Analysis: From Concepts to Applications*. Reading, MA: Addison-Wesley Pub., 1987.

Carelli, M. "The Design and Safety Features of the IRIS Reactor." *Nuclear Engineering and Design* 230.1-3 (2004): 151-67.

Chung, T. J. *Computational Fluid Dynamics*. Cambridge: Cambridge UP, 2002.

COMSOL Multi-Physics User Guide: Version 4.2. COMSOL Inc., Burlington, MA: 2008.

Computational Fluid Dynamics Analysis of Natural Circulation Flows in a Pressurized-Water Reactor Loop under Severe Accident Conditions. Rep. no. NUREG/CR-1922, INEL-94/0016. Washington, DC: U.S. Nuclear Regulatory Commission, March, 2010.

EPRI, Program on Technology Innovation: Probabilistic Risk Assessment Requirements for Passive Safety Systems. Electric Power Research Institute: Palo Alto, CA, 2007.

Freixa, J., and A. Manera. "Analysis of an RPV Upper Head SBLOCA at the ROSA Facility Using TRACE." *Nuclear Engineering and Design* 240.7 (2010): 1779-788.

Galvin, M. R. *OSU-MASLWR Test Facility Modification Description Report*. IAEA Contract Number USA-13386. Oregon State University: Corvallis, OR, 2007.

Gebhart, Benjamin. "Buoyancy Induced Fluid Motions Characteristic of Applications in Technology." *Journal of Fluids Engineering* 101.1 (1979): 5.

Gou, Junli, Suizheng Qiu, Guanghui Su, and Douna Jia. "Thermal Hydraulic Analysis of a Passive Residual Heat Removal System for an Integral Pressurized Water Reactor."*Science and Technology of Nuclear Installations* 2009 (2009): 1-12.

IAEA-TECDOC-626. *Safety Related Terms for Advanced Nuclear Power Plants*. Vienna: International Atomic Energy Agency, 1991.

IAEA-TECDOC-1281. *Passive Decay Heat Removal From the Core Region: Natural Circulation Data and Methods For Advanced Water Cooled Nuclear Power Plant Designs*, Vienna: International Atomic Energy Agency, 2002.

IAEA-TECDOC-1391. *Status of Advanced Light Water Reactor Designs.* Vienna: International Atomic Energy Agency, 2004.

IAEA-TECDOC-1474. *Natural Circulation in Water Cooled Nuclear Power Plants*. Vienna: International Atomic Energy Agency, 2005.

IAEA-TECDOC-1624. *Passive Safety Systems And Natural Circulation In Water Cooled Nuclear Power Plants*. Vienna: International Atomic Energy Agency, 2009.

Ishii, M. *Second Scaling and Scientific Design Study for GE ESBWR Relative to PUMA Facility with Volume Ratio of 1/475*. PU-NE-04-04. West Lafayette, IN: Purdue University, 2004.

Jaluria, Yogesh. *Natural Convection: Heat and Mass Transfer*. Oxford: Pergamon, 1980.

Kolev, N. P., and I. Spasov. *VVER-1000 Coolant Transient Benchmark (Part 2-Vessel Mixing Simultation)*. Nuclear Energy Agency Document No. 6964. Issy-les-Moulineaux, France: Nuclear Energy Agency, 2010.

Kurakov, Y.A., Dragunov, Y. G., Podshibiakin, A. K., Fil, N. S., Logvinov, S. A., Sitnik, Y. K., Berkovich, V.M., Taranov, G. S. *Development and Validation of Natural Circulation Based Systems for new WWER Designs*, IAEA-TECDOC-1281, Vienna: International Atomic Energy Agency, 2002.

Lee, K., and M. Kim. "Experimental and Empirical Study of Steam Condensation Heat Transfer with a Noncondensable Gas in a Small-diameter Vertical Tube." *Nuclear Engineering and Design* 238.1 (2008): 207-16.

Mai, A. T., and G. Ascherl. *OSU MASLWR Test Facility Quick Look Report*. OSU-MASLWR-QLR-SP2. Corvallis, OR: Oregon State University, August, 2011.

Mai, A. T., and G. Ascherl. *OSU MASLWR Test Facility Quick Look Report*. OSU-MASLWR-QLR-SP3. Corvallis, OR: Oregon State University, August, 2011.

Mascari, F., G. Vella, P. Buffa, A. Compagno, and E. Tomarchio. "Passive Safety Systems in View of Sustainable Development." *Final Report on the Round Tables, Erasmus Intensive Programme Project*. Proc. of Intensive Course on Accelerator and Reactor Operations, Sicilia, Italy. December, 2010.

Mascari, F., G. Vella, B.G. Woods, K. Welter, J. Pottorf, E. Young, M. Adorni, and F. D'auria. "Sensitivity Analysis of the MASLWR Helical Coil Steam Generator Using TRACE." *Nuclear Engineering and Design* (2010): 1137-1144.

Mascari, F., G. Vella, B. G. Woods, and F. D'Auria. "Analysis of the OSU-MASLWR Experimental Test Facility." *Science and Technology of Nuclear Installations*(2012): 1-19.

Modro, S. M., J. E. Fisher, K. D. Weaver, J. N. Reyes, Jr., J. T. Groome, P. Babka, and T. M. Carlson. *Multi-Application Small Light Water Reactor Final Report*. DOE Nuclear Energy Research Initiative Final Report. Idaho Falls, ID: Idaho National Engineering and Environmental Laboratory, December, 2003.

Oden, J.T. *Finite Elements: An Introduction.* Englewood Cliffs, NJ: Prentice Hall, 1991.

Pilkhwal, D. S., W. Ambrosini, and N. Forgione. "Analysis of the Unstable Behavior of a Single-phase Natural Circulation Loop with One-Dimensional and Computational Fluid-Dynamic Models." *Annals of Nuclear Energy* 34 (2007): 339-55.

Pottorf, J., F. Mascari, and B. G. Woods. "TRACE, RELAP5 Mod 3.3 and RELAP5- 3D Code Comparison of OSU-MASLWR-001 Test." Proc. of ANS Winter Meeting and Nuclear Technology Expo, Washington, DC, 2009.

"PRIS - Home." *PRIS - Home*. IAEA, 10 July 2013. <http://www.iaea.org/programmes/a2>.

Queral, C., I. Gonzalez, and A. Exposito. "Analysis of Abnormal Operation Procedures in Sequences of Loss of the RHRS at Midloop Operation." *Annals of Nuclear Energy*35.7 (2008): 1321-334.

Reddy, J. N., and David K. Gartling. *The Finite Element Method in Heat Transfer and Fluid Dynamics*. Boca Raton: CRC, 1994.

Symbolic Nuclear Analysis Package (SNAP) User's Manual. Applied Programming Technology, Inc., Bloomsburg, PA: 2007.

Todreas, Neil E., and Mujid S. Kazimi. *Nuclear Systems I—Thermal Hydraulics*. New York: Hemisphere Pub., 1990.

TRACE Version 5.0, Theory and User's Manual. Division of System Analysis, Office of Nuclear Regulatory Research, U.S. Nuclear Regulatory Commission, Washington, DC: 2008.

Wang, Jong-Rong, Hao-Tzu Lin, Yi-Hsiang Cheng, Wei-Chen Wang, and Chunkuan Shih. "TRACE Modeling and Its Verification Using Maanshan PWR Start-up Tests."*Annals of Nuclear Energy* 36.4 (2009): 527-36.

Woods, B. G., M. R. Galvin, and C. J. Bowser. *Problem Specification for the IAEA International Collaborative Standard Problem on Integral PWR Design Natural Circulation Flow Stability and Thermal-Hydraulic Coupling of Containment and Primary System during Accidents*. Publication. Corvallis, OR: Oregon State University, 2010.

Wulff, Wolfgang. "Critical Review of Conservation Equations for Two-phase Flow in the U.S. NRC TRACE Code." *Nuclear Engineering and Design* 241.10 (2011): 4237-260.